Trans-acting mutations reveal non-nuclear modulators of both intrinsic and extrinsic gene expression noise in a eukaryote.

Nena Martin[1], Julie Kleine-Schultjann[1], Quentin Boussau[1], Agnès Dumont[1], Hélène Duplus-Bottin[1], Laurent Modolo[1], Gaël Yvert[1], Patricia J. Wittkopp[2,3] and Fabien Duveau[1,3]

Affiliations:

[1]Laboratory of Biology and Modeling of the Cell, Ecole Normale Supérieure de Lyon, CNRS, Université Claude Bernard Lyon, Université de Lyon, France

[2]Department of Molecular, Cellular, and Developmental Biology, University of Michigan, USA

[3]Department of Ecology and Evolutionary Biology, University of Michigan, USA

Corresponding author:

Fabien Duveau, fabien.duveau@ens-lyon.fr

LBMC, ENS de Lyon, CNRS, UMR5239

46 allée d'Italie

69007 Lyon

France

ABSTRACT

Gene expression regulation is a stochastic process that can be modified by mutations not only in a deterministic manner but also in a probabilistic way, for example by changing the extent of cell-to-cell variability in gene expression (also called “gene expression noise”) without necessarily changing the expected (mean) expression level. Such mutations can act either in *cis* (perturbing expression noise at their own locus) or in *trans* (perturbing expression noise of a gene located elsewhere in the genome). Although systematic studies have successfully analyzed the properties of *cis*-acting mutations modulating gene expression noise, less is known about the type of genetic changes that may alter expression noise in *trans*. Here, we applied genetic mapping on yeast strains (*Saccharomyces cerevisiae*) generated by random mutagenesis and identified three mutations (in *chs1*, *yme2* and *msh1* genes) that changed the expression noise of a reporter gene in the nuclear genome regulated by the yeast *TDH3* promoter. Each of these mutations affected either extrinsic noise (variability due to cell-specific factors), intrinsic noise (inherent variability within each cell), or both. Surprisingly, all three mutations targeted proteins located outside of the nucleus: Yme2 and Msh1 being involved in the maintenance of mitochondrial genome integrity, and Chs1 being necessary for the repair of cell-wall defects in freshly-born daughter cells. Our results reveal that mitochondrial state can modulate the extent of intrinsic expression noise of eukaryotic nuclear genes.

INTRODUCTION

Gene expression levels vary among cells even in isogenic populations originating from a common cell type and maintained in a constant environment. This variability - commonly named *gene expression noise* - results from random fluctuations that inevitably occur along molecular and cellular processes impacting gene expression (reviewed in Pal & Dhar, 2024; Sanchez & Golding, 2013; Verhagen & Hansen, 2025). Expression noise can be modified by genetic changes, leading to differences in cell-to-cell variability among genotypes that can be either detrimental, neutral or beneficial depending on the gene and on the environmental condition; expression noise is therefore a substrate for evolution (M. Richard and Yvert, 2014). As a result, gene expression noise can take diverse forms depending on the shape of the distribution of expression levels observed among cells and how this distribution is modified by genetic changes. In extreme cases, a bimodal (or multimodal) distribution has been observed with two (or more) groups of isogenic cells displaying distinct expression levels of a gene. In certain cases, bimodal expression was shown to be part of a bet-hedging strategy when the two groups of cells were adapted to different environmental conditions (Baptista et al., 2025; Gamba et al., 2015; Levy et al., 2012). Even when the distribution of expression among cells is unimodal, which is the case for most genes (Newman et al., 2006; Taniguchi et al., 2010), genetic variants changing the variance of this distribution can impact population fitness (Duveau et al., 2018; Schmiedel et al., 2019) and therefore be targeted by selection (Metzger et al., 2015). Importantly, a global relationship is known to exist between mean expression and noise, whether among different genes (Newman et al., 2006; Taniguchi et al., 2010), among different genetic variants of a promoter (Carey et al., 2013; Hornung et al., 2012) or among environmental conditions (Bar-Even et al., 2006). Although the confounding effect of mean expression has complicated the study of the genetic sources and functional consequences of variation in expression noise, statistical and experimental approaches have been specifically designed to uncouple variation in these two metrics.

Several studies have shown that total noise in gene expression has two components, *extrinsic* and *intrinsic*, each attributable to distinct sources (Elowitz et al., 2002; Raser & O'Shea, 2004). Technically, extrinsic and intrinsic noise can be measured in cells where transcriptional activities of two copies of the same promoter are distinguishable (for instance using two fluorescent reporter genes of different colors; but see Stewart-Ornstein et al. (2012) for an alternative approach). In this setup, extrinsic noise represents expression variation among isogenic cells (or over time in a cell) that is correlated between the two copies of the promoter, while intrinsic noise represents independent

variation of expression between the two copies. Biologically, e*xtrinsic noise* results from sources generating heterogeneity in global state among cells, with consequences on how individual cells express the gene. In contrast, *intrinsic noise* corresponds to fluctuations that remain in cells after accounting for their state due to the inherent stochasticity of regulatory processes. Experimental and theoretical work have previously studied the properties of these two components and how specific steps of gene regulation contribute to them. The predominant source of intrinsic noise was shown to be transcription, which occurs stochastically in bursts (Blake et al., 2006; Harper et al., 2011; Pedraza & Paulsson, 2008; Quarton et al., 2020; Suter et al., 2011). The extent to which transcription contributes to intrinsic noise depends on chromatin remodeling (Raser & O'Shea, 2004), on nucleosome occupancy (Tirosh & Barkai, 2008), on the presence of TATA boxes in regulatory sequences (Blake et al., 2006; Choi & Kim, 2009; Hornung et al., 2012; Sun & Zhang, 2020) and on the number and type of transcription factors binding to the promoter (Parab et al., 2022; Sharon et al., 2014). Extrinsic noise is known to result from various cell-to-cell differences such as their pool of RNA polymerase (Yang et al., 2014), micro-environment (Snijder et al., 2009), age (P. Liu et al., 2017; Martinez-Jimenez et al., 2017), cell cycle stage (Sukys & Grima, 2025; Zopf et al., 2013), global transcription rate (Sherman et al., 2015), mitochondrial content (Guantes et al., 2015) and proliferation rate (Keren et al., 2015). Extrinsic noise was also shown to be reduced for genes regulated by miRNAs (Siciliano et al., 2013).

All factors modulating gene expression noise are possible targets for mutations and therefore provide a potential substrate for the natural evolution of cell-to-cell variability. As for any trait, two driving forces may influence the evolution of gene expression noise: the effects of random mutations on noise and the effects of selection on the fate of these mutations in natural populations. Regarding the action of selection on expression noise, several important observations have been reported. First, gene expression noise can be evolved experimentally through artificial selection (Wolf et al., 2015; You et al., 2019). Second, several studies provided evidence of negative selection acting against elevated expression noise in natural populations, suggesting that the detrimental effect of elevated noise could be counter-selected separately from any effect of a genetic variant on mean expression (Barroso et al., 2018; Metzger et al., 2015; Puzović et al., 2023; Schor et al., 2017; Vlková & Silander, 2022). Reciprocally, other studies showed that gene expression noise could be positively selected in certain cases, particularly in fluctuating environments (Acar et al., 2008; Eldar & Elowitz, 2010; Rocabert et al., 2020; Schmutzer & Wagner, 2020). When cells are maintained in a steady environment, increasing expression noise of a gene can be either beneficial or detrimental depending on the mean expression level and on the shape of the relationship that exists between the expression level of the gene and the

rate of cell proliferation (Duveau et al., 2018; Schmiedel et al., 2019). In yeast, transcriptome-wide analyses revealed a particularly high level of expression noise for plasma-membrane transporters, which play a critical role in cellular responses to environmental changes (Zhang et al., 2009). Experimental studies in bacteria (Wolf et al., 2015) and yeast (Bódi et al., 2017) showed that elevated expression noise could facilitate the evolution of gene regulation. By generating fitness variation among individuals, expression noise can also potentially reduce the efficacy of selection and therefore affect phenotypic evolution (Mineta et al., 2015; Wang & Zhang, 2011). In multicellular organisms, expression noise was associated with cell fate decision (Balázsi et al., 2011; Coomer et al., 2022; Ohnishi et al., 2014; Pal & Dhar, 2024; A. Richard et al., 2016; Wernet et al., 2006) and in the resistance of cancer cells to chemotherapy (Shaffer et al., 2017). Finding what genetic variants and molecular mechanisms can possibly modulate expression noise is therefore essential for understanding many fundamental biological processes.

In this regard, important discoveries were made about the type of genetic changes that can tune gene expression noise and their mechanisms of action. First, genetic variants segregating in natural populations were found to generate different levels of gene expression noise among individuals. In other words, variability among isogenic cells can itself vary among genetically-diverse individuals. This was first shown in yeast (Ansel et al., 2008; Fehrmann et al., 2013; J. Liu et al., 2015; Metzger et al., 2015) and later in bacteria (Vlková & Silander, 2022), flies (Huang et al., 2015) and human cells (Lu et al., 2016; Morgan et al., 2020; Triqueneaux et al., 2020). Second, as previously demonstrated for changes in mean expression (Wittkopp et al., 2004), a mutation may modify the expression noise of a focal gene in two different ways (Raser & O'Shea, 2004): the mutation may act in *cis* (if the mutation is at the locus of the regulated gene) or in *trans* (if the mutation is at a locus physically distant from the regulated gene). Importantly, a single mutation may act in *cis* on the expression of a nearby gene and in *trans* on the expression of another more distant gene, for example if the first gene is a regulator of the second gene. *Cis* effects of mutations are better accessible for investigations than *trans* effects because of the close proximity in the genome between *cis*-acting mutations and the gene with altered expression. Several studies were therefore conducted on specific genes to understand how *cis*-located mutations modify the expression noise of these genes. A seminal study focusing on the *GAL1* promoter in yeast showed how mutations in the TATA box could modulate noise by altering the dynamics of transcriptional bursts (Blake et al., 2006). In a later study, a more comprehensive random mutagenesis of 22 yeast promoters revealed a mathematical relationship between mean expression and expression noise, showing that mutations primarily altered the frequency of transcriptional bursts while burst size

differed among promoters, producing promoter-specific relationships between mean and noise (Hornung et al., 2012). Using an ingenious high-throughput approach to quantify mean expression and expression noise from thousands of designed synthetic promoters, another yeast study showed that both the number of functional transcription-factor binding sites and the frequency of poly(dT/dA) motifs - which favor nucleosome positioning – were key determinants of expression noise (Sharon et al., 2014). A fourth study compared the effects of 236 artificial mutations and 45 natural polymorphisms in the promoter of the yeast gene *TDH3*, providing evidence of negative selection against *cis*-acting mutations that increased noise of *TDH3* promoter activity (Metzger et al., 2015).

Although there are only few known examples of mutations affecting gene expression noise in *trans*, their effects on noise may differ from those of *cis*-acting mutations. For example, in the case of the yeast *TDH3* promoter, *trans*-acting mutations obtained via random mutagenesis of the genome were found to have a broader distribution of effects on expression noise than *cis*-acting mutations located in the *TDH3* promoter; in addition, random *trans*-acting mutations were as likely to increase as to decrease expression noise, whereas *cis*-acting mutations were more likely to increase expression noise (Metzger et al., 2016). Consistently, a study quantifying expression noise of surface proteins in human cells detected more *trans*-acting than *cis*-acting genetic regulators, suggesting that natural variation modulating gene expression noise was more likely to occur in *trans* (Morgan et al., 2020). Intuitively, another possible difference between *cis* and *trans* effects of mutations could be their impact on intrinsic and extrinsic noise. Indeed, theoretical models predict that *cis*-acting mutations in a regulatory sequence may modulate intrinsic noise by altering the frequency and magnitude of transcriptional bursts (Pedraza & Paulsson, 2008; Zenklusen et al., 2008). It is more difficult to imagine a scenario where a *cis*-acting mutation would modulate extrinsic noise. Mutations affecting expression noise in *trans*, however, could modulate either intrinsic or extrinsic noise. For instance, while mutations in a transcription factor may affect intrinsic noise of its target genes, mutations in a cell cycle regulator may impact extrinsic noise of other genes by generating heterogeneity of states among cells. Given these differences, it is necessary to further characterize what type of mutations can modulate gene expression noise in *trans* and what their mechanisms of action are to understand how expression noise is controlled genetically and evolves. One way to do so is by introducing target mutations in molecular complexes participating to gene expression and determine how they modify cell-to-cell variability in protein levels, as was done for mutations targeting chromatin remodeling (Raser & O'Shea, 2004) or transcription elongation (Ansel et al., 2008; Trinh et al., 2023). Such targeted approach, however, is driven by existing knowledge on gene regulation and does not interrogate the possible roles of

unexpected players. An alternative approach is to identify *trans*-regulators segregating in natural populations using adapted GWAS or QTL mapping methods (Chuffart et al., 2016; Fehrmann et al., 2013; Lu et al., 2016; Morgan et al., 2020; Sarkar et al., 2019; Yvert, 2014). Although this approach is well-suited to characterize genetic variants that have been filtered by selection, it does not capture all possible genetic sources of variation in expression noise. Identifying random mutations that modulate expression noise of a gene in *trans* - regardless of their fitness consequences - is an important complement to understand how the evolution of expression noise is shaped by the mutational process and natural selection (Hill et al., 2021).

Here we used a random mutagenesis screen followed by genetic mapping and functional assays to identify mutations that changed in *trans* the expression noise of a focal gene in yeast. We took advantage of a collection of 1241 mutant strains obtained by chemical mutagenesis of a parental strain expressing a fluorescent reporter gene controlled by the *TDH3* promoter (P_{TDH3}-*YFP*). In its native context, the *TDH3* promoter drives strong constitutive expression of a glyceraldehyde-3-phosphate dehydrogenase involved in glycolysis and gluconeogenesis (Partow et al., 2010). Using flow cytometry, we identified five mutants from the collection that showed altered P_{TDH3}-*YFP* expression noise relative to the parental strain without significant change in mean expression. Via genetic mapping, we identified six candidate causal mutations in these mutants and we validated the effects of three of them using strains engineered to each contain only one of these three candidate mutation (single-site mutants). We then characterized the contribution of these mutations to extrinsic and intrinsic noise using two-color reporters. The three mutations altered the coding sequences of *YME2*, *MSH1* and *CHS1* genes, none of which were previously associated with the control of noise or mean gene expression. In particular, our results suggest a potentially central and unexpected role of mitochondrial genome integrity in the modulation of intrinsic expression noise of nuclear genes.

RESULTS

Mapping mutations with *trans*-acting effects on expression noise

We previously identified mutations that affected the median expression level of a focal gene (P_{TDH3}-*YFP*, where expression of a *YFP* reporter gene is controlled by the *TDH3* promoter) from a yeast collection obtained by ethyl methanesulfonate (EMS) mutagenesis of a reference strain (Duveau et al., 2021; Metzger et al., 2016). Here, we took advantage of this collection to identify and characterize mutations that altered expression noise of the focal gene in *trans* (*i.e.* mutations outside of the *TDH3* promoter and causing increased or decreased cell-to-cell variability of fluorescence level). To this end, we first quantified median expression and expression noise (coefficient of variation of normalized fluorescence; see Methods) of P_{TDH3}-*YFP* in 1241 EMS mutants from the collection and in the reference strain by measuring fluorescence of thousands of cells for each strain using flow cytometry (**Figure 1a**). This initial screen revealed a wide variation of expression noise among mutants that was largely – but not completely – independent from variation in median expression. Next, we selected 254 mutants that showed largest changes of expression noise relative to the reference strain and we quantified their fluorescence a second time in an independent assay (**Figure 1 – figure supplement 1**). Among these 254 mutants, we chose five mutants for further analyses that showed significant changes of expression noise relative to the reference strain in both assays (*t*-test, adjusted $P < 0.01$), with no significant change in median expression in the first assay (*t*-test, adjusted $P \geq 0.05$). Three of these mutants had an increased level of P_{TDH3}-*YFP* expression noise and two mutants had a decreased level of noise (**Figure 1a**, **Table 1**). This procedure ensured that the five selected mutants showed reproducible changes in expression noise that were not explained by variation of median expression levels. By whole-genome re-sequencing (median coverage of 46x), we found between 17 and 47 mutations in the genomes of these five mutants (**Table 1**), which was consistent with the range (14 to 41) of mutations previously identified in other mutants from the same collection (Duveau et al., 2021). Given that the vast majority of mutants in the collection showed no significant change in expression noise, we expected that only one or a few mutations were responsible for the altered expression noise in each of the five selected mutants. We therefore applied a genetic mapping strategy specifically designed to identify these presumably-rare mutations (**Figure 1b**). We used a bulk segregant analysis approach where each haploid mutant was crossed to a wild-type strain also expressing P_{TDH3}-*YFP* and random segregants obtained from the meiosis of resulting diploid cells were sorted by FACS based on their fluorescence levels (see Methods). Among all segregants, the subset of cells that inherited a mutation responsible for

a change in expression noise of the fluorescent reporter (a causative mutation) should show either a broader or a narrower distribution of fluorescence levels than the subset of cells inheriting the wild-type allele. For this reason, we sorted random segregants in three bulks that captured distinct ranges of fluorescence levels: one bulk corresponding to the 2% of cells with lowest fluorescence (low bulk), one bulk corresponding to the 2% of cells with highest fluorescence (high bulk) and one bulk corresponding to the 10% of cells with fluorescence closest to the median fluorescence of all segregants (mid bulk). We reasoned that a causative mutation should be found at different frequencies in the mid bulk than in the low and high bulks. To further increase this difference, we repeated the fluorescence selection twice for each bulk with a few generations of growth between each selection step (**Figure 1b**). For each cross, frequencies of all segregating mutations were then quantified by deep sequencing of genomic DNA extracted from each bulk. Likelihood-ratio tests (*G*-tests) were used to determine if the frequency of each mutation was significantly different between the mid bulk and the combined low and high bulks (**Figure 1 – figure supplement 2**), in which case the mutation was considered causative (or genetically linked to a causative mutation). Using this approach, we found one candidate causative mutations in two out of five mutants analyzed and two candidate mutations in another mutant (**Table 2**). For mutant YPW2162, although no mutation was significantly associated with expression noise, a single mutation was found at very low frequency in all fluorescence bulks (*m2* in **Table 2**). This indicated that the mutation was strongly counter-selected during the procedure used to establish fluorescent bulks, which greatly reduced the statistical power to detect potential association with expression noise. For this reason, we considered mutation *m2* to be possibly causative and further investigated its impact on expression noise in the functional assays described below. For the last mutant (YPW2143), we noticed that the frequency of all 26 mutations was either near zero or near one in the low bulk of segregants. This unexpected observation suggested that a single haplotype was nearly fixed in the low bulk, either due to a strong selective advantage of this haplotype or more likely due to a strong bottleneck in population size (random genetic drift) when this bulk was established. For this reason, we only compared allele frequencies between mid and high bulks, but no mutation was found at a significantly different frequency between these two bulks (**Figure 1 – figure supplement 2c**). Therefore, we used another strategy based on linkage analysis and tetrad dissection to determine which mutation in mutant YPW2143 was associated with variation of expression noise. The candidate mutation we tested first was mutation *m3* (**Table 2**) because it was found at a slightly higher frequency in the high bulk (consistent with the increased noise observed in YPW2143) and this mutation appeared to be counter-selected in both bulks, which reduced the statistical power to detect different frequencies

of the mutation between bulks. After meiosis of diploid cells from the cross between YPW2143 and the mapping wild-type strain, we measured P_{TDH3}-*YFP* expression noise in 84 segregant clones issued from 21 dissected tetrads. We observed a very strong association between expression noise and the presence or absence of mutation *m3* in each clone (**Figure 1 – figure supplement 3**; ANOVA, F value = 792.31, $P = 1.47 \times 10^{-82}$).

Functional validation of effects of candidate mutations on expression noise

Statistical associations described above may be explained by a causal effect of candidate mutations on P_{TDH3}-*YFP* expression noise, but they could also result from genetic linkage with a causative mutation or from unsuspected selection for another trait. To demonstrate the causal impact of each candidate mutation (six mutations in **Table 2**) on expression noise, we used site-directed mutagenesis to introduce each mutation in a common genetic background (reference strain) that does not harbor any other mutations found in EMS mutants and that contains two distinct reporter genes inserted in opposite orientations at the *ho* locus (**Figure 1c**). As further described in the next sections, the use of two reporter genes (*YFP* and *RFP* coding sequences transcribed under control of distinct copies of the *TDH3* promoter) allowed us to distinguish two sources of expression noise. We then used flow cytometry to quantify median expression levels and expression noise of all site-directed mutants, the reference strain and EMS mutants from which candidate mutations were identified (note that EMS mutants do not express the *RFP* reporter gene). In almost all experiments reported below, we included two independent clones for each genotype (*i.e.* two strains established from two colonies from the same transformation) to detect cases where a secondary mutation not shared by all transformed cells would contribute to phenotypic variation (*i.e.* cases where the two independent clones would show statistically different phenotypes).

For three candidate mutations (*m1*, *m2* and *m3*), we observed a significant difference of expression noise between site-directed mutants and the reference strain (*t*-test, adjusted $P < 0.01$), both for YFP (**Figure 2a-c**) and for RFP (**Figure 2 – Figure supplement 2g-i**). In all three cases, the mutation caused an increased in expression noise relative to the allele of the reference strain. In addition, no significant difference of YFP expression noise was observed between each site-directed mutant and the EMS mutant carrying the same mutation (**Figure 2a-c**), indicating that the three candidate mutations were responsible for most, if not all, of the variation of expression noise observed in EMS mutants from which they were identified. As expected, we observed no significant difference of median expression between the reference strain and site-directed or EMS mutants carrying mutations

m1 and *m2* (*t*-test, adjusted $P \geqslant 0.01$), both for YFP (**Figure 2 – figure supplement 1a-b**) and for RFP (**Figure 2 – figure supplement 2a-b**). However, all strains carrying mutation *m3* showed a significant increase of YFP (**Figure 2 – figure supplement 1c**) and RFP (**Figure 2 – figure supplement 2c**) median expression levels relative to the reference strain (*t*-test, adjusted $P < 0.01$), which was unexpected based on the initial screen (**Figure 1a**) where the EMS mutant carrying mutation *m3* did not show an increased median expression level. We further investigated the cause of this apparent inconsistency below (**Figure 6 – figure supplement 2**).

For the other three candidate mutations tested (*m4*, *m5* and *m6*), no significant change in expression noise was observed between site-directed mutants and the reference strain for YFP (**Figure 2d-f**) and RFP (**Figure 2 – figure supplement 2j-l**); except for one of the two tested clones carrying mutation *m5* and only for RFP, which we considered to be a false positive. These mutations also did not significantly impact the median expression level of YFP (**Figure 2 – figure supplement 1d-f**) and RFP (**Figure 2 – figure supplement 2d-f**). Because mutations *m5* and *m6* were identified from the same EMS mutant, we hypothesized that these mutations may be required together to significantly impact expression noise. We therefore constructed a double mutant carrying both *m5* and *m6*, but this mutant did not show any significant change of expression noise relative to the reference strain (**Figure 2 – figure supplement 3**). In these experiments, the two EMS mutants from which *m4*, *m5* and *m6* mutations were identified showed a significant change of expression noise relative to the reference strain, as expected. Several hypotheses may explain why we did not find a causative mutation for these two EMS mutants (see Discussion).

A missense mutation in *YME2* gene increases intrinsic noise of P_{TDH3}-*YFP* expression.

To further investigate potential mechanisms of action for each causative mutation, we next measured how these mutations affected two distinct sources of noise: intrinsic and extrinsic noise. Even though intrinsic and extrinsic noise both contribute to the total expression noise of a gene, they are confounded when expression is measured from a single allele. However, these sources of noise can be distinguished when measuring expression from two reporter genes (in our case P_{TDH3}-*YFP* and P_{TDH3}-*RFP*) in individual cells (**Figure 3a**), as previously demonstrated (Elowitz et al., 2002). Indeed, while intrinsic noise creates differences of expression levels between the two reporters within a cell, extrinsic noise creates expression variation among cells that is well correlated between the two reporters (**Figure 1c**). Intrinsic noise is expected to result from stochastic processes involved in the independent transcription, translation and post-translational regulation of each reporter gene, while extrinsic noise

results from more global differences among cells such as differences in physiological states or in the amount of transcription factors regulating both reporters (Raser & O'Shea, 2005). We calculated intrinsic and extrinsic noise of mutant and reference strains from YFP and RFP fluorescence levels of individual cells as described in Fu & Pachter (2016) (see Methods).

We first focused on mutation *m1* corresponding to a missense mutation located in the coding sequence of the *YME2* gene (*G1234a* substitution; **Table 3**). Site-directed mutants carrying the mutant allele *yme2(G1234a)* showed an increased intrinsic noise relative to the reference strain (**Figure 3b**; *t*-test, adjusted $P < 0.001$ for both clones). This effect is visible through the lower correlation observed between YFP and RFP expression levels of mutant cells than wild-type cells (**Figure 3 – figure supplement 1**). The impact of *yme2(G1234a)* mutation on extrinsic noise was less clear as only one of the two tested clones showed a significant increase in extrinsic noise (**Figure 3c**; *t*-test, adjusted $P < 0.001$ for clone 1 and adjusted $P \geqslant 0.05$ for clone 2). Overall, the impact of *yme2(G1234a)* mutation on intrinsic noise explained most of the variation in total expression noise of the two reporter genes (**Figure 3d**). This is particularly surprising since YME2p is an integral protein of the mitochondria inner membrane with known functions linked to fusion and fission of mitochondrial nucleoids and integrity of the mitochondrial genome (Hanekamp & Thorsness, 1996; Park et al., 2006). Indeed, YME2p is not known to directly regulate the expression of nuclear genes. An indirect effect of mitochondrial activity on transcriptional or post-transcriptional regulation of nuclear genes would be expected to affect the expression of both reporter genes in a coordinated fashion, resulting in variation of extrinsic noise, which is not what we observed. Therefore, we tested whether potential experimental artifacts may explain the elevated intrinsic noise of *yme2(G1234a)* mutant. In particular, the detection of intrinsic noise may not only by caused by biological noise, but also by technical noise in the measurements of YFP an RFP fluorescence using flow cytometry. To exclude this possibility, we fused the coding sequences of *YFP* and *RFP* downstream of the *TDH3* promoter sequence (P_{TDH3}-*YFP-RFP*) and inserted the resulting transgene at the *ho* locus in genetic backgrounds carrying either the wild-type *YME2* allele or the *yme2(G1234a)* mutation. We reasoned that expressing a YFP-RFP protein fusion would lead to the same amount of yellow and red chromophores within a cell (variation can still exist among cells), which would completely prevent the detection of biological intrinsic noise (**Figure 3e**). Therefore, any difference of intrinsic noise detected in this context could be attributed to technical noise affecting the detection of YFP and RFP signals. We observed no significant effect of *yme2(G1234a)* mutation on intrinsic noise detected in strains expressing P_{TDH3}-*YFP-RFP* (**Figure 3f**), while the mutation significantly increased levels of extrinsic noise (**Figure 3g**) and total noise (**Figure**

3h). This result confirmed that the impact of *yme2(G1234a)* mutation on intrinsic noise detected with two reporter genes was caused by actual differences in the amount of YFP and RFP molecules within each cell.

We noticed in flow cytometry data a small but statistically significant decrease of median cell size (estimated from forward scatter signal) in *yme2(G1234a)* mutants relative to the reference strain (**Figure 4a**). When clustering cells in five quantiles based on cell size for each genotype, we observed that the increase of intrinsic noise associated with *yme2(G1234a)* mutation was more pronounced in smaller cells (**Figure 4b**). The extrinsic noise of wild-type and mutant cells was indistinguishable regardless of their size, even though a negative relationship was globally observed between extrinsic noise and the size of genetically identical cells (**Figure 4c**). In budding yeast with asymmetric cell division, smallest cells in non-synchronized populations often correspond to daughter cells just after division. Although variation of intrinsic noise is typically thought to result from alteration in processes regulating gene expression (Hypothesis 1 in **Figure 4d**), an alternative hypothesis would be that the effect of *yme2(G1234a)* mutation on intrinsic noise was caused by altered partitioning of YFP and RFP molecules in daughter cells after division, potentially because of their reduced size compared to wild-type daughter cells (Hypothesis 2 in **Figure 4d**). To test these hypotheses, we constructed a P_{TDH3}-*YFP-RFP* gene fusion where coding sequences of *YFP* and *RFP* were separated by a short sequence encoding the cleavage site for the tobacco etch virus (TEV) protease (ENLYFQS peptide sequence). This construct was inserted at *ho* locus in strains that constitutively express the wild-type TEV or the improved uTEV3 protease from Sanchez and Ting (2020), with either the wild-type or *G1234a* mutant allele of *YME2*. We reasoned that sources of noise acting on expression at any step from transcription to translation would be undetectable in these strains because YFP and RFP are expressed from the same coding sequence. However, if the increased intrinsic noise was caused by altered partitioning of YFP and RFP molecules, we should still be able to detect it in these strains because YFP-RFP proteins are cleaved into YFP and RFP peptides that are free to segregate independently in mother and daughter cells after division (**Figure 4d**). Western blotting with an antibody against RFP showed that YFP-RFP was fully cleaved in strains expressing the improved uTEV3 protease (undetectable level of YFP-RFP fusion protein), but only partially cleaved in strains expressing the wild-type TEV (**Figure 4e**). Therefore, we measured expression noise in strains expressing uTEV3. We observed no detectable effect of mutation *yme2(G1234a)* on intrinsic noise in strains producing YFP and RFP peptides from cleavage of YFP-RFP fusion proteins (**Figure 4f**; *t*-test, adjusted $P > 0.05$), regardless of cell size (**Figure 4h**). However, a significant increase of extrinsic noise was observed for *yme2(G1234a)* strains

relative to wild-type strains (**Figure 4g**; *t*-test, adjusted $P < 0.001$ for clone 1, adjusted $P < 0.01$ for clone 2). These results are not consistent with the hypothesis that *yme2(G1234a)* mutation affects expression noise via altered partitioning of proteins during cell division. Instead, the mutation must cause an increased intrinsic noise by acting on a process regulating gene expression at some point from transcription to protein degradation, via an unknown mechanism.

A nonsense mutation in *CHS1* increases extrinsic noise via impaired chitin septum reparation in daughter cells.

We next quantified the impact of mutation *m2* on extrinsic and intrinsic noise using site-directed mutants that expressed both P_{TDH3}-*YFP* and P_{TDH3}-*RFP*. *m2* is a nonsense mutation in the *CHS1* gene (*G1752a* substitution) that introduces an early stop codon reducing the open reading frame by 48.4% (**Table 3**). We found that *chs1(G1752a)* allele had no clear impact on intrinsic noise (**Figure 5a**; *t*-test, adjusted $P \geqslant 0.05$ for clone 1 and $P < 0.01$ for clone 2 with decreased intrinsic noise). However, it significantly increased extrinsic noise (**Figure 5b**; *t*-test, adjusted $P < 0.01$ for clone 1 and $P < 0.001$ for clone 2) and total noise (**Figure 5c**; *t*-test, adjusted $P < 0.01$ for clone 1 and $P < 0.001$ for clone 2) relative to the reference allele. Consistent with this increase in extrinsic noise, *chs1(G1752a)* cells showed stronger correlation of YFP and RFP expression levels than wild-type cells, with a higher proportion of mutant cells showing either low or high expression of both reporters (**Figure 5 – figure supplement 1**). As expected, we also detected an increased extrinsic noise in *chs1(G1752a)* mutant cells that expressed a YFP-RFP fusion protein (**Figure 5 – figure supplement 2**).

We next investigated what mechanisms could explain the effect of *chs1(G1752a)* mutation on expression noise based on the known function of *CHS1*. *CHS1* encodes a chitin synthase specifically involved in the repair of the chitin septum after cell division in daughter cells (Cabib et al., 1989, 1992), which are the smaller cells resulting from asymmetric division in budding yeast. Detachment between mother and daughter cells involves partial degradation of the septum on the daughter side, which can sometimes damage the cell wall of daughter cells and lead to their lysis in the absence of repair. *chs1(G1752a)* allele generates an early stop codon that leads to a truncated protein lacking several residues and domains that are essential for *chs1* function (Chen et al., 2023); therefore, it is likely to be a null allele of *chs1*. Flow cytometry data showed an enrichment of cells with a smaller size for the *chs1(G1752a)* site-directed mutant relative to the reference strain (**Figure 5d**), consistent with an accumulation of daughter cells with damaged or lysed cell wall in the mutant. When splitting wild-type and *chs1(G1752a)* samples in different intervals of cell size, we observed that the median

expression level of P_{TDH3}-*YFP* did not depend on cell size (**Figure 5e**). Therefore, the increased expression noise of *chs1(G1752a)* strain is not explained by a difference of median expression level between damaged daughter cells and larger cells in this mutant. Instead, we observed a large increase of extrinsic noise mostly in the smallest cells of the *chs1(G1752a)* mutant: larger *chs1(G1752a)* cells and wild-type cells of all sizes showed much lower extrinsic noise (**Figure 5f**). This observation is consistent with an increased extrinsic noise in damaged daughter cells that accumulate in the *chs1(G1752a)* mutant.

To further show that the effect of *chs1(G1752a)* mutation on extrinsic noise was due to impaired chitin septum repair, we measured expression noise of wild-type and mutant cells grown in presence of glucosamine in the culture medium. Supplementing the culture medium with glucosamine is known to promote chitin synthesis via the activity of CHS3p (Bulik *et al.*, 2003), preventing damage to the chitin septum in daughter cells. Therefore, any consequence of *chs1(G1752a)* mutation caused by impaired chitin septum repair is expected to be suppressed in presence of glucosamine. We indeed observed that the extrinsic noise of the smallest *chs1(G1752a)* mutant cells decreased with increasing doses of glucosamine in the culture medium (**Figure 5g**). At 15 mM glucosamine, there was almost no difference of extrinsic noise and of cell size between wild-type and *chs1(G1752a)* cells. When considering all cell sizes (**Figure 5 – figure supplement 3c**), the increase of extrinsic noise in *chs1(G1752a)* cells relative to wild-type cells varied from 136% in absence of glucosamine (*t*-test, $P = 3.35 \times 10^{-7}$) to only 12% in presence of 15 mM glucosamine in the culture medium (*t*-test, $P = 5.8 \times 10^{-3}$). We also observed a gradual decrease of median cell size with increasing dose of glucosamine, a pattern that was more pronounced for wild-type cells than for *chs1(G1752a)* cells (**Figure 5 – figure supplement 3a**). This is consistent with the previous finding that yeast cells grown in presence of glucosamine retain less water, for unknown reasons (Bulik *et al.*, 2003). Importantly, the doses of glucosamine used did not significantly impact cell growth rates during the first phase of growth after glucosamine was added to the medium (**Figure 5 – figure supplement 4**). Altogether, these observations strongly suggest that *chs1(G1752a)* mutation increases extrinsic noise of P_{TDH3} activity exclusively in daughter cells with damaged chitin septum, a phenomenon that is suppressed in presence of glucosamine. The mechanism linking chitin septum repair to extrinsic noise of gene expression remains to be characterized.

Density-dependent effect of a missense mutation in *MSH1* gene on intrinsic and extrinsic noise.

Mutation *m3* is a missense mutation located in the coding sequence of the *MSH1* gene (*G1262a* substitution; **Table 3**). As mentioned above, we observed considerable variation of P_{TDH3}-*YFP* median expression and expression noise in the EMS mutant carrying mutation *m3* (YPW2143) between independent experiments. In the initial mutagenesis screen (**Figure 1a**), mutant YPW2143 showed a modest decrease of median expression (-0.9%) and a large increase of expression noise (+72.8%) relative to the reference strain. However, in a subsequent experiment (**Figure 2d**, **Figure 2 – figure supplement 1c**), the same mutant showed a substantial increase of median expression (+6.5%) and a much lower increase of expression noise (+6.3%). Since these two experiments were performed in different laboratories, the observed phenotypic variation could be caused by uncontrolled variation in experimental conditions. We hypothesized that the initial density of cell cultures – a parameter difficult to control exactly when handling a large number of samples in parallel – might influence the effect of *msh1(G1262a)* mutation on P_{TDH3}-*YFP* expression. To test this hypothesis, we initiated cell cultures from four different dilutions of a preculture and incubated these cultures for the same duration (20 hours) at 30°C before quantifying absorbance as a proxy for final cell density and expression using flow cytometry. This experimental procedure was applied to haploid strains expressing both P_{TDH3}-*YFP* and P_{TDH3}-*RFP* reporters with either the wild type allele or the *G1234a* allele of *MSH1*. We found a strong association between the initial dilution of cell cultures and the effects of *msh1(G1234a)* mutation on expression noise of either P_{TDH3}-*YFP* (**Figure 6a**) or P_{TDH3}-*RFP* (**Figure 6b**). Expression noise increased with initial cell density both for the reference strain and for the *msh1(G1262a)* mutant, but this trend was stronger for the *msh1(G1262a)* mutant, resulting in higher expression noise for the mutant relative to the reference strain at the highest initial density tested (*i.e.* 16:500 dilution). At the lowest initial cell density (*i.e.* 1:500 dilution), we observed a negligible increase of expression noise for P_{TDH3}-*YFP* (+4.2%; *t*-test, adjusted $P = 0.41$) and P_{TDH3}-*RFP* (+6.4%; *t*-test, adjusted $P = 0.035$) in the *msh1(G1262a)* mutant relative to the reference strain (**Figure 6 – figure supplement 2**). In contrast, at the highest initial cell density (*i.e.* 16:500 dilution), expression noise was increased by 45.7% for P_{TDH3}-*YFP* (*t*-test, adjusted $P = 3.0 \times 10^{-4}$) and by 34% for P_{TDH3}-*RFP* (*t*-test, adjusted $P = 9.9 \times 10^{-4}$) in *msh1(G1262a)* mutant cells (**Figure 6 – figure supplement 2**). We also observed a complex relationship between initial cell density and median expression of P_{TDH3}-*YFP* and P_{TDH3}-*RFP* (**figure 6 – figure supplement 2**): median expression remained constant among the different initial densities tested for the reference strain; however, for *msh1(G1262a)* mutant cells, median expression changed significantly depending on initial cell density and this variation was not the same for P_{TDH3}-*YFP* and P_{TDH3}-*RFP* median expression. The fact that initial cell density altered the effect of *msh1* mutation on

expression noise and median expression can explain the variability we previously observed between independent experiments. However, variation of initial cell density is not necessarily the direct cause of expression variation. A more direct cause could be a variation of final cell densities after growth of cultures initiated at different cell densities. This seems unlikely, though, as we observed significant differences of intrinsic (*t*-test, adjusted $P = 1.98 \times 10^{-3}$) and extrinsic (*t*-test, adjusted $P = 4.42 \times 10^{-2}$) noise for *msh1* mutant cells diluted at 2:500 and at 4:500 (**Figure 6 – figure supplement 2**) despite no significant difference of final cell densities (**Figure 6 – figure supplement 2b**; *t*-test, adjusted $P = 0.24$). Cultures initiated at different cell densities are expected to reach different phases of growth after 20 h of incubation at 30°C, which could explain why we observed density-dependent effects of *msh1(G1262a)* mutation on median expression and expression noise.

We found that *msh1(G1262a)* mutation impacted both extrinsic and intrinsic noise (**Figure 6c**), but only at the highest initial cell density tested (*i.e.* 16:500 pre-culture dilution) and the effect on intrinsic noise was greater that the effect on extrinsic noise (**Figure 6 – figure supplement 2**). No significant difference of intrinsic noise (*t*-test, adjusted $P = 0.69$) and extrinsic noise (*t*-test, adjusted $P = 0.16$) was observed between *msh1(G1262a)* mutant cells and wild-type cells for a 1:500 pre-culture dilution, while a 244% increased intrinsic noise (*t*-test, adjusted $P = 2.8 \times 10^{-3}$) and a 41% increased extrinsic noise (*t*-test, adjusted $P = 0.058$) was observed in mutant relative to wild-type cells for a 16:500 pre-culture dilution. The effect of *msh1* mutation on intrinsic noise is visible at the single cell level via the lower correlation observed between YFP and RFP expression levels of mutant cells relative to wild-type cells (**Figure 6 – figure supplement 1**).

MSH1 encodes a DNA-binding protein of the mitochondria involved in the repair of mitochondrial DNA. Disruption of this gene is known to cause a high frequency of respiratory-deficient cells (*ρ*- petite cells), which may generate cell-to-cell heterogeneity and could provide a simple explanation for the increased expression noise observed in the *msh1(G1262a)* mutant. We compared the frequencies of *ρ*- cells in wild-type and *msh1(G1262a)* mutant strains after growth in a rich medium (YPD) containing a fermentable carbon source (see Methods) and using two different pre-culture dilutions (1:500 and 8:500). Both *ρ*+ and *ρ*- cells can grow in this medium. As expected, we observed a much lower frequency of *ρ*- cells in the wild-type strain (1.3% and 0.3% *ρ*- cells for pre-culture dilutions of 1:500 and 8:500; **Figure 6d**) than in the *msh1(G1262a)* mutant strain (94.5% and 88.6% *ρ*- cells for pre-culture dilutions of 1:500 and 8:500; **Figure 6d**). We isolated a *ρ*- colony from the *msh1(G1262a)* mutant strain and noticed, as expected, that it produced 100% of *ρ*- cells after growth in YPD medium. We reasoned that if the impact of *msh1(G1262a)* mutation on expression

noise was explained by the co-existence of *ρ*+ and *ρ*- cells in the mutant strain, then expression noise should be reduced in the *msh1(G1262a)* strain with 100% of *ρ*- cells, and its noise should no longer depend on initial cell density. However, fixing the frequency of *ρ*- cells to 100% did not reduce the effect of *msh1(G1262a)* mutation on intrinsic and extrinsic noise (**Figure 6d**; **Figure 6 - figure supplement 3**). In addition, the expression noise of *msh1(G1262a)* strain was higher in cultures initiated at high cell densities than in cultures initiated at low cell density regardless of the frequency of *ρ*- cells in the population (**Figure 6d**; **Figure 6 - figure supplement 3**). These observations indicate that the effect of *msh1(G1262a)* mutation on expression noise is not directly explained by cell-to-cell heterogeneity in respiratory capacity caused by the mutation.

DISCUSSION

In this study, we used random mutagenesis followed by genetic mapping to identify three *trans*-acting mutations that increased cell-to-cell variability of expression of a yeast reporter gene. This unbiased approach made it possible to discover any mutation that could possibly alter the expression noise of the focal gene. Indeed, all three mutations identified here were located in the coding sequence of genes that were not known regulators of *TDH3* promoter activity and were therefore not expected to regulate P_{TDH3}-*YFP* expression noise. Importantly, these three mutations had very little impact on the median expression of P_{TDH3}-*YFP*. Their action on expression noise can therefore not be explained by the well-known scaling of expression noise with expression mean (Newman et al., 2006). The three mutations targeted proteins with different biochemical functions involved in different – but not necessarily unrelated – cellular processes. *chs1(G1752a)* non-sense mutation increased extrinsic noise exclusively in the smallest cells of yeast populations, which was likely caused by damaged cell walls of daughter cells improperly repaired in the absence of chitin synthase I activity. The second mutation targeted the inner mitochondrial membrane protein Yme2 and increased intrinsic noise of P_{TDH3} expression. The third mutation, targeting the Msh1 ATPase involved in mitochondrial DNA repair, also increased P_{TDH3} intrinsic noise and this effect varied with the growth phase of cells. Intriguingly, although *yme2(G1234a)* and *msh1(G1262a)* mutations impacted genes with distinct functions, both genes are important for the maintenance of mitochondrial genome integrity, leaving open the possibility that these mutations modulate intrinsic expression noise via a common mechanism. After describing the potential limits of our screen-based approach, we discuss this possibility, as well as the main implications of these results, below.

We decided to identify genetic modulators of expression noise by performing a random mutagenesis screen rather than testing candidate genes because it allowed the discovery of unknown mechanisms without ascertainment biases. Although EMS mutagenesis mostly induces G:C to A:T substitutions, which could slightly bias the screen towards GC-rich genes and coding sequences (relative to regulatory sequences), we do not expect this potential bias to significantly impact our conclusions. Indeed, *YME2*, *CHS1* and *MSH1* coding sequences are not particularly enriched in G or C nucleotides (GC content is 39.7%, 36.8% and 37.0% in these three genes relative to 39.6% among all ORFs) and, in the yeast genome, GC content is not much lower in intergenic sequences (34.4%) than in ORFs (39.6%). We note that bulk-segregant analysis (BSA-seq), which is generally very powerful to map causal mutations in yeast (Duveau et al., 2014; Ehrenreich et al., 2010; Magwene et al., 2011), was only successful here for two of the five mutants that we analyzed (we identified the third causal mutation by another approach based on tetrads). Several possibilities may explain the limited power of BSA-seq in the present study. First, the statistical power to map a variant impacting expression noise is expected to be lower than to the power to map a variant impacting mean expression (Sarkar et al., 2019). Second, based on previous simulations (Duveau et al., 2014), our procedure included three cycles of growth and FACS selection. This is predicted to increase detection power, but only for mutations that do not impair fitness during the growth phase of each cycle. It is therefore possible that some mutations causing elevated expression noise escaped BSA-seq detection because they also impacted growth. Another possibility is that the effect of these mutations may be particularly sensitivite to microenvironmental conditions, which could have differed between the characterization of the mutants and the conditions of BSA-seq selection. In the present mapping study where the genetic diversity between the two parental strains was low, tetrad analysis proved to be more powerful than BSA-seq to map mutations altering gene expression noise.

Few studies previously characterized *trans*-acting genetic variants impacting expression noise. Besides pioneering work showing the effect of chromatin remodelers on noise using gene deletions (Raser & O'Shea, 2004), expression-noise modulators were also identified as natural polymorphisms in genes involved in cell-sensing and responses to environmental variation. The first examples discovered were the *MUP1* and *ERC1* genes, which regulate the import of extracellular methionine in yeast cells, and where natural polymorphisms affected noise in expression of the methionine-sensitive reporter P_{MET17}-*GFP* (Fehrmann et al., 2013). Another example was later identified in humans, where a disease-associated variant in the *PDE4D* phosphodiesterase - controlling cAMP signalling - was associated with noise in expression of the HLA-DR receptor at the surface of CD8+ T cells and of the CD38

receptor at the surface of CD4+CD45RA+ naive T cells (Lu et al., 2016). Therefore, we could have expected our screen to reveal mutations perturbing cell sensing, but this was not the case. Our screen also did not reveal mutations in transcription factors known to regulate *TDH3* promoter activity, or in the TATA box binding protein (TBP), which were obvious candidates because mutations in transcription factor binding sites and in the TATA box of the *TDH3* promoter are known to sometimes alter expression noise independently from mean expression (Duveau et al., 2018; Hornung et al., 2012; Loell et al., 2022; Metzger et al., 2015). We note that the number of mutations we mapped (3) is small in comparison to the size of the mutational target represented by these genes in the genome (~0.05% of the genome) and it is possible that a larger screen could have revealed such genes. It is also possible that most mutations altering these candidate genes are lethal – TBP and many transcription factors are essential proteins – and thus could not be recovered from our mutagenesis screen. Conversely, it is not necessarily surprising that the classes of genes we identified here have not been previously associated with *trans*-modulation of gene expression noise. Indeed, previous reports focused on natural variants which, unlike the artificial random mutations studied here, had been exposed to the filter of natural selection. The mutations we identified here would probably be counter-selected in nature since they cause dysfunctions in cell wall repair and mitochondrial genome integrity. The classes of genes we identified as *trans*-acting noise modulators therefore illustrate the complementarity between the analysis of natural variants and the analysis of laboratory mutations.

In a previous study, we screened the same collection of EMS mutants to identify 69 *trans*-acting mutations that changed the median expression of P_{TDH3}-*YFP* (Duveau et al., 2021). These mutations were located in genes with different functions (iron metabolism, purine synthesis, transcription) from the three genes we identified here, indicating that different cellular processes are involved in the regulation of median expression level and expression noise. However, all of these mutations (those impacting noise and those impacting median expression) were non-synonymous coding mutations outside annotated regulatory sequences. Therefore, when not exposed to natural selection, random mutations in coding sequences are more likely to alter gene expression (either median level or noise) of another gene in *trans* than mutations in regulatory sequences. To draw more general conclusions about the genetic modulation of expression noise variation, more mutations will need to be identified, in different systems, cell types and organisms, and for the regulation of multiple genes.

The identity of two of the three mutations we identified (*yme2(G1234a)* and *msh1(G1262a)*) suggests that the integrity of the mitochondrial genome is needed to limit expression noise of the P_{TDH3} nuclear gene promoter. Previous studies linked mitochondrial variability among clonal yeast or human

cells to the variability of various cellular traits, including proliferation and transcription rates (Dhar et al., 2019; Guantes et al., 2015; Neves et al., 2010). In these past studies, cell-to-cell variability in mitochondrial content or activity acted as an extrinsic source of expression noise: cells inherited different numbers of mitochondria after division, causing correlated variation in the expression of many genes among cells (Johnston et al., 2012). The situation we observe here is different: the *yme2* and *msh1* mutations increased the variability of expression of two reporter genes of P_{TDH3} activity within the same cell (intrinsic noise), but not their co-variation among cells (extrinsic noise). This is a very surprising observation because it cannot be explained by the classic extrinsic model, where the mutation would generate variable mitochondrial defects among cells that would in turn cause differences of gene expression among these cells. Instead, our results suggest a more complex model: the mutation amplifies stochastic variability within cells without necessarily generating diverse mitochondrial states among cells. In this model of increased intrinsic noise, the same mitochondrial defect in different cells can lead to different expression levels. How may this happen? It is known that intrinsic noise can be altered by changing the frequency and magnitude of transcriptional or translational bursts. A factor decreasing burst frequency while increasing burst size could increase intrinsic noise without altering mean expression (Pedraza & Paulsson, 2008; Tan & van Oudenaarden, 2010; Zenklusen et al., 2008), as we observed in *yme2(G1234a)* and *msh1(G1262a)* mutants. Thus, we can hypothesize that a signal is activated in response to mitochondrial defects and transmitted to the molecular complexes involved in transcription or translation. A promising candidate for such a signal would be the retrograde response. This pathway is activated in response to mitochondria dysfunction and enables cells to compensate for the lack of mitochondrial activity via the regulation of nuclear genes (Butow & Avadhani, 2004; Z. Liu & Butow, 2006). The retrograde response was best characterized in yeast and was also described in other eukaryotes, including human cells, which revealed that its mechanisms and functions are partially conserved across species (Jazwinski & Kriete, 2012). We hypothesize that *yme2(G1234a)* and *msh1(G1262a)* mutations may both activate the retrograde response by causing mitochondrial defects, which could then lead to alteration of transcriptional bursting at the *TDH3* promoter, generating intrinsic noise. The known binding site (GGTCAC) of the retrograde transcription factor (Rtg1-Rtg3 heterodimer; Jia et al., 1997; X. Liao & Butow, 1993) is absent in the *TDH3* promoter, suggesting it is not a direct target of the pathway. However, previous findings suggest that the expression level of *CIT2* – the best-characterized target gene of the retrograde pathway (X. S. Liao et al., 1991) – may impact *TDH3* promoter activity, thereby an indirect effect of the retrograde response is possible. Indeed, we previously showed that mutations in

the Cyc8-Tup1 complex, a direct regulator of *CIT2* transcription (Conlan et al., 1999), altered *TDH3* promoter activity (Duveau et al., 2021). Further work is necessary to determine whether activation of the retrograde response can indeed increase intrinsic noise of the *TDH3* promoter, and whether *yme2(G1234a)* and *msh1(G1262a)* mutations act via this mechanism. If this is the case, it will then become interesting to investigate whether mitochondrial retrograde signaling has a similar effect on expression noise of other genes and in other species.

What can be the consequences of an increase in expression noise? Previous studies showed that varying the expression noise of *TDH3* or other genes could have a small but detectable impact on fitness (Duveau et al., 2018), highlighting how genetic modifiers of noise could be subjected to natural selection. The mutations we identified here compromise the integrity of important cellular functions (mitochondria and cell wall) and this direct effect is likely their major - negative - impact on fitness. The fact that they also modulate noise in gene expression could also cause marginal fitness changes, especially if this modulation is not restricted to the expression of *TDH3* but affects expression noise of other genes involved in other biological processes.

In conclusion, the present study provides examples of *trans*-acting mutations affecting gene expression noise, revealing an unexpected link between mitochondrial defects and intrinsic variability in expression of a nuclear gene. In the future, identifying more *trans*-acting mutations, and quantifying their pleiotropic effects on expression noise at the transcriptomic scale and on fitness (as done in Vande Zande et al., (2022) for mutations impacting median expression levels) will be essential to understand how random mutations contribute to natural variation of expression noise.

MATERIALS AND METHODS

Biological resources

All yeast strains, oligonucleotides and plasmids used in this study are listed in Supplementary File 1. A genealogy of yeast strains with a brief summary of their genotypes can be found in Supplementary File 2. Laboratory stocks were traced using MyLabStocks web application (Chuffart & Yvert, (2014); https://gitbio.ens-lyon.fr/LBMC/yvertlab/mylabstocks).

Reference strain & EMS mutants

The collection of 1241 mutant strains obtained by ethyl methanesulfonate (EMS) mutagenesis of the reference strain YPW1139 was described in Metzger et al. (2016) and Duveau et al. (2021). YPW1139 was itself obtained from YPW978, a *MATα* haploid strain with S288c genetic background carrying alleles of *RME1* and *TAO3* from SK1 strain that conferred increased sporulation efficiency (Deutschbauer & Davis, 2005) and alleles of *SAL1*, *CAT5* and *MIP1* from RM11 strain that conferred decreased frequency of respiratory deficient (petites) cells (Dimitrov et al., 2009). YPW1139 was obtained by introducing at the *ho* locus a reporter gene that contained the *TDH3* promoter upstream of the *Venus YFP* coding sequence and the *CYC1* terminator along with a *KanMX4* drug resistance gene. As shown in Supplementary Files 1 & 2, all strains constructed in this study were derived from YPW1139.

Strain constructions

We describe below different procedures that were applied to generate yeast strains used in this study. For each genotype, we systematically constructed and used in experiments two strains that originated from two independent colonies obtained after the same transformation. Comparing phenotypes of these independent transformants allowed us to distinguish true effects of a targeted genetic change from undesired effects of potential spontaneous secondary mutations.

Reference strains with two fluorescent reporters

To be able to distinguish intrinsic and extrinsic sources of expression noise, we constructed strains GY2458 and GY2459 by inserting a P_{TDH3}-*RFP*-T_{CYC1} construct at *ho* locus in the genome of strain YPW1139. The resulting genotype is *ho::*P_{TDH3}-*YFP*-T_{CYC1}-*KanMX4*-T_{CYC1}-*RFP*-P_{TDH3} with the two reporter genes in opposite orientation. We used the *mCherry* variant of *RFP*. The genomic insertion was done using a CRISPR/Cas9 approach adapted to yeast (Laughery et al., 2015). First, we used overlap extension PCR to generate a P_{TDH3}-*RFP* fragment with homologies to the insertion site at 5' and 3' ends. P_{TDH3} was amplified by PCR from genomic DNA of strain YPW1139 using oligonucleotides 1Q65 and 1S07. *RFP*-T_{CYC1} was amplified by PCR from genomic DNA of strain GY2433 using oligonucleotides 1S04 and 1S05. Equimolar amounts of both amplicons were fused by overlap extension PCR, and 70 bp of homology to the insertion site was added by a final PCR with oligonucleotides 1S06 and 1S08. In parallel, we generated plasmid pGY639 by cloning hybridized oligonucleotides 1R98 and 1R99 between BclI and SwaI restriction sites of plasmid pML104 (encoding guide RNA and Cas9). The repair fragment and pGY639 were transformed in YPW1139 using a classic LiAc/polyethylene glycol and heatshock protocol (Gietz & Schiestl, 2007). Transformants were

selected on SD -Ura agar plate (synthetic defined medium lacking uracil). Successful transformation was verified by PCR and sequencing of the insert. Two positive transformants were transferred to a YPG plate to counter select petite cells and then transferred to a SD + 5-FOA plate (0.9 g/L 5-Fluoroorotic acid) to counter select cells carrying the pGY639 plasmid. The two strains were stored at -70°C in 15% glycerol.

Single-site mutants

Point mutations identified via genetic mapping were inserted individually in the genome of strain GY2458. *yme2(G1234a)*, *chs1(G1752a)*, *ald4(C-344t)*, *nop19(C-575t)* and *rsn1(G86a)* mutations were inserted using a similar CRISPR/Cas9 approach as described above and in Duveau *et al.* (2021). For each mutation, a specific recognition site of the guide RNA was cloned in plasmid pML104 corresponding to a sequence adjacent to a PAM motif and near the mutation site in the genome. The repair fragment was obtained by hybridization of two complementary 90-bases oligonucleotides containing the target mutation and flanking genomic sequences (Supplementary File 1). *msh1(G1262a)* mutation was obtained using the *delitto perfetto* approach (Stuckey et al., 2011), because a suitable recognition site for the guide RNA could not be found near the mutation site. First, we inserted a cassette containing *Ura3* and *hphMX4* selection markers (amplified by PCR from plasmid pCORE-UH) at the mutation site in *msh1*. Transformants were selected consecutively on SD medium lacking uracil and on YPD medium complemented with 300 mg/L of hygromycin B (Sigma-Aldrich H3274-1G). Correct insertion of the *Ura3-hphMX4* cassette without mutation was verified by PCR and Sanger sequencing. Second, the *Ura3-hphMX4* cassette inserted at *msh1* locus was replaced by a repair fragment that contained *msh1(G1262a)* mutation. This time transformants were selected on SD medium complemented with 0.9 mg/L of 5-FOA. Correct insertion of the mutation was validated by Sanger sequencing. However, resulting strains were unable to grow on a non-fermentable carbone source (petites), a phenotype frequently observed in *msh1* mutant. We restored respiratory efficiency by crossing these strains with YPW1240 (*MAT***a** strain with same genetic background as YPW1139) and by selecting *MATα*; *msh1(G1262a)*; *ho::*P_{TDH3}*-YFP-*T_{CYC1}*-KanMX4-*T_{CYC1}*-RFP-*P_{TDH3} segregating cells after meiosis of the diploid. For each single-site mutant, two independent clones were stored at -80C in 15% glycerol.

YFP-RFP gene fusion

We edited the genome of strains YPW1139 (*MATα*) and YPW1240 (*MAT***a**) using CRISPR/Cas9 to fuse the *RFP* coding sequence at the 3' end of the *YFP* coding sequence with addition of a 30-bp linker sequence between the two reporters. The repair fragment was obtained by PCR amplification of *RFP*

from GY2433 genomic DNA using oligonucleotides 1U75 and 1U76. CRISPR plasmid pGY666 was obtained by cloning hybridized oligonucleotides 1U79 and 1U80 in pML104. Correct insertion was verified by PCR and Sanger sequencing. We then inserted separately mutations *yme2(G1234a)* and *chs1(G1752a)* in the genome of the *MATα* strain that expressed the YFP-RFP fusion protein. The *yme2(G1234a)* single-site mutant was crossed to the *MAT***a** strain with *YFP-RFP* gene fusion. We then performed tetrad dissection after meiosis of the resulting diploid, and selected segregant clones with *MATα; yme2(G1234a)*; *ho::*P_{TDH3}*-YFP-RFP* genotype. *chs1(G1752a)* mutation was introduced using the CRISPR/Cas9 approach described above.

YFP-RFP *gene fusion with uTEV cleaving site*

We also constructed strains with a P_{TDH3}*-YFP-RFP* gene fusion at *ho* where coding sequences of YFP and RFP were separated by a short sequence encoding a cleavage site (ENLYFQS polypeptide) for the tobacco etch virus protease uTEV (Kapust et al., 2001). Using CRISPR/Cas9, we first inserted the uTEV cleavage site between YFP and RFP coding sequences in the genome of strains described above carrying a *YFP-RFP* gene fusion and with or without *yme2(G1234a)* mutation. CRISPR plasmid pGY682 was obtained by cloning hybridized oligonucleotides 1W21 and 1W22 in pML104. The repair fragment containing uTEV cleavage site and homology to 3' end of *YFP* and 5' end of *RFP* coding sequences was obtained by PCR amplification of oligonucleotides 1W23 and 1W24. Correct insertion was verified by PCR and Sanger sequencing. Second, we inserted a P_{TDH3}*-uTEV* construct at *LYS2* locus in these strains using CRISPR/Cas9 gene editing. The CRISPR plasmid targeting a guide RNA at *LYS2* was obtained by cloning hybridized oligonucleotides and in pML104. The repair fragment was obtained by overlap extension PCR. P_{TDH3} was amplified by PCR from genomic DNA of strain YPW1139 using oligonucleotides 1R33 and 1W26. *uTEV* coding sequence was amplified from plasmid pRK792 (obtained from Addgene) using oligonucleotides 1W27 and 1W28. Equimolar amounts of both amplicons were fused by overlap extension PCR, and 70 bp of homology to the insertion site was added by a final PCR with oligonucleotides 1W29 and 1W30. Transformants were selected as described above for reference strains. Correct insertion was verified by PCR and Sanger sequencing using oligonucleotides 1W31, 1W32 and 1W33.

Sequencing genomes of EMS mutants

The genome of the parental strain YPW1139 was sequenced in a previous study (Duveau et al., 2021). Here, we sequenced the genomes of EMS mutant strains YPW2088, YPW2162, YPW2143,

YPW2210 and YPW2153 to identify all point mutations that were present in each strain. After growth of each strain in 5 mL of YPD medium for 16 hours at 30°C, genomic DNA was extracted from ~2 x 10^8 cells per strain using a Wizard genomic DNA purification kit (Promega). Illumina sequencing libraries were then prepared using a DNA Library Prep kit from ActiveMotif. Samples were sequenced on a MiSeq instrument by ProfileXpert, using a MiSeq standard V2 2 x 250 bp sequencing kit. The sequencing depth was ~40x per genome (15 M paired-end reads). Sequencing data were analyzed with a Nextflow pipeline. Sequences corresponding to P5 and P7 Illumina adapters were removed using *cutadapt*, then trimmed reads were aligned to S288c reference genome using*bowtie2*. Variant calling was performed using *freebayes*, and false positive calls were filtered out based on mapping quality MQ. We also removed variants shared by strain YPW1139 and mutant strains, as well as mutations found in at least four mutant strains.

Mapping mutations altering expression noise

BSA-seq approach

We previously used a BSA-seq approach to identify mutations associated with variation of P_{TDH3}-*YFP* median expression (Duveau et al., 2021). Here, we adapted this approach for mapping mutations associated with variation of P_{TDH3}-*YFP* expression noise. First, each haploid mutant strain (resistant to G418) was crossed to the mapping strain YPW1240 (resistant to Nourseothricin) on YPG agar plates. Hybrids were selected after replication on YPD agar complemented with 60 mg/L of Nourseothricin and 200 mg/L of G418. Then,meiosis was induced by incubation for 5 days on YPA agar plates (10 g/L Bactopeptone, 10 g/L Bacto Yeast extract, 2% Kac). Random spores were isolated after incubation in 0.3 µg/L zymolyase 100T for 1 hour at 30°C as previously described (Duveau et al., 2021). Briefly, spores and vegetative cells were pelleted by centrifugation in a microcentrifuge tube, resuspend in 100 µL H_2O and then vigorously vortexed for 2 minutes. At this stage, spores adhered to tube walls, allowing elimination of vegetative cells and undigested tetrad via several washes with 1 mL of sterile water. Spores were then resuspended in 0.02% Triton-X using brief sonication. Next, 10^6 spores that did not express RFP (*MATα*) were sorted for each sample by FACS (BD FACS Aria II) at the University of Michigan Flow Cytometry Core. RFP fluorescence was quantified using a 561 nm laser for excitation and a 582/15 nm optical filter for emission. Sorted cells were cultivated in 1 mL of YPD for 24 hours at 30°C. We next sorted each sample into three bulks of 10^5 cells based on cell fluorescence levels using FACS. YFP fluorescence was quantified using a 488 nm laser for excitation

and a 530/30 nm optical filter for emission. The low fluorescence bulk corresponded to cells sorted among the 2% cells in the population with the lowest YFP fluorescence. The high fluorescence bulk corresponded to cells sorted among the 2% cells in the population with the highest YFP fluorescence. The mid fluorescence bulk corresponded to cells sorted among the 10% cells in the population with a fluorescence closest to the median YFP fluorescence. When establishing gates for cell sorting, we were particularly careful to keep the median cell size (area of forward scatter) as similar as possible among the three bulks. Sorted cells were then cultivated for 24 hours in 1.5 ml of YPD. Next, we proceeded with a second round of cell sorting based on YFP fluorescence. 10^5 cells were sorted by FACS for each fluorescence bulk. For each fluorescent bulk, we only sorted cells with YFP levels from the same portion of the population as in the previous round of FACS. After growth for 24 hours in 1.5 ml of YPD, a third round of cell sorting and growth was performed using the same procedure. Next, genomic DNA was extracted from each sample using a Gentra Puregene yeast/Bact kit (Qiagen). DNA libraries were prepared from 1 ng of genomic DNA using a Nextera XT DNA Library Prep kit (Illumina). Deep sequencing of DNA libraries was performed on a HiSeq 4000 instrument (Illumina) at the University of Michigan Sequencing Core Facility, using a 2 x 150 bp sequencing kit. Demultiplexing of sequencing reads were performed using *bcl2fastq2* v2.17. Sequencing data were next analyzed using a Nextflow pipeline on clusters of the PSMN at ENS de Lyon. The first steps of the pipeline were the same as described above for the sequencing of EMS mutants. Variant calling was performed using *freebayes*, which provided the number of reads supporting each allele at each variant site. We then used custom *R* scripts to only retain variants that were identified in the genome of the corresponding EMS mutant for each sample. Finally, likelihood ratio tests (*G*-tests) were used to determine for each variant site whether the proportion of wild-type and mutant alleles was statistically different in the mid fluorescence bulk and in the combined low and high fluorescence bulks. We reasoned that a mutation associated with an increased expression noise should be found at a lower frequency in the mid bulk than in combined data from low and high bulks. We expected to observe the opposite pattern for a mutation associated with a decreased expression noise, and no significant difference among bulks for a mutation without effect on expression noise and not linked to a causative mutation.

Tetrad analysis approach

Mutation *msh1(G1262a)* was the best candidate to explain the increased expression noise of mutant YPW2143 after using BSA-seq, but no significant association could be established due to unexpected allele frequencies in one of the three segregant bulks. To statistically test the association between

expression noise and *msh1* genotype, we used linkage analysis based on tetrad dissection. First, we induced meiosis in the diploid strain YPW2318 (obtained by crossing YPW2143 mutant with YPW1240 mapping strain) by incubation for 5 days in YPA medium (10 g/L Bactopeptone, 10 g/L Bacto Yeast extract, 2% KAc). After sporulation, tetrads were digested in 0.5 mg/mL zymolyase 20T (Seikagaku) and 1M sorbitol for 10 minutes at 30°C. 32 tetrads were dissected with a platinum needle mounted on a inverted microscope, resulting in the isolation of the 4 spores from each tetrad on YPD agar plates with 1M sorbitol. After 48 h of incubation at 30°C, colonies were replicated with sterile velvets on selective media to determine how three markers segregated among the 4 spores in each tetrad: *NatMX4* was selected on Nourseothricin (60 mg/L), *KanMX4* was selected on G418 (200 mg/L) and *HphMX* was selected on Hygromycin B (200 mg/L). In addition, the segregation of a red fluorescent reporter inserted at the *MAT* locus (*mata2::yEmRFP-HphMX)* was characterized using a fluorescence stereomicroscope (Nikon SMZ800N). 22 tetrads showed a 2:2 segregation of all markers with a co-segregation of red fluorescence and Hygromycin B resistance, as expected. We then quantified P_{TDH3}-*YFP* median expression and expression noise for the 88 segregants from these 22 tetrads using flow cytometry as described below. In parallel, we used Sanger sequencing of PCR amplicons obtain with oligonucleotides 1T05 and 1T06 to determine the genotype at *MSH1* locus in the 88 segregants. Statistical association between *MSH1*genotype and expression noise was determined using a linear model with expression noise treated as a continuous response variable and genotypes at *MSH1*, *MAT* and *NatMX4* treated as categorical explanatory variables.

Quantification of median expression and expression noise using flow cytometry

Measurements of median expression and expression noise of the P_{TDH3}-*YFP* reporter gene in the 1241 EMS mutants and control strains YPW1139 and YPW978 were performed at the University of Michigan as previously described (Duveau et al., 2021; Metzger et al., 2016), using a BD Accuri C6 flow cytometer (BD Biosciences). Subsequent experiments to measure P_{TDH3}-*YFP* expression in single-site mutants were performed at ENS Lyon following a similar procedure to prepare samples, but using a MACS Quant VYB flow cytometer (Miltenyi Biotec). For each experiment, yeast strains were revived from -80°C glycerol stocks on YPG plates (20 g/L yeast extract, 10 g/L peptone, 5% glycerol v/v and 20 g/L agar) at least 3 days and no more than 2 weeks before starting the experiment. After 2 days of incubation at 30°C, YPG plates were kept at room temperature. Then, a small amount of cells (~10^5 cells) was inoculated in each well of a 96-deep well plate containing 0.5 mL of filter-sterilized YPD medium (20 g/L yeast extract, 10 g/L peptone, 20 g/L dextrose from Fisher bioreagents) and one 3-mm glass bead per well according to a randomized plate design. We observed that changing the

brand of reagents used to make YPD medium could lead to inconsistent measures of expression noise. Culture plates were incubated for 24 h at 30°C with 250 rpm orbital shaking. Cells were maintained in suspension both because of the shaking and the presence of a single glass bead in each well. After this first phase of growth, 2 µL of culture from each well (~ 2 x 10^5 cells) were transferred to another plate containing 0.5 mL of fresh YPD per well and a second growth phase was carried on by incubating new plates at 30°C for 18 h with 250 rpm orbital shaking. For the experiment where the second culture was initiated at different cell densities (Figure 6), we transferred 1, 2, 4 or 16 µL of culture in different wells and we estimated cell density after growth by measuring the optical density at 660 nm of 0.2 mL of each culture using a Sunrise (Tecan) plate reader. Then, for all experiments, 200 µL from each sample were transferred to 96-well plates with 1.2 µm filters (Millipore MSBVS1210). Culture medium was aspirated with vacuum, then cells were washed twice in 200 µL of phosphate-buffer saline (PBS) before fixation in 200 µL of 2% paraformaldehyde (PFA) for 8 minutes. After aspiration, cells were resuspended in 200 µl of PBS containing 0.1 M Glycine for 12 minutes, and washed twice in 200 µL of PBS. A final 1/20 dilution was applied by transferring 5 µL of each sample into 195 µL of PBS in a flat bottom 96-well plate (Falcon). Plates were stored up to 24 hours at 4°C prior to flow cytometry acquisition.

Forward scatter and fluorescence were recorded for 10,000 events per sample with the MACS Quant VYB. A 488-nm laser was used for excitation and a 525/50 optical filter was used for acquisition of YFP signal, while a 561-nm laser was used for excitation and a 615/20 optical filter was used for acquisition of RFP signal. Flow cytometry data were analyzed using custom R scripts (Supplementary File 3) with a similar approach as in Duveau et al. (2018), except for certain points mentioned below. First, we filtered out artifactual events and doublets (events corresponding to multiple cells) based on values of the area and height of forward scatter (FSC.A and FSC.H) as previously described. Then, we excluded cells that were clear outliers in each fluorescence channel using flowClust package. Raw fluorescence values of cells are strongly correlated with forward scatter (a proxy for cell size). We therefore computed normalized fluorescence values that were independent from cell size, as previously described (Duveau et al., 2018). For each sample, we then computed the median cell size among cells, as well as the median fluorescence and the coefficient of variation (CV) of fluorescence for each fluorescence channel (YFP and RFP) as measures of expression noise. Extrinsic and intrinsic noise were calculated using formula from Fu and Pachter (2016). First, we applied quantile normalization to YFP and RFP fluorescence values of cells (after cell size normalization) using *normalize.quantiles* function from R package *preprocessCore*. Then, intrinsic noise was calculated as:

$$intrinsic = \frac{\frac{1}{n}\left(\sum_{i=1}^{n}\left(\left(RFP_i - YFP_i\right)^2\right)\right)}{2 \cdot \overline{RFP} \cdot \overline{YFP}},$$

and extrinsic noise was calculated as:

$$extrinsic = \frac{\frac{1}{n}\left(\sum_{i=1}^{n}\left(RFP_i \cdot YFP_i\right)\right) - 2 \cdot \overline{RFP} \cdot \overline{YFP}}{2 \cdot \overline{RFP} \cdot \overline{YFP}},$$

where n is the number of cells in a sample, RFP_i and YFP_i are quantile-normalized fluorescence levels of each cell and $\overline{RFP}$ and $\overline{YFP}$ are means of quantile-normalized fluorescence levels among cells. For each sample, median cell size, median fluorescence, CV of fluorescence, intrinsic noise and extrinsic noise were also calculated for five subsets of cells defined based on five quantiles (quintiles) of FSC.A values (area of forward scatter). Statistical comparisons between genotypes or conditions were performed via pairwise *t*-tests using data from replicate samples (samples sharing the same genotype and condition). Benjamini-Hochberg procedure (FDR) was used to adjust *P* values for multiple testing.

Western blot

The protease from tobacco etch virus (TEV) cleaves the specific site ENLYFQS in proteins (Kapust et al., 2001; Parks et al., 1994), resulting into two residues when the target sequence is inserted in a protein sequence. A western blot on whole-cell protein extract was performed to determine how complete was the cleavage of YFP-ENLYFQS-RFP fusion protein by the classic TEV and improved uTEV protease both in wild-type and *yme2(G1234a)* cells. Control genotypes that expressed either no RFP, RFP alone or YFP-RFP fusion protein were also included (seven strains in total). YFP-RFP and RFP are detected using a primary antibody targeted against mCherry and distinguished based on band sizes after electrophoresis. GAPDH constitutive control were detected with anti-GAPDH antibody for all proteins extract.

Yeast strains were thawed from glycerol stocks kept at –80°C onto YPG agar plates 3 days before experiment. After 2 days of incubation at 30°C, YPG plates were placed at room temperature. The day before the experiment, a small amount of cells (~10^5 cells) was inoculated in 4 mL of YPD medium and incubated overnight at 30°C with 250 rpm orbital shaking. 1 mL of cell culture was then transferred to 50 mL of YPD medium and incubated for another 4 hr at 30°C to reach the exponential phase of growth. All cells were pelleted by centrifugation and resuspended in 1 mL of sterile water.

After another centrifugation at 10,000 g for 1 minute, cell pellets were resuspended on ice in 300 µL of fresh lysis buffer (0,1 % w/v sodium deoxycholate, 1 mM EDTA pH8, 50 mM HEPES-KOH pH 7.5, 140 mM NaCl, 1 % w/v Triton W-100 and proteinase inhibitors (Sigma P8215). Reagents were mixed by pipetting up and down. To disrupt cell walls and membranes, we added 500 µL of cold acid-washed glass beads (Sigma G8772) and the tubes were placed on a PreCellys apparatus. Tubes were shaken at 6,800 rpm through 2 cycles, each cycle consisting of 10 s ON, 10 s OFF, 10 s ON. Tubes were placed for 5 min on ice between the two cycles. Lysates were collected in a microtube and stored at -80°C. Protein concentration was measured using the Bio-Rad Protein Assay (#500-0006) from optical density at 595 nm (Bradford) based on linear regression curve made with standards. The samples were diluted in lysis buffer to load 50 µg of proteins and denatured 5 min at 95°C.

Proteins were separated on a 12 % SDS-PAGE gel electrophoresis at 100 V for 2 hours and then transferred to nitrocellulose membrane at 0,2 µM by semi-dry transfer. The membrane was blocked 1 hour at room temperature with 5 % non-fat dry milk in Tris-buffered saline (TBS) containing 0,02 % Tween. The membrane was incubated with primary antibodies against mCherry in TBS with 0,02% Tween and 0,3% milk (1:1000; Invitrogen, PA5-34974) overnight at 4°C. The membrane was washed three times during 10 minutes in TBS with 0,02% Tween and incubated with the secondary antibodies against rabbit in TBS with 0,02% Tween and 0,3% milk (1:10000; Odyssey; 926-32210) for 1 hour at room temperature. The membrane was washed as before and the protein band was visualized by a ChemiDoc MP imaging system (Biorad) with ECL kit (Thermo Scientific) and analyzed using ImageJ. YFP-RFP fusion protein had an expected size of 55 kDa and the RFP residue alone had an expected size of 26 kDa. The membrane was washed one last time and incubated with GAPDH-HRP conjugate antibody in TBS with 0,02% Tween and 0,3% milk [1:2000; AbCam; ab85760] for 1 hour at room temperature. The GAPDH protein bands were revealed as before, with an expected size of 36 kDa.

FIGURES

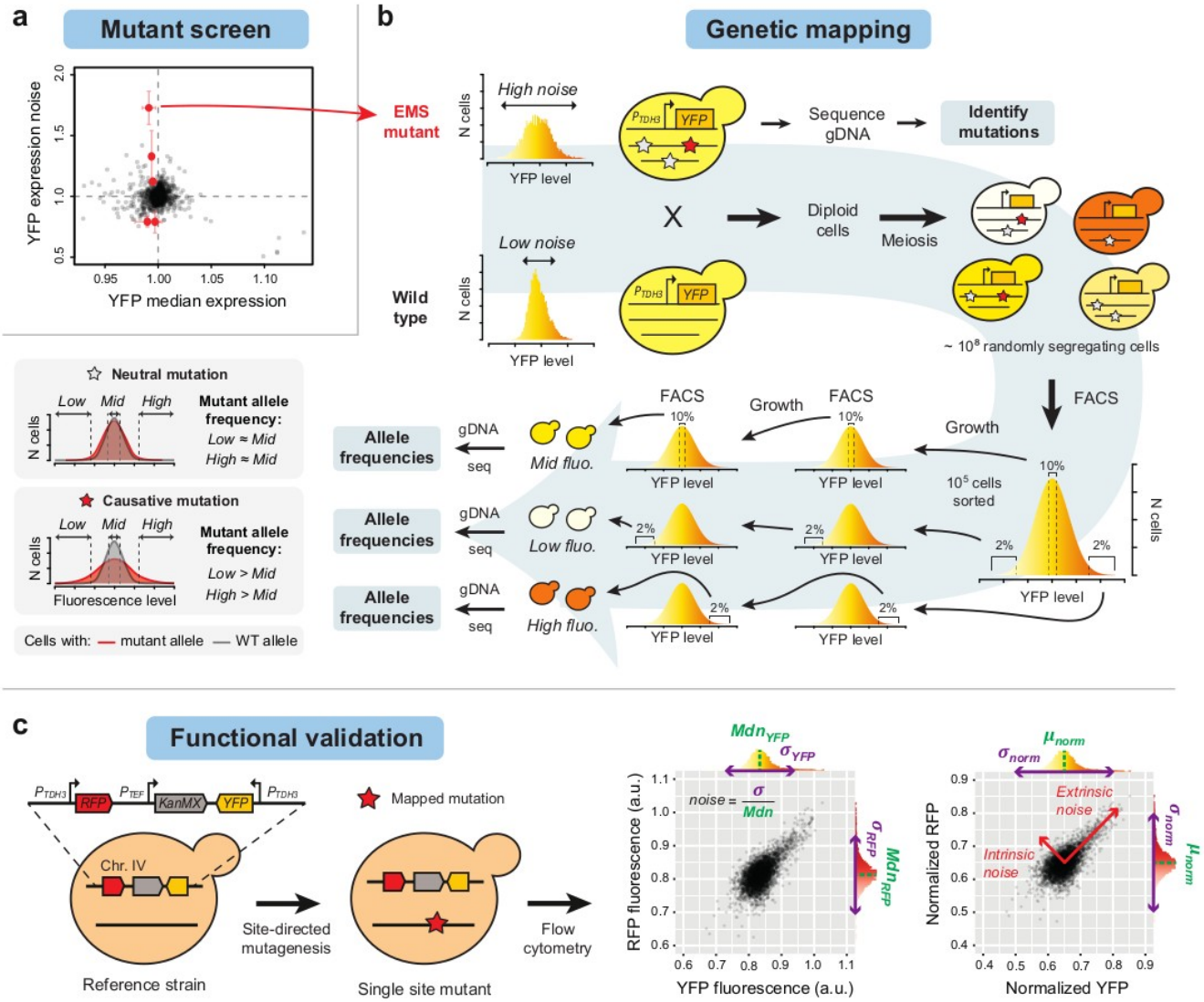

Figure 1. Identification of mutations affecting cell-to-cell variability of expression of a target gene. (a) A mutagenesis screen was performed to identify 5 strains (red dots) with altered expression noise and unchanged median expression of the P_{TDH3}-*YFP* reporter. These five strains were identified among a collection of 1241 strains obtained by ethyl methanesulfonate (EMS) mutagenesis (Duveau *et al.* 2021); their altered expression noise was further validated in another independent experiment (**Figure supplement 1**). Each dot represents the mean expression value among four replicate samples relative to the mean expression of the unmutagenized reference strain. Error bars show 95% confidence intervals. **(b)** Scheme of the bulked segregant analysis and whole-genome sequencing mapping strategy (BSA-seq) used to determine which mutations were statistically associated with expression noise. All mutations present in the 5 selected mutant strains were identified by whole-genome sequencing. In parallel, each mutant strains was crossed to a reference strain to

obtain a large population of segregating cells after meiosis of the resulting diploids. Segregating cells were sorted by FACS in three bulks based on their fluorescence levels. Each bulk was further enriched for a particular fluorescence level by two additional rounds of growth and cell sorting. Whole-genome sequencing was then performed at ~100x coverage to quantify frequencies of segregating mutations in the three bulks. A mutation that does not impact *YFP* expression noise is expected to be found at similar frequencies in the three bulks, while a mutation impacting expression noise or genetically linked to a causative mutation is expected to be found at different frequencies in the bulk of cells with average fluorescence levels and in the two bulks of cells with extreme fluorescence levels. **(c)** Strategy used to confirm the effects of mapped mutations on expression noise. Mapped mutation were individually introduced in the genome of a strain expressing two different reporter genes (*RFP* and *YFP*), each under control of a copy of the *TDH3* promoter. These single-site mutants allowed us to quantify the effects of each mutation not only on expression noise of the two fluorescent reporters, but also on intrinsic and extrinsic noise (from the covariation of fluorescence of the two reporters, see Methods).

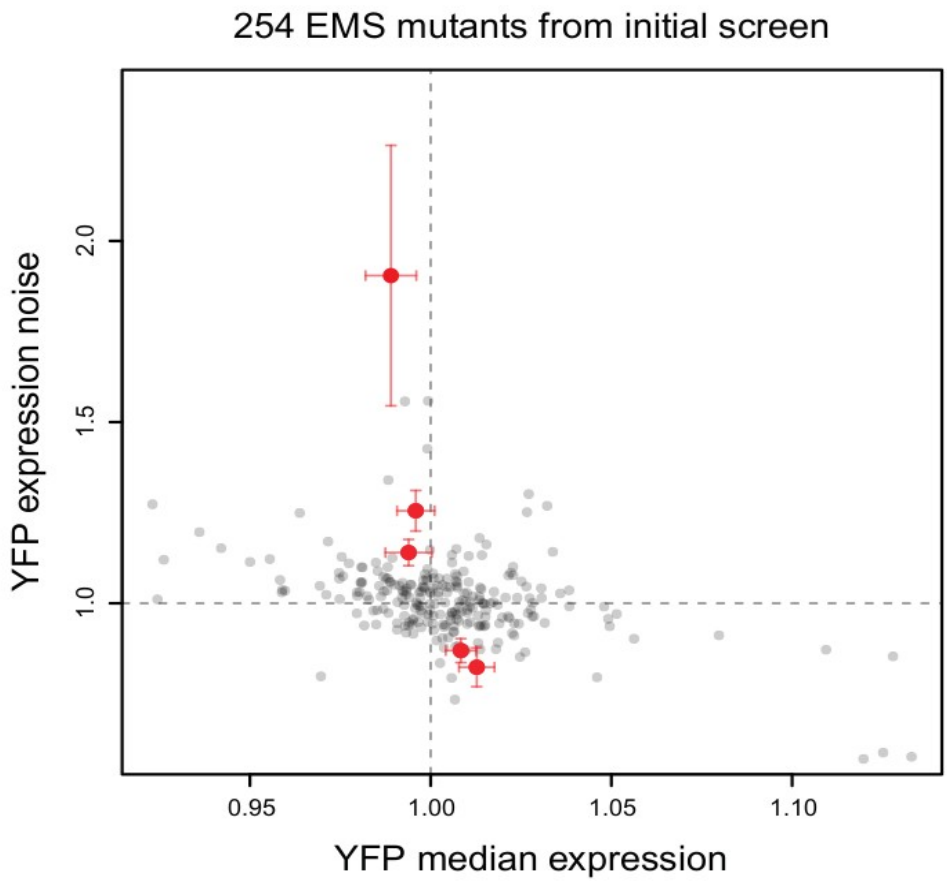

Figure 1 – figure supplement 1. Second fluorescence screen used to select mutant strains with reproducible changes of expression noise for genetic mapping. Median expression and expression noise of YFP were quantified in 254 mutant strains that showed significant changes of YFP expression (median and/or noise) relative to the reference strain in the initial screen (**Figure 1a**). Each dot represents the mean expression value among four replicate samples relative to the mean expression of the unmutagenized reference strain. The five strains selected for genetic mapping are shown in red. Error bars show 95% confidence intervals.

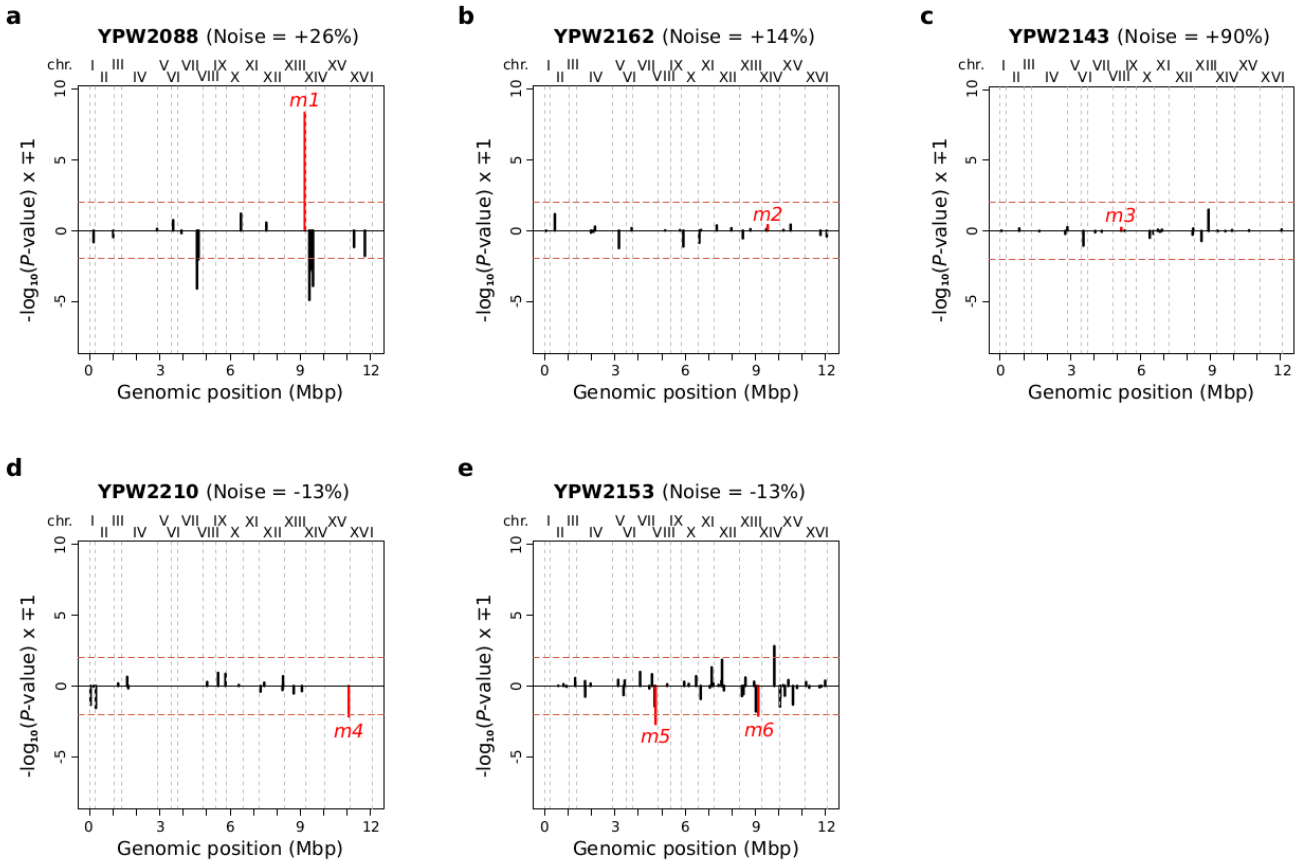

Figure 1 – figure supplement 2. Statistical comparisons of allele frequencies between different fluorescent bulks at each mutation site in the genome of segregants from five crosses. For each mutation site (each vertical bar) in **(a)**, **(b)**, **(d)**, and **(e)**, the *P*-value was computed using a *G*-test (as described in Methods) to compare read counts with mutant and wild-type alleles between i) low and high fluorescence bulks combined and ii) mid fluorescence bulk. For the cross involving mutant YPW2143 **(c)**, we only compared high and mid fluorescence bulks because a single haplotype was

nearly fixed in the low fluorescence bulk. *P*-values were adjusted using the Benjamini-Hochberg procedure to control the false-discovery rate. To visualize directions of effects, we represented $-\log_{10}(P)$ values with a positive sign if a mutation was found at higher frequency in the low and high bulks than in the medium bulk (*i.e.* mutation associated with increased expression noise) and a negative sign if a mutation was found at lower frequency in the low and high bulks than in the medium bulk (*i.e.* mutation associated with decreased expression noise). Vertical dotted lines show boundaries between chromosomes. Horizontal red dotted lines show *P*-value thresholds of 0.01 for mutations with positive and negative effects. The six mutations for which we attempted to validate the effect on expression noise in **Figure 2** are represented in red.

a

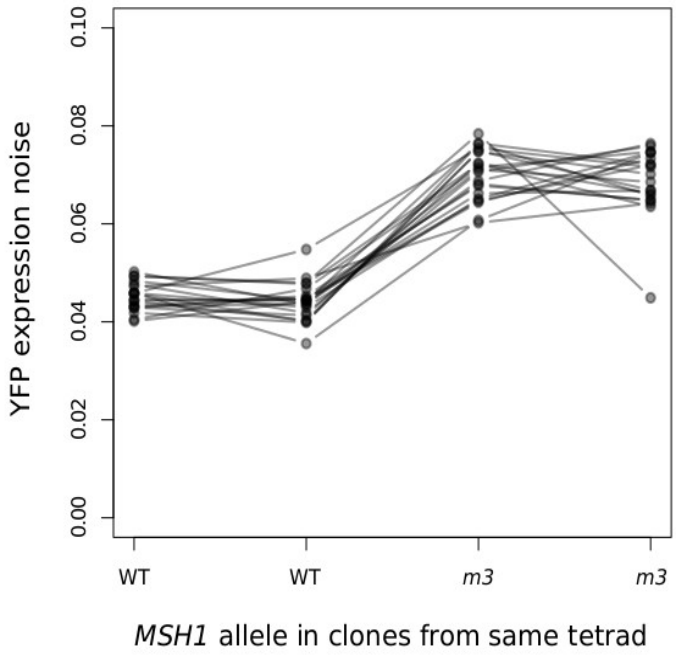

b

Analysis of variance table

	Df	*Sum Sq*	*Mean Sq*	*F value*	*Pr(>F)*
MSH1	1	4.39E-02	4.39E-02	7.92E+02	1.47E-82
TETRAD	19	1.19E-03	6.27E-05	1.13E+00	3.20E-01
PLATE	3	4.08E-03	1.36E-03	2.45E+01	4.54E-14
MAT	1	1.15E-03	1.15E-03	2.06E+01	8.31E-06
MARKER	1	1.52E-04	1.52E-04	2.74E+00	9.89E-02
Residuals	272	1.51E-02	5.55E-05		

Figure 1 – figure supplement 3. Linkage analysis showing a strong association between expression noise and segregation of *m3* mutation (*msh1(G1262a)*) in F2 hybrids. P_{TDH3}-*YFP* expression noise was quantified by flow cytometry and *msh1* genotype was determined by Sanger sequencing in 80 F2 clones isolated from 20 tetrads. F1 diploid cells were obtained by crossing mutant YPW2143 with the mapping strain YPW1240. **(a)** Each dot shows the mean expression noise measured from 6094 to 8799 cells in 3 or 4 replicate populations for each F2 clone. Lines connect the four clones issued from the same tetrad. **(b)** Results of an ANOVA used to determine the statistical significance of the additive effects of the following explanatory variables on expression noise: i) *MSH1* genotype, ii) the tetrad of origin of each clone, iii) the culture plate (each replicate was grown in a different plate), iv) the mating type and v) the drug resistance marker segregating in F2 clones. The adjusted *R*-squared

of the linear model used in the ANOVA is 0.7489 and the associated *F*-statistic is 36.43 (*P*-value = 3.30 x 10^{-72}).

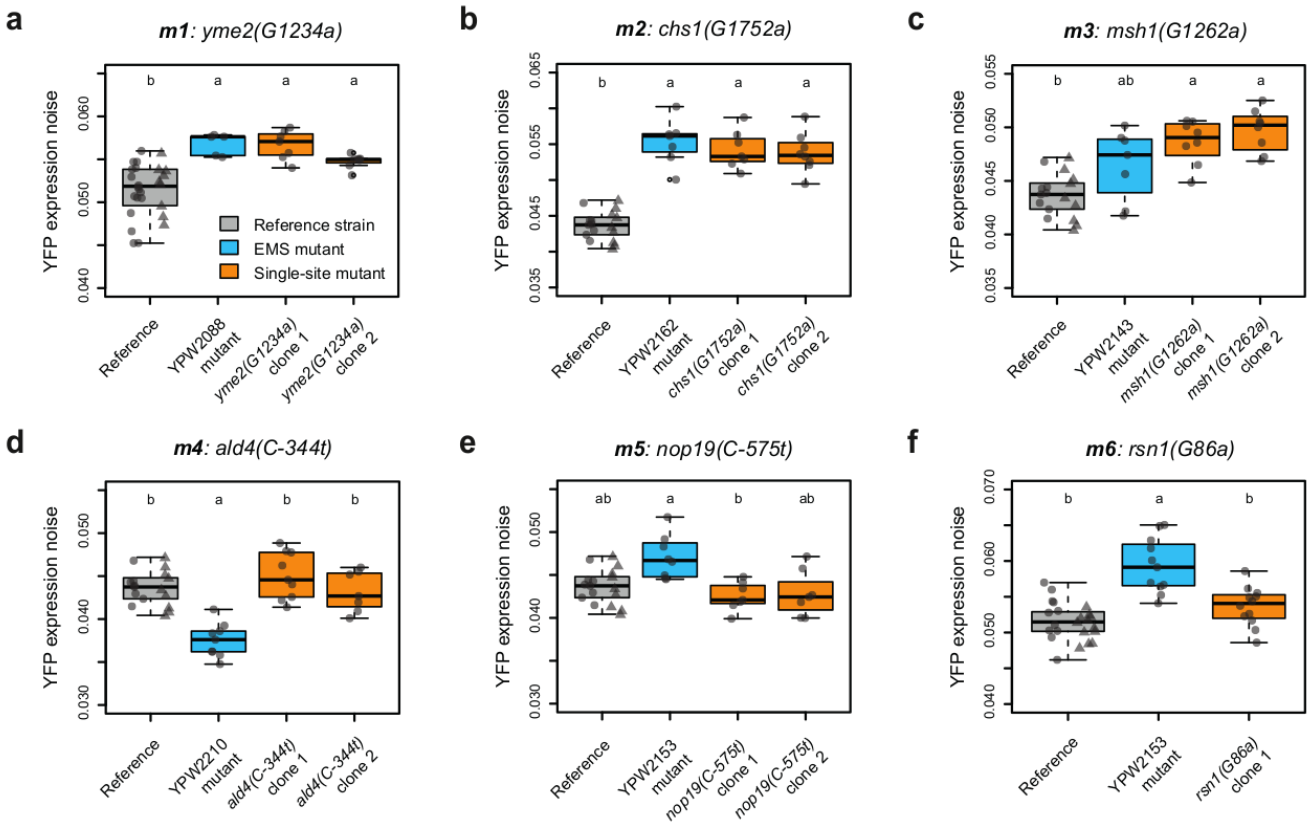

Figure 2. Testing the effects of six mapped mutations on YFP expression noise using single-site mutants. Thick lines, boxes and whiskers represent the median, interquartile range (IQR) and 1.5 IQR of expression noise measured among 7 to 26 samples, with colors corresponding to different genotypes as indicated in the legend of panel **(a)**. Dots represent the expression noise of individual samples measured from 2102 to 4707 cells. For the reference genotype, circles and triangles represent data collected for two independent clones obtained from the same transformation experiment. For genotypes carrying single mutations, data collected for independent clones from the same transformation are shown in two orange boxes. Pairwise t-tests were performed to compare the mean expression noise among replicates between pairs of genotypes, with p-values adjusted using Benjamini-Hochberg correction. For each panel, the mean expression noise is statistically different between two genotypes (adjusted p-value < 0.05) if no letter is shared above the boxes of the two genotypes. Above each plot, positions of mutations are indicated relative to the start codon of the gene with positive and

negative numbers if mutations are respectively downstream (*i.e.* in coding sequence) and upstream of the start codon. Capital and lowercase letters indicate respectively reference and alternate nucleotides at each mutation site.

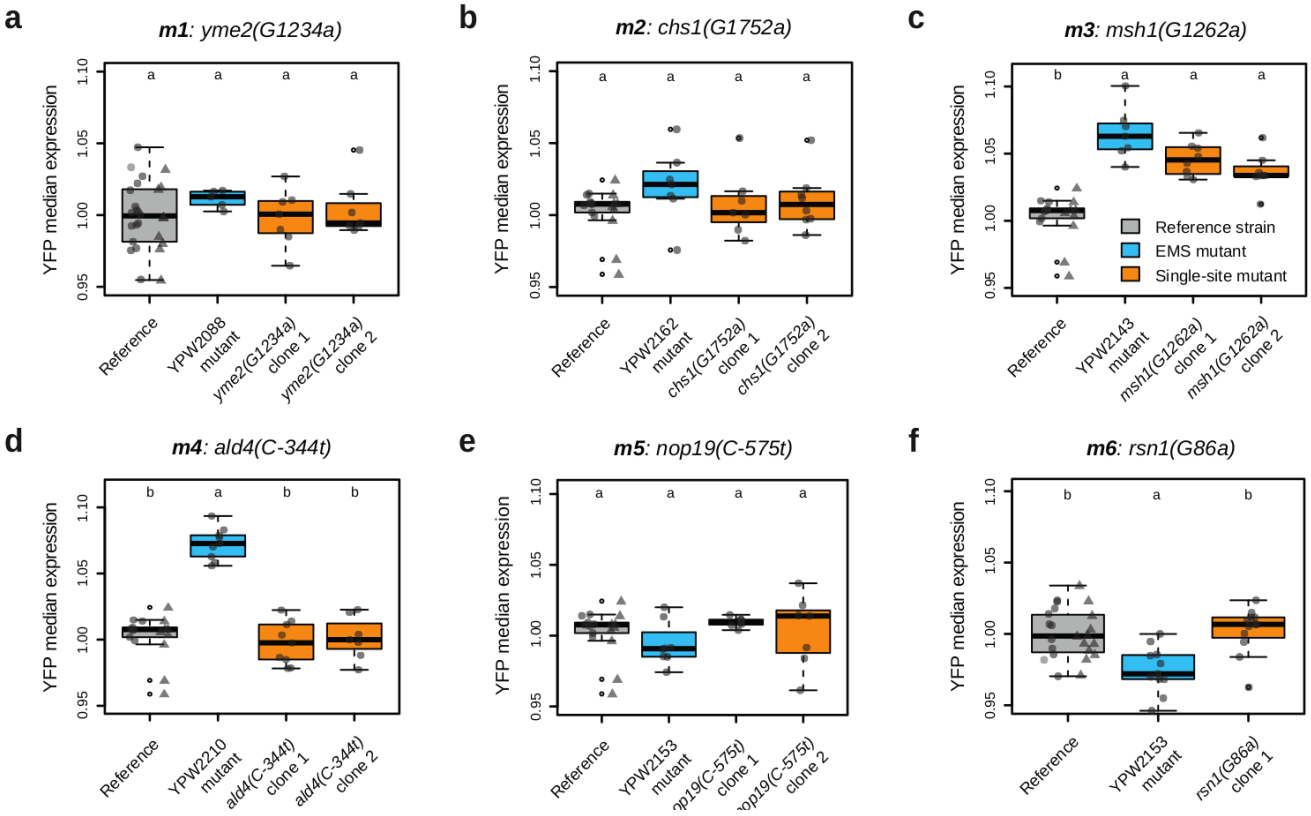

Figure 2 – figure supplement 1. Testing the effects of six mapped mutations on YFP median expression using single-site mutants. Thick lines, boxes and whiskers represent the median, interquartile range (IQR) and 1.5 IQR of median expression measured among 7 to 26 samples, with colors corresponding to different genotypes as indicated in the legend of panel **(c)**. Dots represent the median expression of individual samples measured from 2102 to 4707 cells. For the reference genotype, circles and triangles represent data collected for two independent clones obtained from the same transformation experiment. For genotypes carrying single mutations, data collected for independent clones from the same transformation are shown in two orange boxes. Pairwise *t*-tests were performed to compare the mean of median expression levels among replicates between pairs of genotypes, with *p*-values adjusted using Benjamini-Hochberg correction. For each panel, the median expression is statistically different between two genotypes (adjusted *p*-value < 0.05) if no letter is shared above the boxes of the two genotypes. Above each plot, positions of mutations are indicated

relative to the start codon of the gene with positive and negative numbers if mutations are respectively downstream (*i.e.* in coding sequence) and upstream of the start codon. Capital and lowercase letters indicate respectively reference and alternate nucleotides at each mutation site.

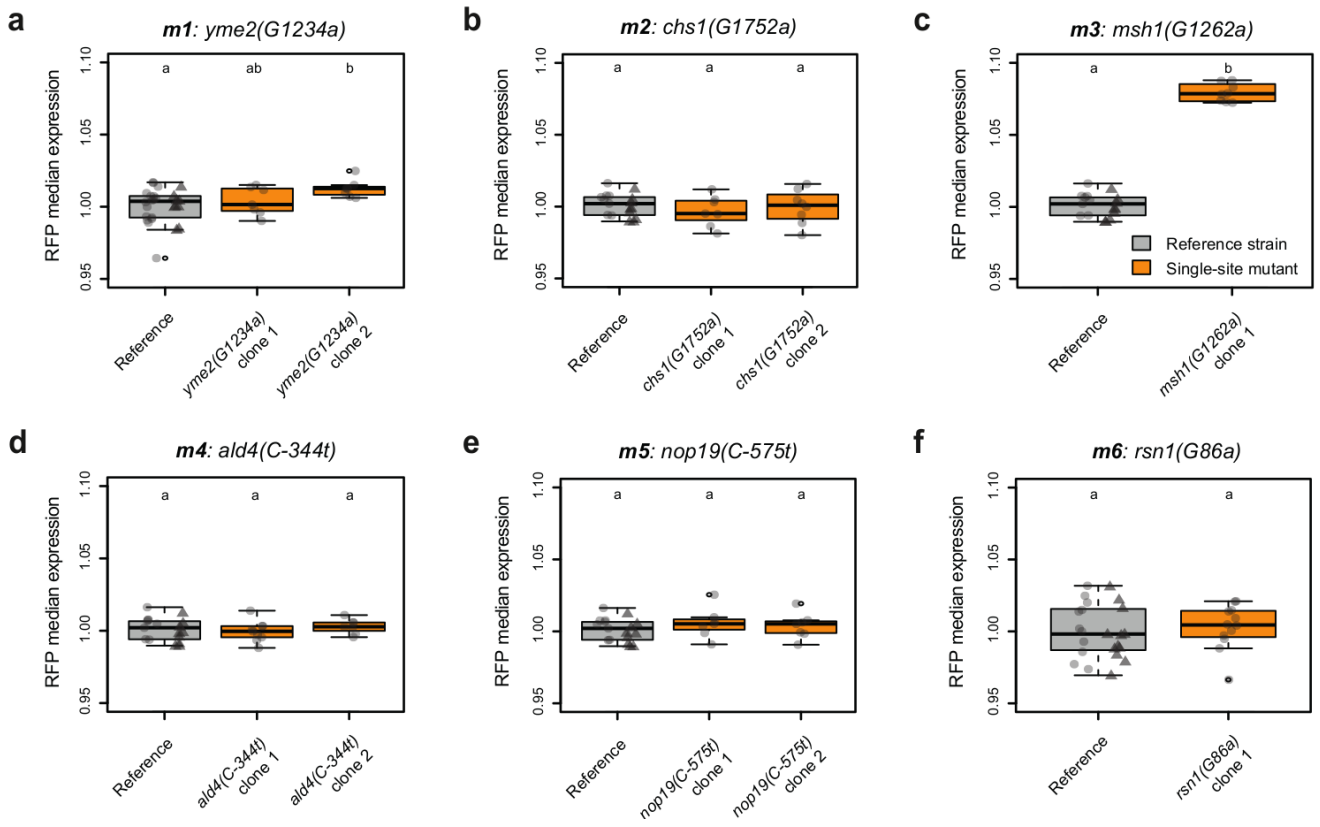

Figure 2 – figure supplement 2. Testing the effects of six mapped mutations on RFP median expression and expression noise using single-site mutants. Thick lines, boxes and whiskers represent the median, interquartile range (IQR) and 1.5 IQR of median expression **(a-f)** or expression noise **(g-l)** measured among 7 to 26 samples, with colors corresponding to different genotypes as indicated in the legend of panel **(c)**. Dots represent the median expression or expression noise of individual samples measured from 2102 to 4707 cells. For the reference genotype, circles and triangles represent data collected for two independent clones obtained from the same transformation experiment. For genotypes carrying single mutations, data collected for independent clones from the same transformation are shown in two orange boxes. Pairwise *t*-tests were performed to compare the mean of median expression levels (or expression noise) among replicates between pairs of genotypes, with *p*-values adjusted using Benjamini-Hochberg correction. For each panel, the median expression (or

expression noise) is statistically different between two genotypes (adjusted *p*-value < 0.01) if no letter is shared above the boxes of the two genotypes. Above each plot, positions of mutations are indicated relative to the start codon of the gene with positive and negative numbers if mutations are respectively downstream (*i.e.* in coding sequence) and upstream of the start codon. Capital and lowercase letters indicate respectively reference and alternate nucleotides at each mutation site.

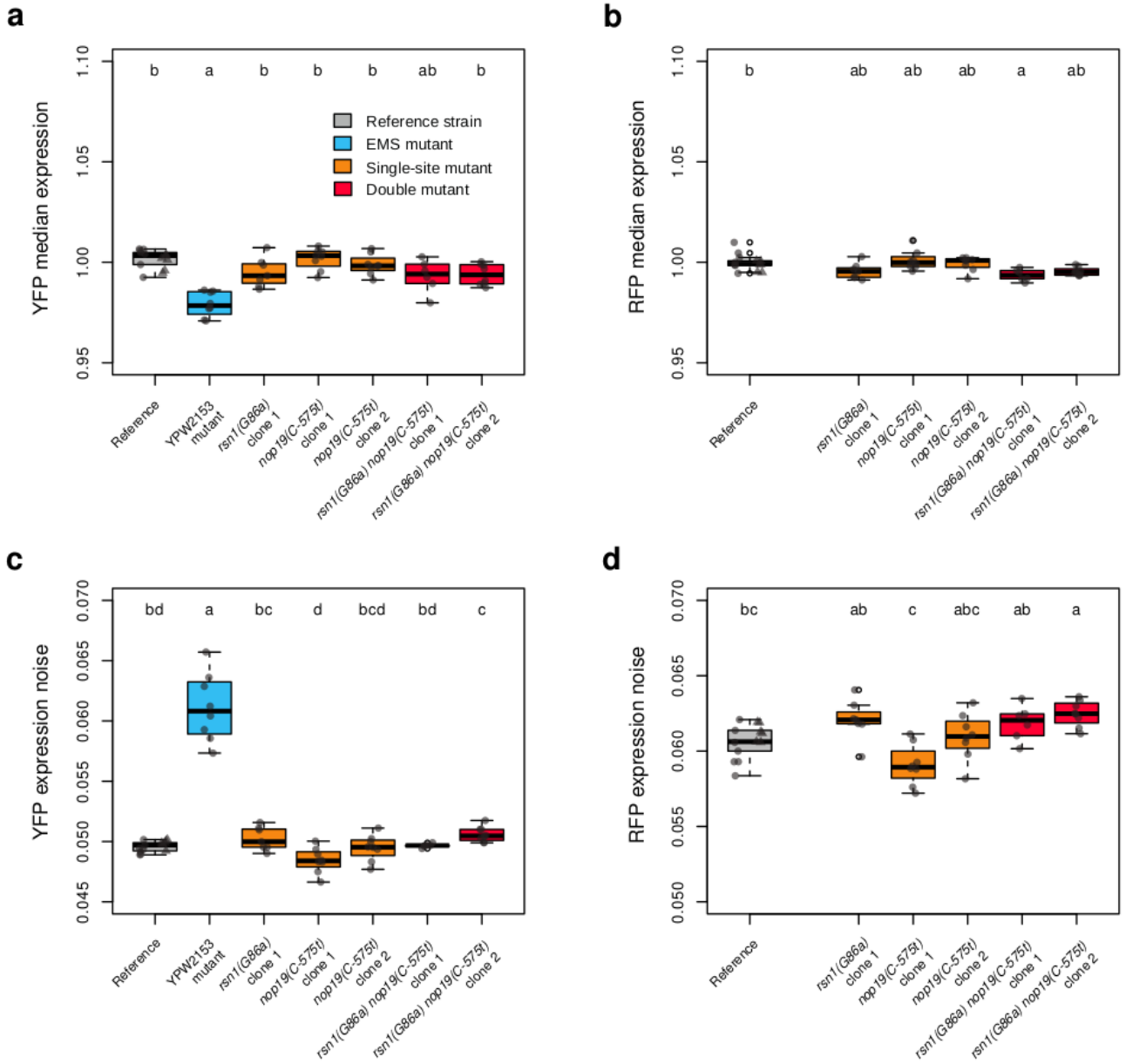

Figure 2 – figure supplement 3. Combined effects of *rsn1(G86a)* and *nop19(C-575t)* mutations on YFP and RFP median expression and expression noise. Thick lines, boxes and whiskers represent the median, interquartile range (IQR) and 1.5 IQR of **(a)** YFP median expression,

(b) RFP median expression, **(c)** YFP expression noise and **(d)** RFP expression noise measured among 6 to 14 samples. Colors corresponding to different genotypes as indicated in the legend of panel **(a)**. Dots represent expression values of individual samples measured from 4226 to 4551 cells. For the reference genotype, circles and triangles represent data collected for two independent clones obtained from the same transformation experiment. For genotypes carrying single mutations, data collected for independent clones from the same transformation are shown in two orange boxes. Pairwise *t*-tests were performed to compare the mean of median expression levels among replicates between pairs of genotypes, with *p*-values adjusted using Benjamini-Hochberg correction. For each panel, the median expression is statistically different between two genotypes (adjusted *p*-value < 0.05) if no letter is shared above the boxes of the two genotypes. Above each plot, positions of mutations are indicated relative to the start codon of the gene with positive and negative numbers if mutations are respectively downstream (*i.e.* in coding sequence) and upstream of the start codon. Capital and lowercase letters indicate respectively reference and alternate nucleotides at each mutation site.

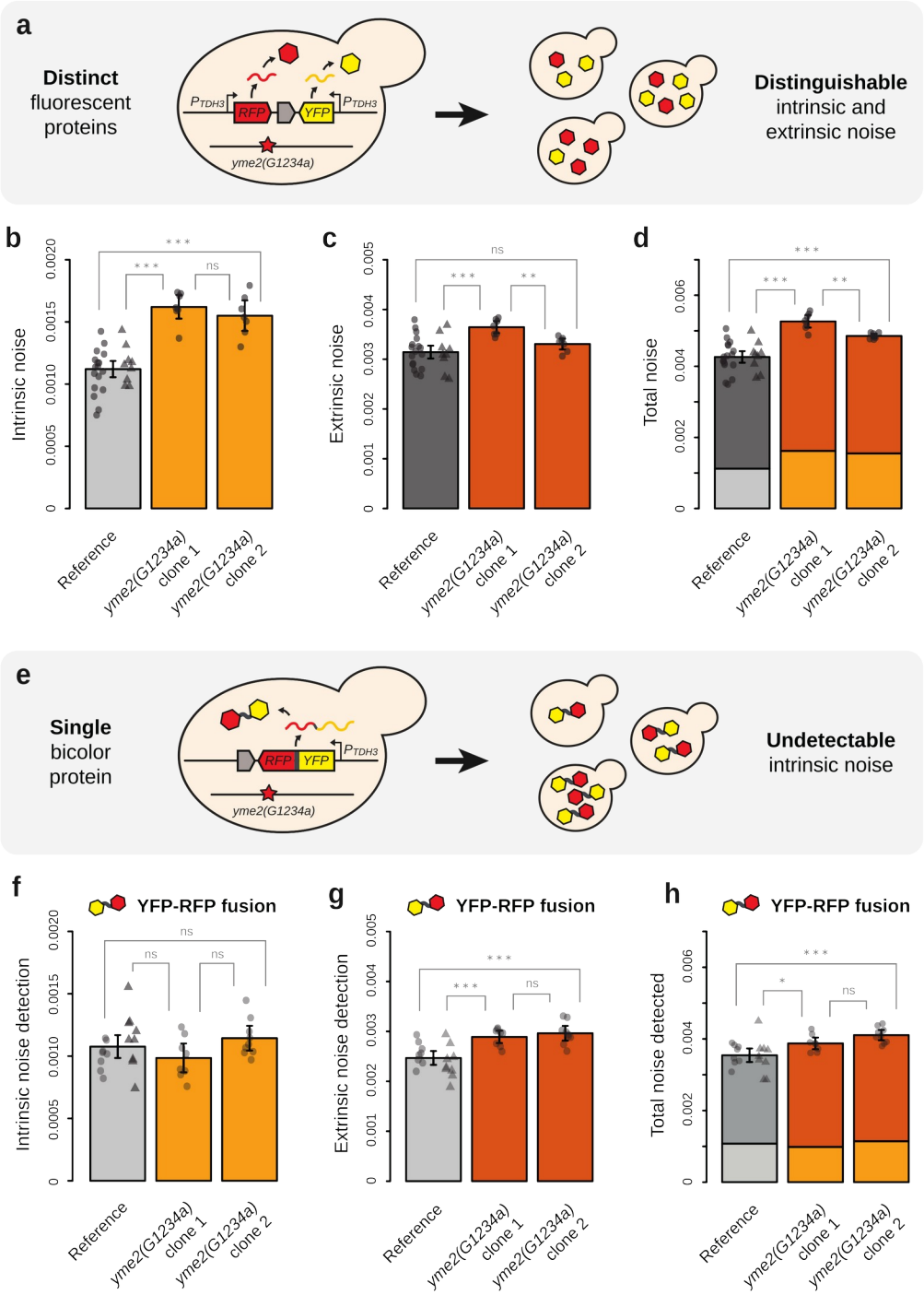
a
Distinct fluorescent proteins
PTDH3
RFP
YFP
PTDH3
yme2(G1234a)
Distinguishable intrinsic and extrinsic noise
b
Intrinsic noise
c
Extrinsic noise
d
Total noise
Reference
yme2(G1234a) clone 1
yme2(G1234a) clone 2
e
Single bicolor protein
RFP
YFP
PTDH3
yme2(G1234a)
Undetectable intrinsic noise
f
YFP-RFP fusion
Intrinsic noise detection
g
YFP-RFP fusion
Extrinsic noise detection
h
YFP-RFP fusion
Total noise detected

Figure 3. Quantifying the effects of a non-synonymous mutation in *yme2* on intrinsic and extrinsic noise using a dual reporter system. (a) A construct consisting of P_{TDH3}-*RFP* and P_{TDH3}-*YFP* reporter genes transcribed from opposite strands and separated by a *KanMX4* drug resistance cassette was inserted at the *ho* locus in genetic backgrounds with wild-type or mutant (*G1234a)* alleles of *yme2*. By quantifying both YFP and RFP fluorescence of individual cells using flow cytometry, it is possible to distinguish the effects of *yme2* mutation on intrinsic and extrinsic noise of P_{TDH3} activity. **(b)** Intrinsic, **(c)** extrinsic and **(d)** total noise of P_{TDH3} activity in strains carrying the dual reporter system with wild-type (light and dark gray bars) or mutant (light and dark orange bars) alleles of *yme2*. Bars show mean values among 7 to 26 replicate populations. Error bars are 95% confidence intervals of means. Dots show values of individual samples obtained from 4312 to 4689 cells. **(e)** A construct consisting of fused *YFP* and *RFP* coding sequences expressed under control of a single P_{TDH3} copy was inserted at *ho* locus in genetic backgrounds with wild-type or mutant (*G1234a)* alleles of *yme2*. This system was used to test whether the change in intrinsic noise detected in **(b)** using the dual reporter system was a technical artifact or not. Indeed, the mutation should not have detectable impact on intrinsic noise when the two fluorescent proteins are fused, because their expression is forced to covary. **(f)** Detected intrinsic noise, **(g)** detected extrinsic noise and **(h)** detected total noise in strains expressing YFP-RFP fusion proteins and with wild-type (light and dark gray bars) or mutant (light and dark orange bars) alleles of *yme2*. Bars show mean values among 8 to 17 replicate populations. Error bars are 95% confidence intervals of means. Dots show values of individual samples obtained from 4424 to 4714 cells. In **(d,h)**, light and dark bars indicate respectively the contributions of intrinsic and extrinsic noise to total noise. **(b-d,f-h)** For the reference genotype, circles and triangles represent data collected for two independent clones obtained from the same transformation experiment. For *yme2* mutants, data collected for independent clones from the same transformation are shown in two different colored bars. Pairwise *t*-tests were performed to compare mean values between bars: ns $P \geq 0.05$, * $0.05 > P \geq 0.01$, ** $0.001 > P \geq 0.001$, *** $P < 0.001$.

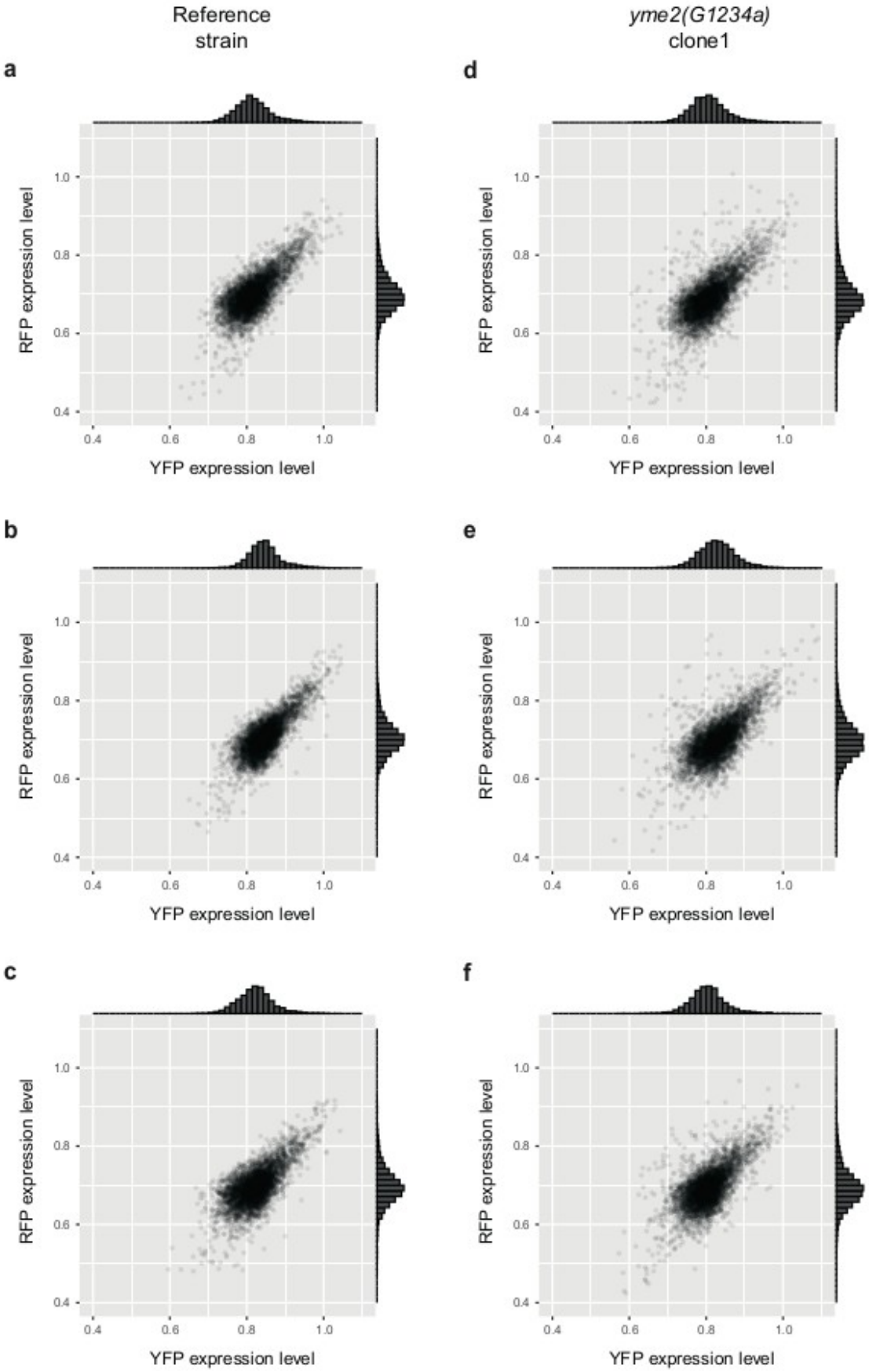
Reference strain
yme2(G1234a) clone1
a
b
c
d
e
f
RFP expression level
YFP expression level
0.4
0.6
0.8
1.0

Figure 3 – figure supplement 1. YFP and RFP expression levels of individual cells from wild-type and *yme2(G1234a)* strains expressing P_{TDH3}-*YFP* and P_{TDH3}-*RFP* reporter genes. Expression of the two fluorescent reporters in **(a-c)** three replicate populations of strain GY2458 carrying a wild-type allele of *YME2* and **(d-f)** three replicate populations of strain GY2634 carrying mutation *G1234a* in *YME2* coding sequence (4312 to 4689 cells per sample). Histograms show the distribution of data on each axis. Correlations between YFP and RFP expression levels are visually lower for *yme2(G1234a)* cells than wild-type cells, consistent with the increased intrinsic noise quantified from mutant cells.

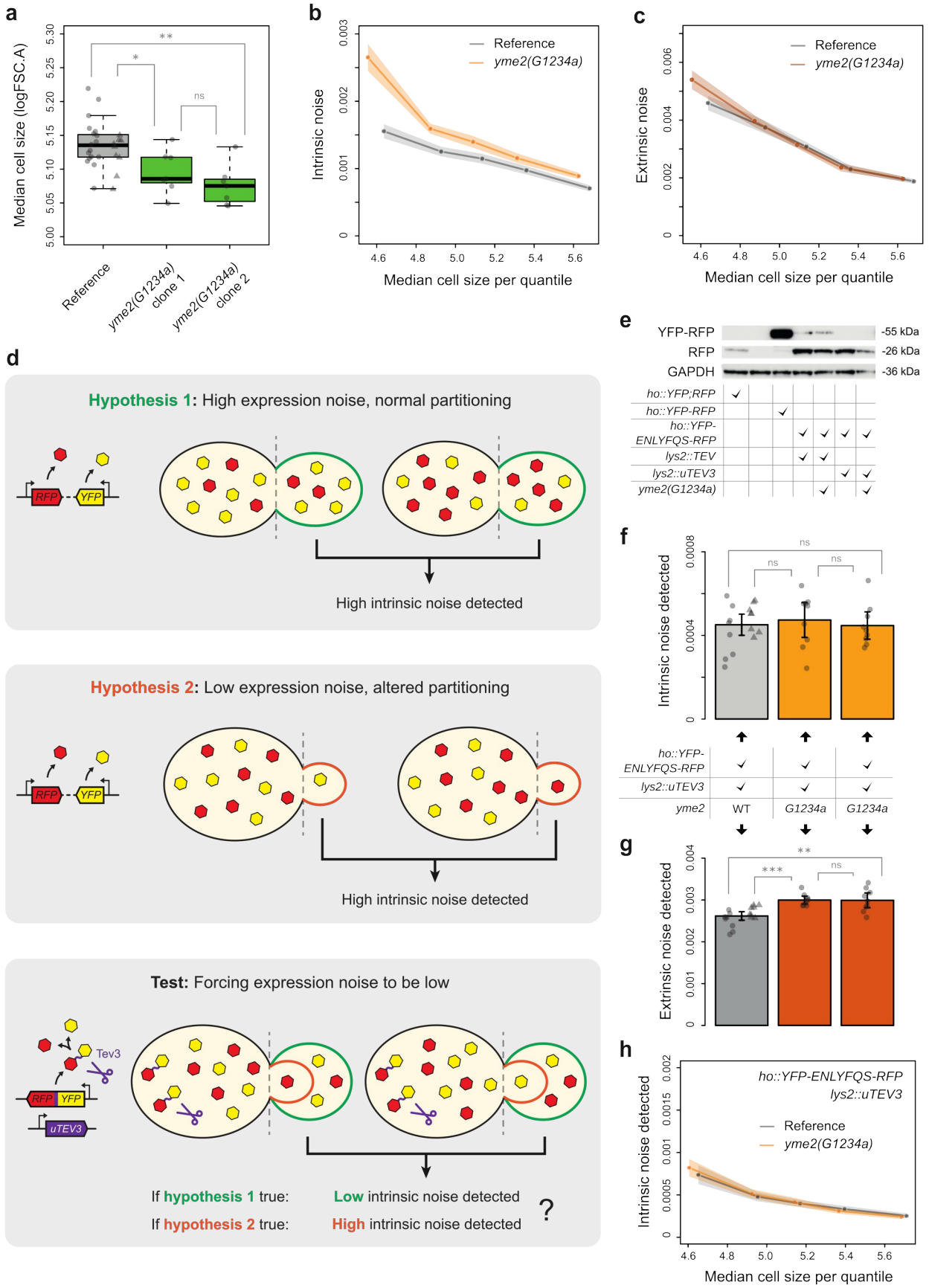
a
Median cell size (logFSC.A)
5.00
5.05
5.10
5.15
5.20
5.25
5.30
**
*
ns
Reference
yme2(G1234a) clone 1
yme2(G1234a) clone 2
b
Intrinsic noise
0
0.001
0.002
0.003
Reference
yme2(G1234a)
4.6
4.8
5.0
5.2
5.4
5.6
Median cell size per quantile
c
Extrinsic noise
0
0.002
0.004
0.006
Reference
yme2(G1234a)
4.6
4.8
5.0
5.2
5.4
5.6
Median cell size per quantile
d
Hypothesis 1: High expression noise, normal partitioning
RFP
YFP
High intrinsic noise detected
Hypothesis 2: Low expression noise, altered partitioning
RFP
YFP
High intrinsic noise detected
Test: Forcing expression noise to be low
Tev3
RFP
YFP
uTEV3
If hypothesis 1 true: Low intrinsic noise detected
If hypothesis 2 true: High intrinsic noise detected
?
e
YFP-RFP
RFP
GAPDH
-55 kDa
-26 kDa
-36 kDa
ho::YFP;RFP
ho::YFP-RFP
ho::YFP-ENLYFQS-RFP
lys2::TEV
lys2::uTEV3
yme2(G1234a)
f
Intrinsic noise detected
0
0.0004
0.0008
ns
ns
ns
ho::YFP-ENLYFQS-RFP
lys2::uTEV3
yme2
WT
G1234a
G1234a
g
Extrinsic noise detected
0
0.001
0.002
0.003
0.004
**
***
ns
h
Intrinsic noise detected
0
0.0005
0.001
0.0015
0.002
ho::YFP-ENLYFQS-RFP
lys2::uTEV3
Reference
yme2(G1234a)
4.6
4.8
5.0
5.2
5.4
5.6
Median cell size per quantile

Figure 4 – *yme2(G1234a)* mutation increases intrinsic noise via altered gene expression and not via altered protein partitioning at cell division. (a) Median size of wild-type and *yme2(G1234a)* mutant cells quantified from forward scatter area (FSC.A) in flow cytometry data. Thick lines, boxes and whiskers represent the median, interquartile range (IQR) and 1.5 IQR of median cell size measured among 7 to 26 samples. Dots represent the median cell size of individual samples measured from 4312 to 4689 cells. For the reference genotype, circles and triangles represent data collected for two independent clones obtained from the same transformation experiment. For genotypes carrying single mutations, data collected for independent clones from the same transformation are shown in two green boxes. Pairwise *t*-tests were performed to compare median cell sizes between boxes: ns $P \geq 0.05$, * $0.05 > P \geq 0.01$, ** $0.001 > P \geq 0.001$, *** $P < 0.001$. **(b)** Intrinsic noise and **(c)** extrinsic noise of five groups of cells with different cell sizes for strains with wild-type (gray) and *G1234a* (orange) alleles of *yme2*. Cell groups correspond to five fractions of the population of cells delimited by 5-quantiles of cell sizes (same number of cells in each group but different cell sizes). Dots indicate the median cell size (x-axis) and intrinsic **(b)** or extrinsic **(c)** noise (y-axis) of each cell group (906 cells per group in 24 replicate samples for wild-type and 909 cells per group in 18 replicate samples for *yme2* mutant). Shaded areas represent 95% confidence intervals. **(d)** Schemes representing i) two alternative hypotheses to explain how *yme2(G1234a)* mutation can lead to higher intrinsic noise detection and ii) a strategy to test these hypotheses. In hypothesis 1, higher intrinsic noise is explained by higher variability of expression of the two fluorescent reporters (yellow and red hexagons), either via altered regulation of transcription or translation. In hypothesis 2, higher detection of intrinsic noise is not caused by altered regulation of expression, but instead by altered partitioning of fluorescent proteins at cell division. If fewer proteins are inherited by daughter cells (because of smaller bud size or other mechanisms), this could lead to higher variability of colors detected by fluorescence in daughter cells and therefore higher intrinsic noise detected. A strategy to test these hypotheses is to express a YFP-RFP fusion protein that can be cleaved by a protease in two separate YFP and RFP fluorescent proteins after translation. With this system, we expect *yme2* mutation to have no detectable impact on intrinsic noise if it acts at the expression level (hypothesis 1) because the expression of the two reporters is forced to covary. However, we expect to detect increased intrinsic noise if *yme2* mutation acts on protein partitioning (hypothesis 2) because cleaved proteins can segregate independently at cell division. **(e)** Western blot used to detect the presence of YFP-RFP fusion protein, RFP single protein and GAPDH constitutive control in seven genotypes (as indicated below the plot). YFP-RFP and RFP

are detected using an antibody against mCherry and distinguished based on the size of bands after electrophoresis. GAPDH is detected with anti-GPADH antibody. The last two lanes on the right show complete cleavage of YFP-ENLYFQS-RFP fusion protein by uTEV3 protease both in wild-type and *yme2(G1234a)* cells. ENLYFQS is the peptide sequence targeted by the protease. **(f)** Detected intrinsic noise and **(g)** extrinsic noise in strains expressing YFP-ENLYFQS-RFP fusion protein cleaved by uTEV3 and with wild-type (light and dark gray bars) or mutant (light and dark orange bars) alleles of *yme2*. Bars show mean values among 9 to 16 replicate populations. Error bars are 95% confidence intervals of means. Dots show values of individual samples obtained from 4061 to 4673 cells. For the reference genotype, circles and triangles represent data collected for two independent clones obtained from the same transformation experiment. For *yme2(G1234a)* strains, data collected for independent clones from the same transformation are shown in two different colored bars. Pairwise *t*-tests were performed to compare mean values between bars: ns $P \geq 0.05$, * $0.05 > P \geq 0.01$, ** $0.001 > P \geq 0.001$, *** $P < 0.001$. **(h)** Intrinsic noise of five groups with different cell sizes for strains expressing YFP-ENLYFQS-RFP fusion protein cleaved by uTEV3 with wild-type (gray) and mutant *G1234a* (orange) alleles of *yme2*. Cell groups correspond to five fractions of the population of cells delimited by 5-quantiles of cell sizes. Dots indicate the median cell size (x-axis) and intrinsic noise (y-axis) of each cell group (902 cells per group in 17 replicate samples per group for wild-type and 906 cells per group in 18 replicate samples per group for *yme2(G1234a)*). Shaded areas represent 95% confidence intervals of intrinsic noise.

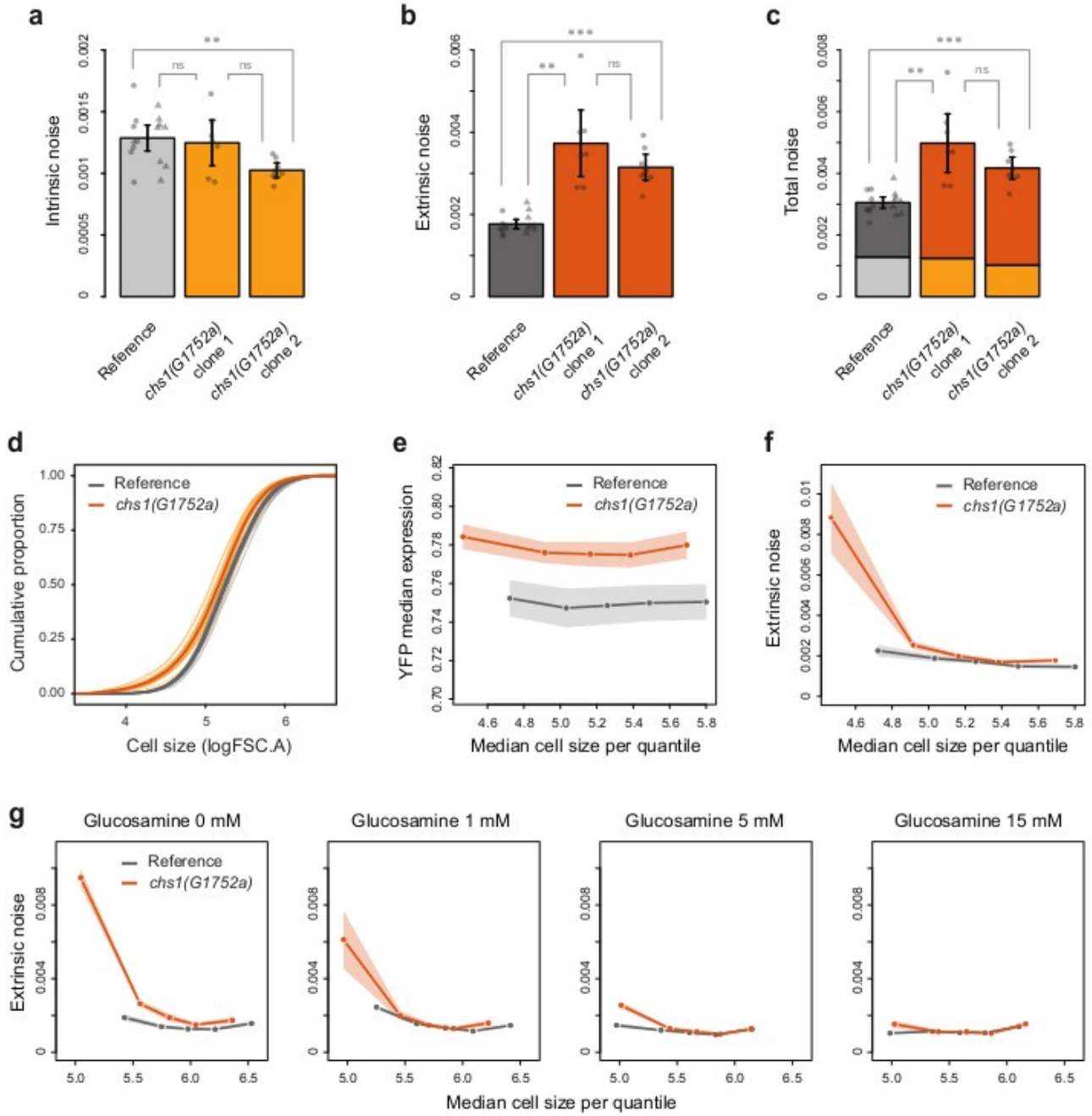

Figure 5 – *chs1(G1752a)* mutation increases extrinsic noise exclusively in small cells in absence of glucosamine precursor for chitin synthesis. (a) Intrinsic, **(b)** extrinsic and **(c)** total noise of P_{TDH3} activity in strains carrying the dual reporter system (P_{TDH3}-*YFP* and P_{TDH3}-*RFP*) with wild-type (light and dark gray bars) or mutant (light and dark orange bars) alleles of *chs1*. Bars show mean values among 7 to 16 replicate populations. Error bars are 95% confidence intervals of means. Dots show values of individual samples obtained from 3684 to 4657 cells. **(d)** Cumulative distribution of cell sizes for wild-type (gray lines) and *chs1(G1752a)* cells (orange lines) expressing the dual reporter system,

shown for individual samples (thin lines) or for all samples sharing the same genotype (thick lines). Cell sizes were quantified by flow cytometry (FSC.A: area of forward scatter). The number of samples and cells analyzed is the same as in **(a-c)** as data are from the same experiment. **(e)** YFP median expression and **(f)** extrinsic noise of five groups of cells with different cells sizes for strains with wild-type (gray) and *G1752a* (orange) alleles of *chs1*. Cell groups correspond to five fractions of the population of cells delimited by 5-quantiles of cell sizes (same number of cells in each group but different cell sizes). Dots indicate the median cell size (x-axis) and YFP median expression **(e)** or extrinsic **(c)** noise (y-axis) of each cell group (1790 cells per group in 16 replicate samples for wild-type and 1603 cells per group in 15 replicate samples for *chs1* mutant). **(g)** Extrinsic noise of cells of different sizes measured after growth in media with different concentrations of glucosamine (0, 1, 5 or 15 mM) for strains with wild-type (gray) and *G1752a* (orange) alleles of *chs1*. Cells were grouped based on median cell size as explained for **(e-f)**. Dots indicate the median cell size (x-axis) and extrinsic noise (y-axis) for 1660 to 1878 cells per group measured in 5 to 16 replicates. **(e-g)** Shaded areas represent 95% confidence intervals.

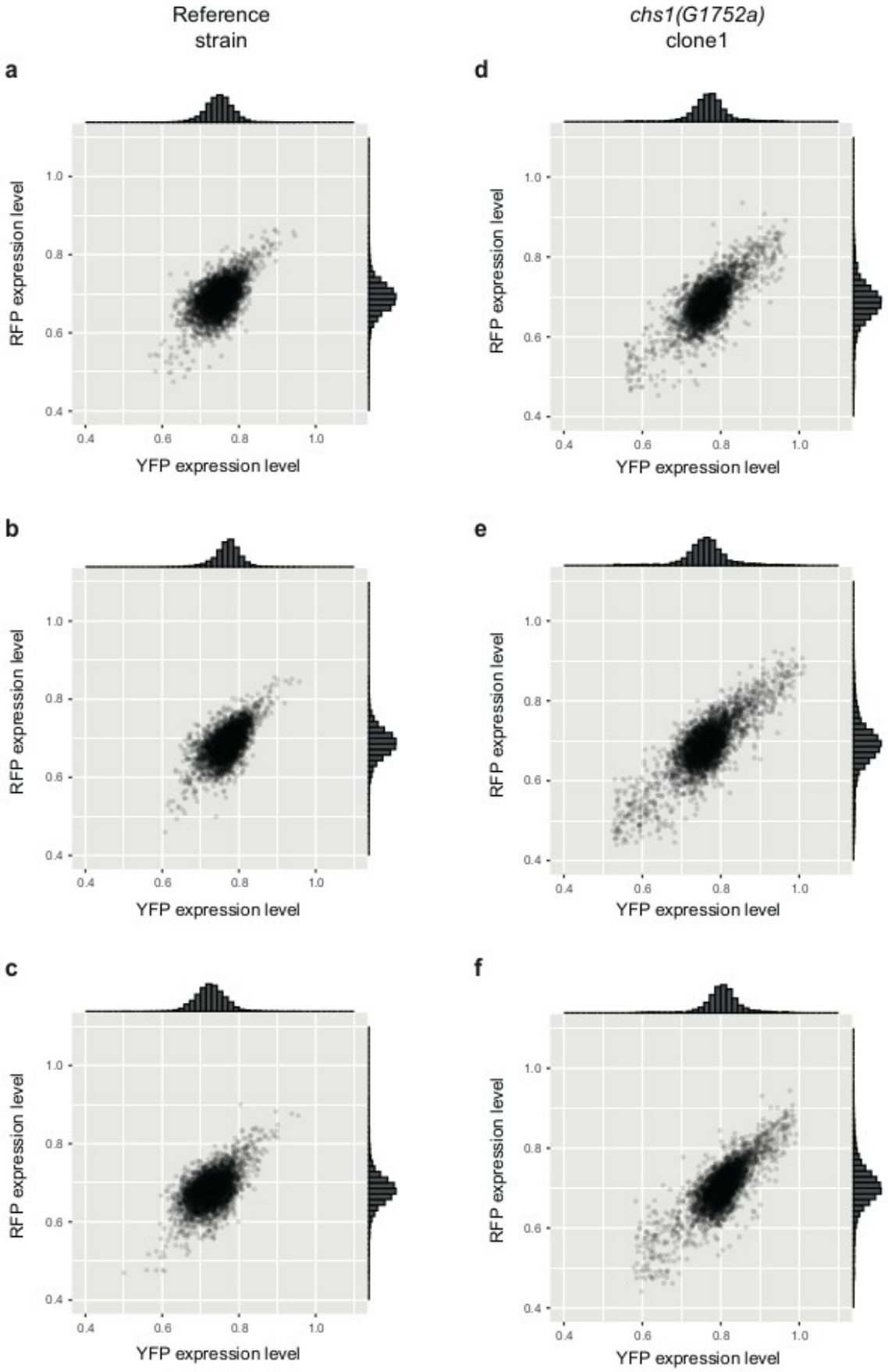
Reference strain
chs1(G1752a) clone1
a
b
c
d
e
f
RFP expression level
YFP expression level
0.4
0.6
0.8
1.0

Figure 5 – figure supplement 1. YFP and RFP expression levels of individual cells from wild-type and *chs1(G1752a)* strains expressing P_{TDH3}-*YFP* and P_{TDH3}-*RFP* reporter genes. Expression of the two fluorescent reporters in **(a-c)** three replicate populations of strain GY2458 carrying a wild-type allele of *CHS1* and **(d-f)** three replicate populations of strain GY2534 carrying mutation *G1752a* in *CHS1* coding sequence (3917 to 4627 cells per sample). Histograms show the distribution of data on each axis. The variability and covariation of YFP and RFP expression levels are both visually higher for *chs1(G1752a)* cells than for wild-type cells, consistent with the increased extrinsic noise quantified from mutant cells.

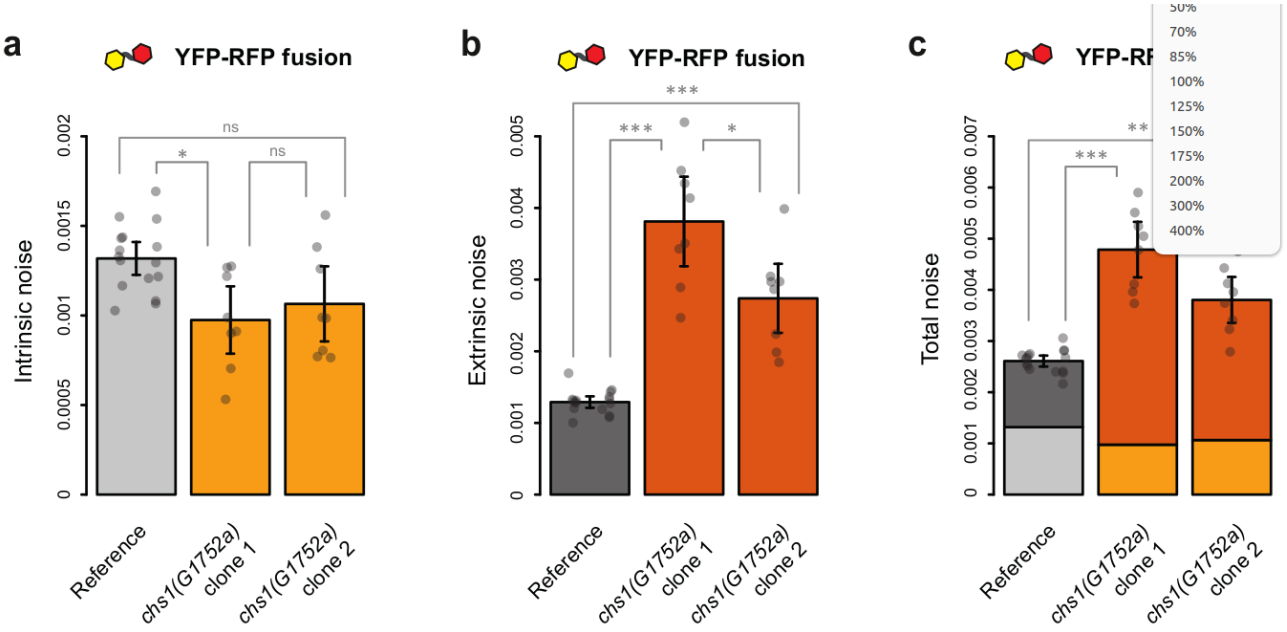

Figure 5 – figure supplement 2. Fusion of YFP and RFP fluorescent proteins does not change the detected effect of *chs1(G1752a)* mutation on extrinsic noise. (a) Detected intrinsic noise, **(b)** detected extrinsic noise and **(c)** detected total noise in strains expressing YFP-RFP fusion proteins and with wild-type (light and dark gray bars) or mutant (light and dark orange bars) alleles of *chs1*. Bars show mean values among 8 to 16 replicate populations. Error bars are 95% confidence intervals of means. Dots show values of individual samples obtained from 4196 to 4899 cells. Pairwise *t*-tests were performed to compare mean values between bars: ns $P \geq 0.05$, * $0.05 > P \geq 0.01$, ** $0.001 > P \geq 0.001$, *** $P < 0.001$.

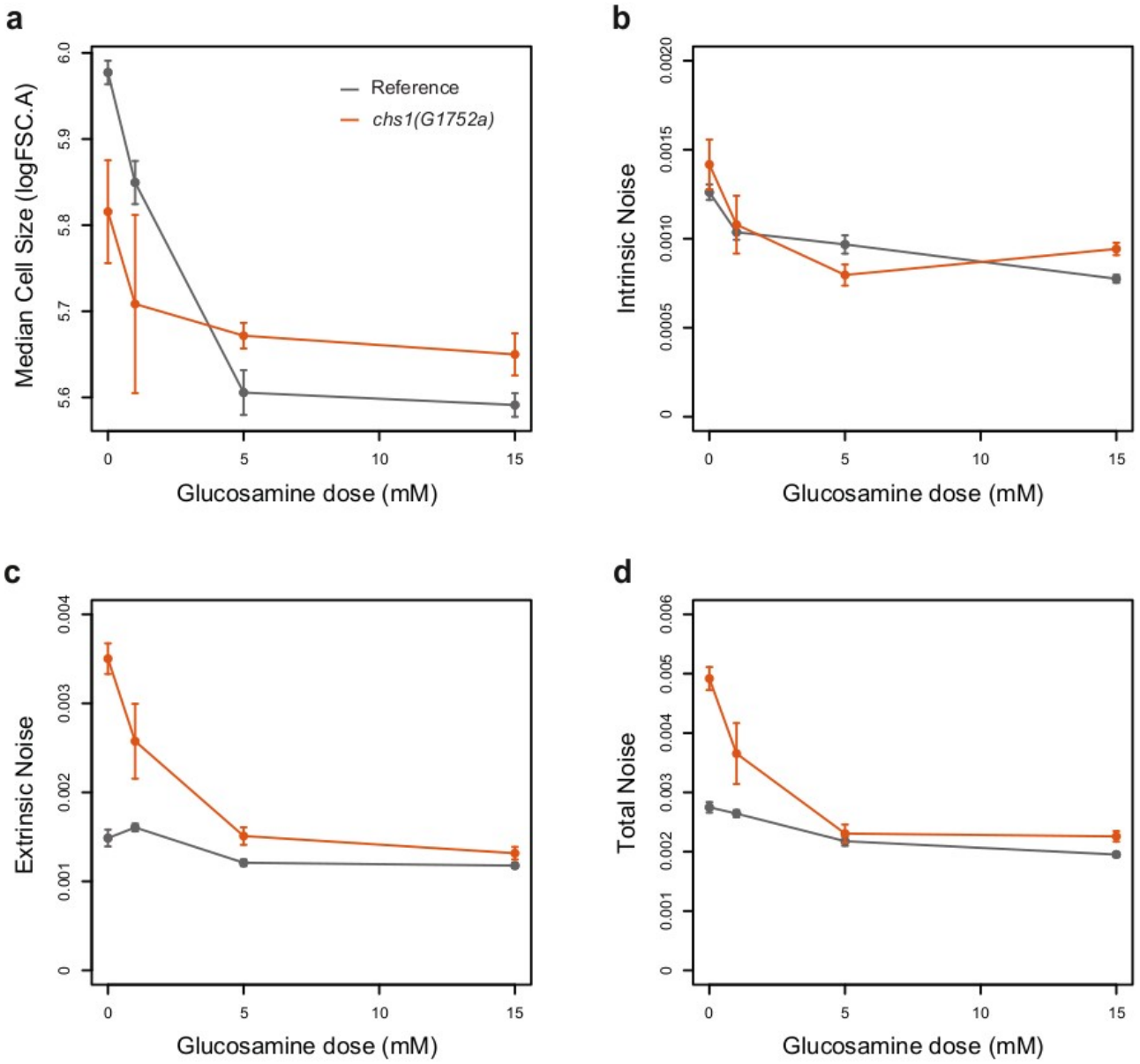

Figure 5 – figure supplement 3. Impact of glucosamine concentration on (a) median cell size, (b) intrinsic noise, (c) extrinsic noise and (d) total noise. These traits were quantified in wild-type (gray dots) and *chs1(G1752a)* (orange dots) strains expressing P_{TDH3}-*YFP* and P_{TDH3}-*RFP* reporter genes. Error bars show 95% confidence intervals of means measured among 5 to 16 replicate samples.

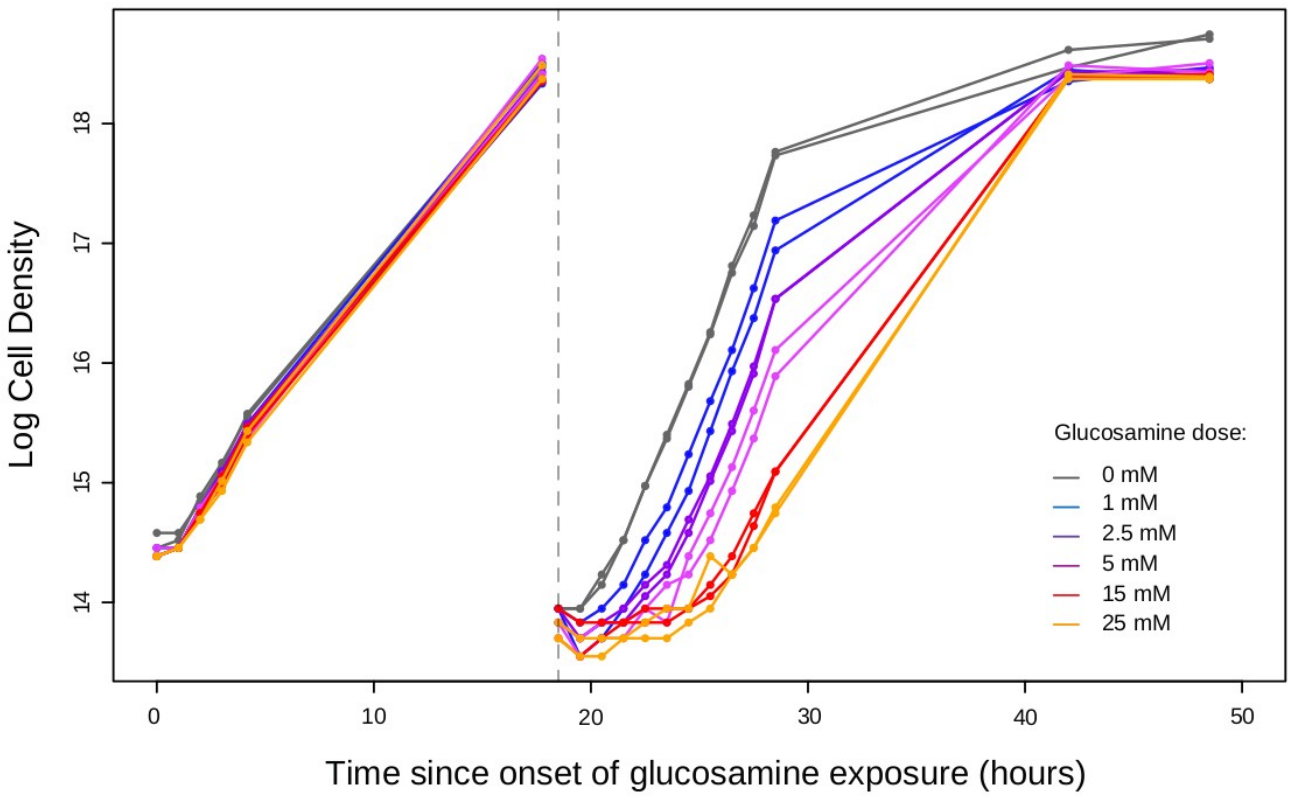

Figure 5 – figure supplement 4. Growth of wild-type cell populations exposed to different concentrations of glucosamine. Densities of cell cultures were quantified at different time points (dots) over two cycles of growth using a spectrophotometer. At $t = 0$, cells were transferred to different media containing the indicated concentrations of glucosamine (colors), then grown for 18.5 hours, diluted to fresh media containing the same concentrations of glucosamine and grown again for 30 hours.

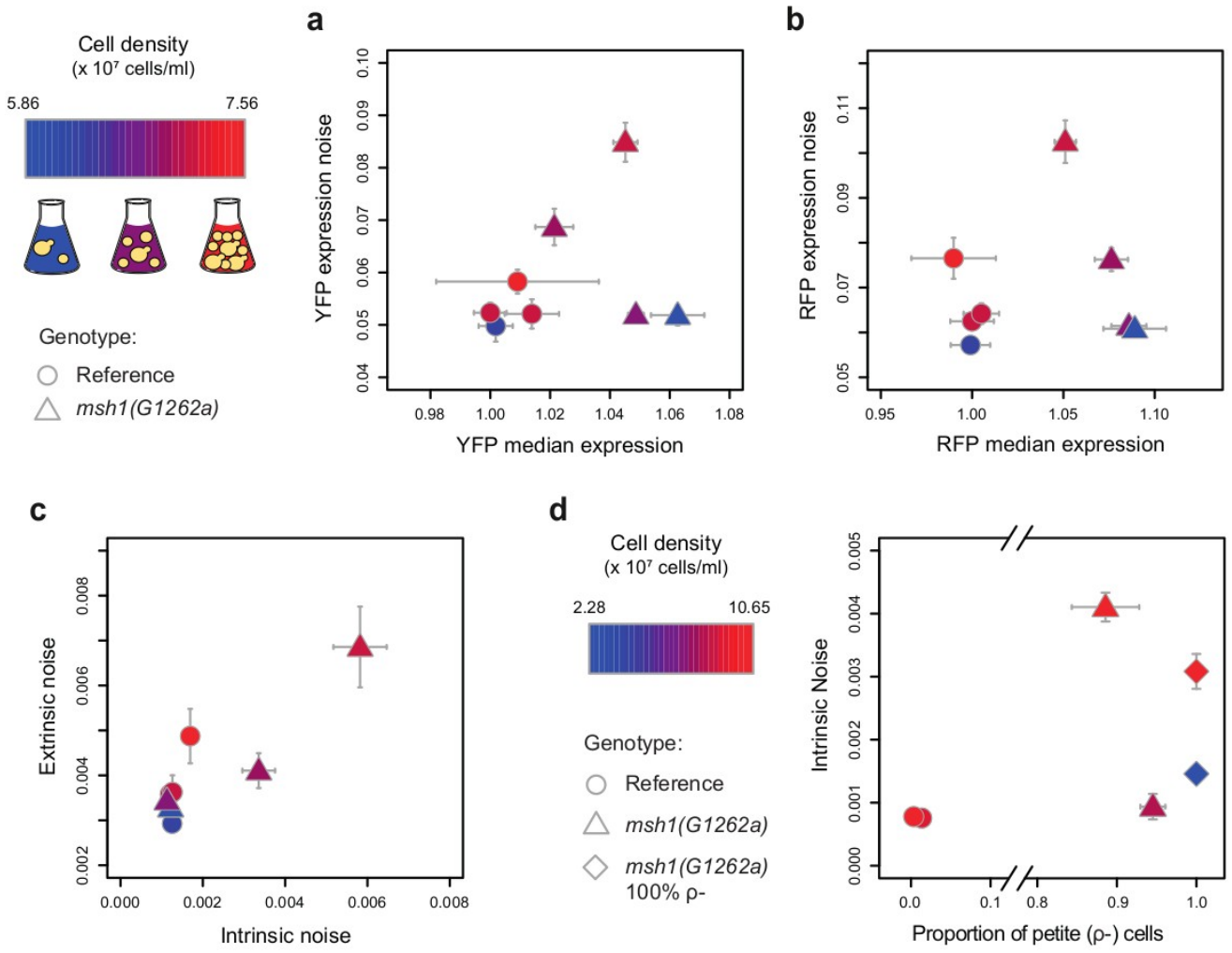

Figure 6. The effect of *msh1(G1262a)* mutation on expression noise depends on cell density. Expression noise was quantified either from YFP fluorescence **(a)**, RFP fluorescence **(b)** or both **(c)** in strains carrying the dual reporter system (P_{TDH3}-*YFP* and P_{TDH3}-*RFP*) with wild-type (circles) or mutant (triangles) alleles of *msh1*. **(d)** Intrinsic noise plotted against the proportion of respiratory deficient cells (petites ρ-) for a strain with wild-type allele of *msh1* (circle), a strain derived from a ρ+ cell with *msh1(G1262a)* mutation (triangle) and a strain derived from a ρ- cell with *msh1(G1262a)* mutation (diamond). The proportion of ρ- cell was quantified for each strain as described in Materials and methods. **(a-d)** Dots indicate mean values among 4 replicates and error bars are 95% confidence intervals of the mean. Colors indicate the average density of cell cultures measured after growth and just before fixing cells to quantify their fluorescence levels, with color legend shown on top left for **(a-c)** and at the bottom for **(d)**.

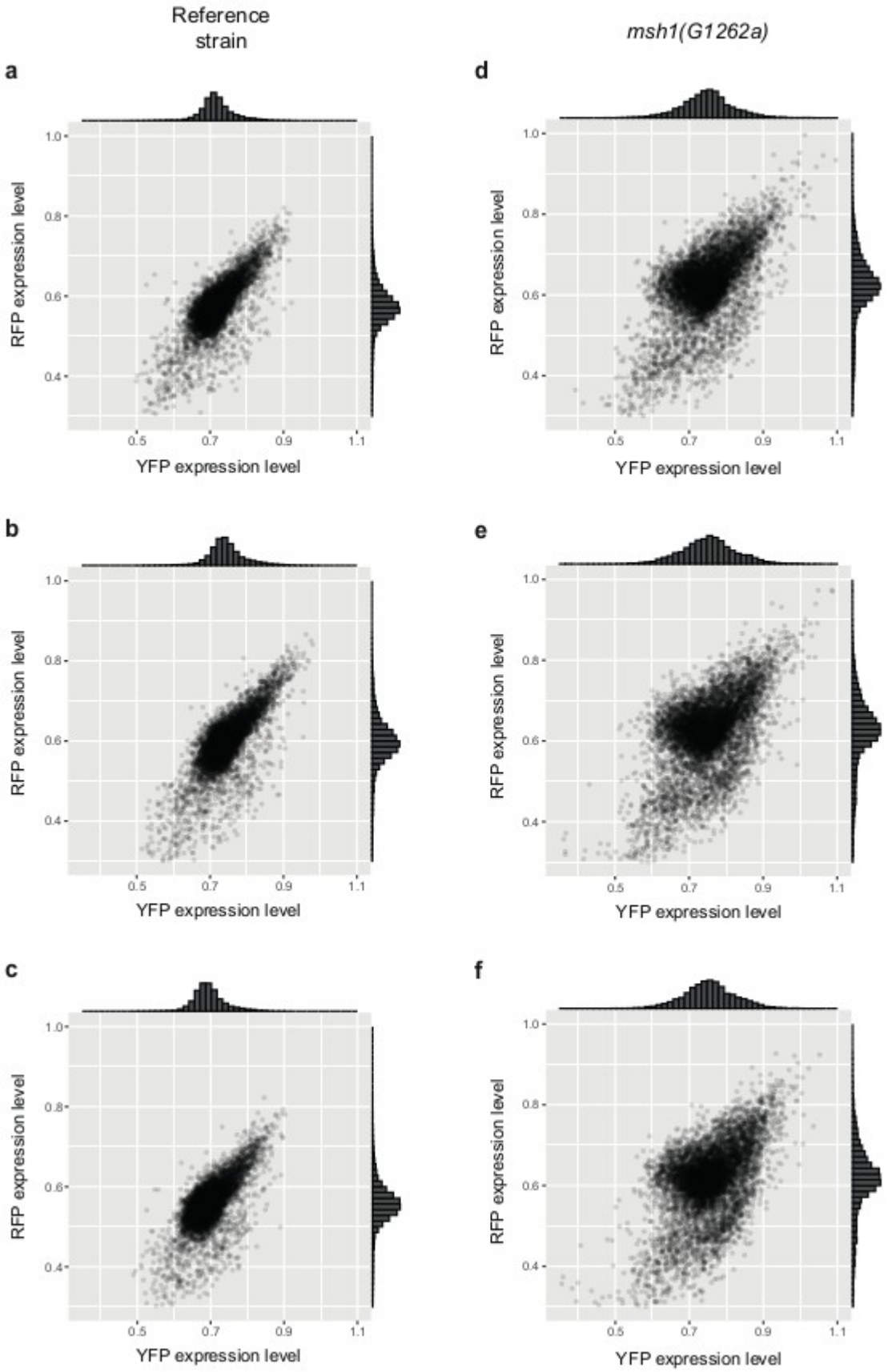
Reference strain
msh1(G1262a)
a
b
c
d
e
f
RFP expression level
YFP expression level
1.0
0.8
0.6
0.4
0.5
0.7
0.9
1.1

Figure 6 – figure supplement 1. YFP and RFP expression levels of individual cells from wild-type and *msh1(G1262a)* strains expressing P_{TDH3}-*YFP* and P_{TDH3}-*RFP* reporter genes. Expression of the two fluorescent reporters in **(a-c)** three replicate populations of strain GY2458 carrying a wild-type allele of *MSH1* and **(d-f)** three replicate populations of strain GY2534 carrying mutation *G1262a* in *MSH1* coding sequence (7885 to 8394 cells per sample). Histograms show the distribution of data on each axis.

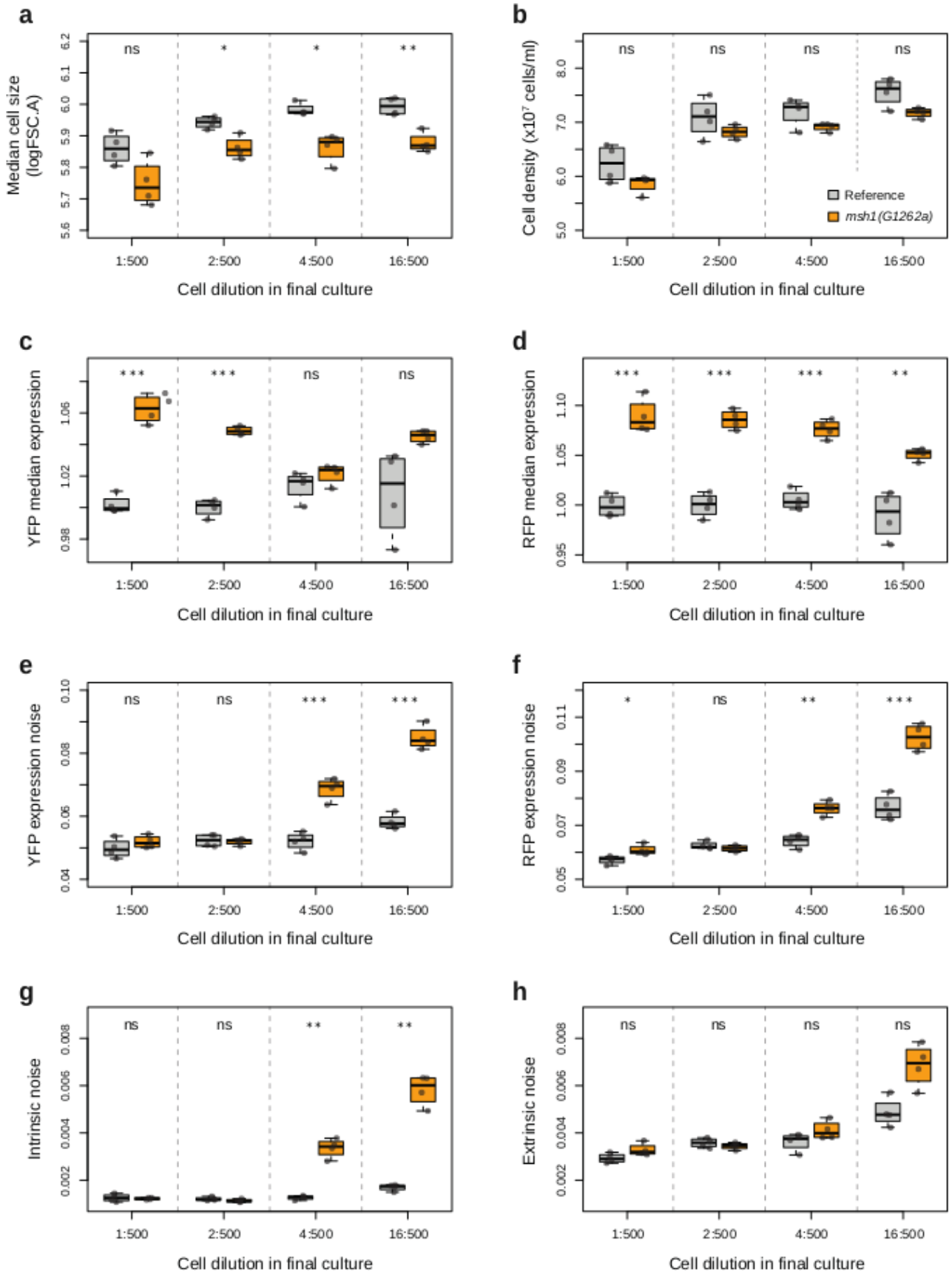
a
Median cell size (logFSC.A)
ns
*
*
**
1:500
2:500
4:500
16:500
Cell dilution in final culture
b
Cell density (x10^7 cells/ml)
ns
ns
ns
ns
Reference
msh1(G1262a)
Cell dilution in final culture
c
YFP median expression
***
***
ns
ns
Cell dilution in final culture
d
RFP median expression
***
***
***
**
Cell dilution in final culture
e
YFP expression noise
ns
ns
***
***
Cell dilution in final culture
f
RFP expression noise
*
ns
**
***
Cell dilution in final culture
g
Intrinsic noise
ns
ns
**
**
Cell dilution in final culture
h
Extrinsic noise
ns
ns
ns
ns
Cell dilution in final culture

Figure 6 – figure supplement 2. Effect of *msh1(G1262a)* mutation on 8 quantitative traits depending on cell culture dilutions. (a) Median cell size, **(b)** cell density, **(c)** YFP median expression, **(d)** RFP median expression, **(e)** YFP expression noise, **(f)** RFP expression noise, **(g)** intrinsic noise and **(h)** extrinsic noise were quantified in strains with the dual reporter system carrying wild-type (gray) or *G1262a* (orange) alleles of *msh1*. **(a-h)** Thick lines, boxes and whiskers represent the median, interquartile range (IQR) and 1.5 IQR of traits indicated on y-axis measured among 4 replicate samples. Dots represent mean values for individual samples measured from 7203 to 9218 cells. Starting from a culture at saturation (~10^8 cells/ml), cells were diluted to 500 µl of fresh SD medium at 4 different dilution ratios as indicated on x-axis and incubated for another 18 hours at 30°C before fixation and phenotyping by flow cytometry. As intended, the different dilution ratios resulted in different cell densities after incubation as shown in **(b)**. Pairwise *t*-tests were performed to compare mean phenotypic values among replicates between wild-type and *msh1(G1262a)* strains for each dilution ratio, with p-values adjusted using Benjamini-Hochberg correction: ns $P \geq 0.05$, * $0.05 > P \geq 0.01$, ** $0.001 > P \geq 0.001$, *** $P < 0.001$.

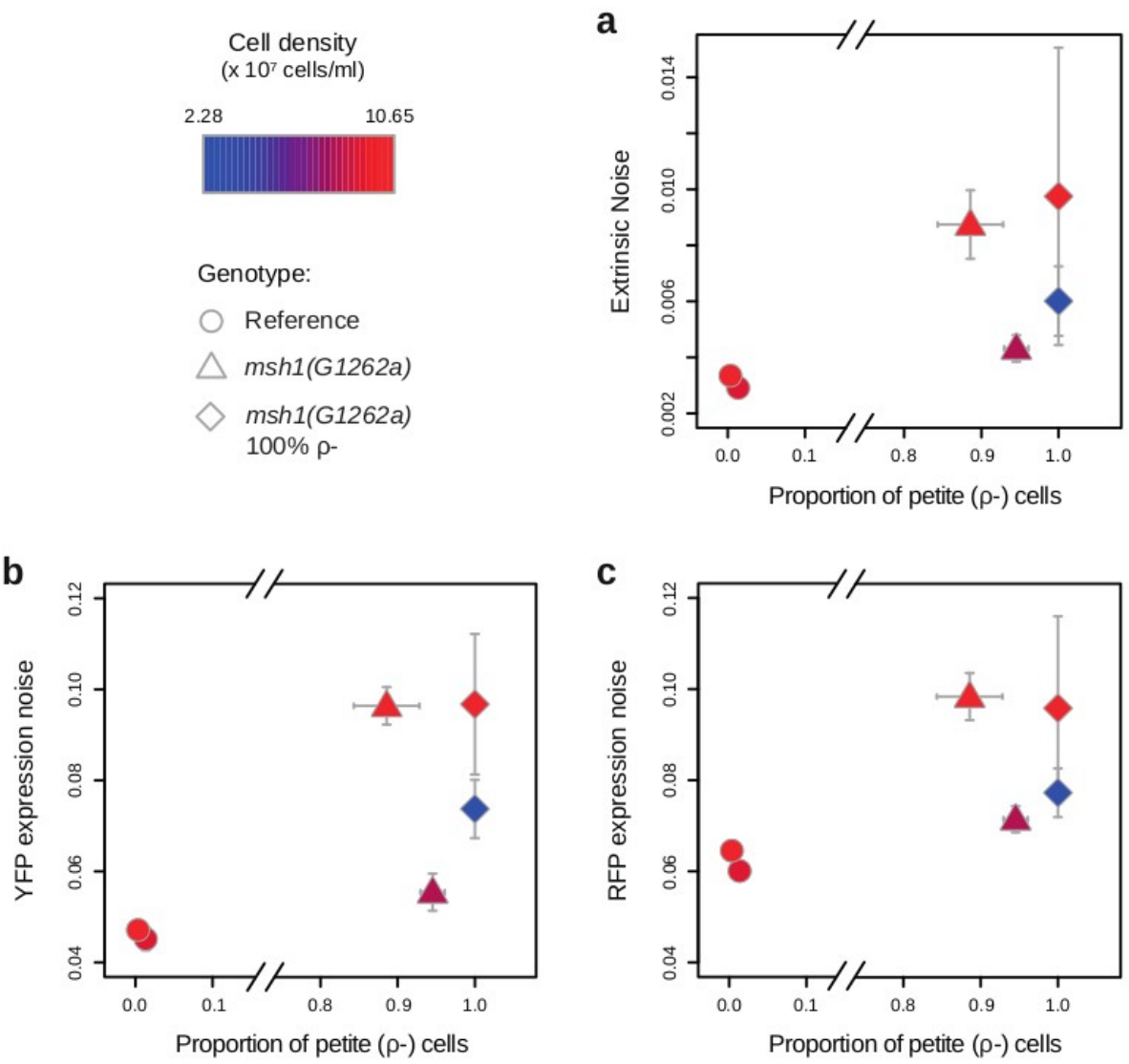

Figure 6 – figure supplement 3. Cell density changes the effect of *msh1(G1262a)* on expression noise independently from an increased proportion of respiratory deficient cells. (a) Extrinsic noise, **(b)** YFP expression noise and **(c)** RFP expression noise plotted against the proportion of respiratory deficient cells (petites ρ-) for a strain with wild-type allele of *msh1* (circle), a strain derived from a ρ+ cell with *msh1(G1262a)* mutation (triangle) and a strain derived from a ρ- cell with *msh1(G1262a)* mutation (diamond). The proportion of ρ- cell was quantified for each strain as described in Materials and methods. Dots indicate mean values among 4 replicates and error bars are 95% confidence intervals of the mean. Colors indicate the average density of cell cultures measured after growth and just before fixing cells to quantify their fluorescence levels, with color legend shown on top left.

TABLES

Strain name	Type	YFP median expr. (relative) Assay 1	YFP noise (relative) Assay 1	YFP noise (absolute) Assay 1	YFP median expr. (relative) Assay 2	YFP noise (relative) Assay 2	YFP noise (absolute) Assay 2
YPW1139	Reference	1	1	0.0152	1	1	0.0165
YPW2088	EMS mutant	0.994	1.329	0.0203	0.996	1.255	0.0208
YPW2162	EMS mutant	0.995	1.123	0.0172	0.994	1.140	0.0188
YPW2143	EMS mutant	0.991	1.728	0.0261	0.989	1.904	0.0309
YPW2210	EMS mutant	0.990	0.792	0.0121	1.008	0.870	0.0146
YPW2153	EMS mutant	0.997	0.791	0.0120	1.013	0.824	0.0134

Table 1. Properties of the reference strain and of the 5 mutants with altered P_{TDH3}-*YFP* expression noise included in the genetic mapping experiments.

Mutation	Chr.	Position (nt)	Nucleotide change	EMS mutant	Mutant noise	Frequency low bulk	Frequency middle bulk	Frequency high bulk	*P*-value
m1	XIII	871,392	C→T	YPW2088	Increase	0.66	0.24	0.36	4×10^{-9}
m2	XIV	278,253	G→A	YPW2162	Increase	0.04	0.01	0.01	0.41
m3	VIII	350,835	G→A	YPW2143	Increase	NA	0.11	0.03	NA
m4	XV	1,039,495	C→T	YPW2210	Decrease	0.37	0.61	0.50	0.007
m5	VII	995,063	C→T	YPW2153	Decrease	0.37	0.56	0.38	0.002
m6	XIII	798,603	G→A	YPW2153	Decrease	0.44	0.57	0.39	0.004

Table 2. Candidate mutations showing statistical association with variation of P_{TDH3}-*YFP* expression noise or low frequency in all fluorescence bulks.

Mutation	Gene	Function	Position in protein	Amino acid change
m1	*YME2*	Integral inner mitochondrial membrane protein; role in maintaining mitochondrial nucleoid structure and number; mutants exhibit an increased rate of mitochondrial DNA escape; shows some sequence similarity to exonucleases	412	Asp→Asn
m2	*CHS1*	Chitin synthase I; requires activation from zymogenic form in order to catalyze the transfer of N-acetylglucosamine (GlcNAc) to chitin; required for repairing the chitin septum during cytokinesis; transcription activated by mating factor	584	Trp→Stop
m3	*MSH1*	DNA-binding protein of the mitochondria; involved in repair of mitochondrial DNA; has ATPase activity and binds to DNA mismatches; has homology to E. coli MutS; transcription is induced during meiosis	428	Arg→His

Table 3. Mutations with confirmed effect on P_{TDH3}-*YFP* expression noise.

AUTHORS CONTRIBUTION

FD and PJW conceived the study; FD and LM supervised the work; NM, FD, QB, AD and HDB performed experiments; FD, JKS and QB analyzed data; FD, GY and PJW interpreted results; FD wrote the manuscript; GY reviewed and edited the manuscript. These contributions may change prior to publication.

ACKNOWLEDGEMENTS

We thank Gérard Triqueneaux for sharing protocols, the SFR Biosciences Gerland-Lyon Sud (UAR3444/US8) and University of Michigan Flow Cytometry Core for access to flow cytometers and technical assistance, the University of Michigan Sequencing Facility and ProfileXpert for Illumina sequencing, the Pôle Scientifique de Modélisation Numérique for computing resources. We also thank developers of R, Bioconductor, Ubuntu and Git.

FUNDING

Agence Nationale de la Recherche – JCJC VORTEX (ANR-20-CE12-0022)

- Fabien Duveau

Fonds de Recherche ENS Lyon – Projet Emergent 2020-2022 (R02/B-R02-FR-S60)

- Fabien Duveau

Horizon Europe, European Research Council Consolidator eGRIDE (101126053_ERC-2023-COG)

- Fabien Duveau

National Institutes of Health (R01GM108826)

- Patricia Wittkopp

National Institutes of Health (R35GM118073)

- Patricia Wittkopp

National Science Foundation (MCB-1929737)

- Patricia Wittkopp

European Molecular Biology Organization – Long-Term Fellowship (1114-2012)

- Fabien Duveau

The funders had no role in study design, data collection and interpretation, or the decision to submit the work for publication.

DATA AVAILABILITY

Illumina sequencing data have been deposited on the European Nucleotide Archive of the EBI under Study PRJEB104107 (https://www.ebi.ac.uk/ena/browser/home). This includes data for genome sequencing of the five EMS mutant strains described in the study, as well as data for deep genome sequencing of three bulks of segregants sorted based on fluorescence (BSA-seq data) for each of the five mutants crossed to the mapping strain YPW1240. Flow cytometry data will be available in the FlowRepository (https://flowrepository.org/) under experiment ID XXX.

1354 REFERENCES

Acar, M., Mettetal, J. T., & van Oudenaarden, A. (2008). Stochastic switching as a survival strategy in fluctuating environments. *Nature Genetics*, *40*(4), 471–475. https://doi.org/10.1038/ng.110

Ansel, J., Bottin, H., Rodriguez-Beltran, C., Damon, C., Nagarajan, M., Fehrmann, S., François, J., & Yvert, G. (2008). Cell-to-Cell Stochastic Variation in Gene Expression Is a Complex Genetic Trait. *PLoS Genetics*, *4*(4), e1000049. https://doi.org/10.1371/journal.pgen.1000049

Balázsi, G., van Oudenaarden, A., & Collins, J. J. (2011). Cellular decision making and biological noise: From microbes to mammals. *Cell*, *144*(6), 910–925. https://doi.org/10.1016/j.cell.2011.01.030

Baptista, I. S. C., Dash, S., Arsh, A. M., Kandavalli, V., Scandolo, C. M., Sanders, B. C., & Ribeiro, A. S. (2025). Bimodality in E. coli gene expression: Sources and robustness to genome-wide stresses. *PLOS Computational Biology*, *21*(2), e1012817. https://doi.org/10.1371/journal.pcbi.1012817

Bar-Even, A., Paulsson, J., Maheshri, N., Carmi, M., O'Shea, E., Pilpel, Y., & Barkai, N. (2006). Noise in protein expression scales with natural protein abundance. *Nature Genetics*, *38*(6), 636–643. https://doi.org/10.1038/ng1807

Barroso, G. V., Puzovic, N., & Dutheil, J. Y. (2018). The Evolution of Gene-Specific Transcriptional Noise Is Driven by Selection at the Pathway Level. *Genetics*, *208*(1), 173–189. https://doi.org/10.1534/genetics.117.300467

Blake, W. J., Balázsi, G., Kohanski, M. A., Isaacs, F. J., Murphy, K. F., Kuang, Y., Cantor, C. R., Walt, D. R., & Collins, J. J. (2006). Phenotypic consequences of promoter-mediated transcriptional noise. *Molecular Cell*, *24*(6), 853–865. https://doi.org/10.1016/j.molcel.2006.11.003

Bódi, Z., Farkas, Z., Nevozhay, D., Kalapis, D., Lázár, V., Csörgő, B., Nyerges, Á., Szamecz, B., Fekete, G., Papp, B., Araújo, H., Oliveira, J. L., Moura, G., Santos, M. A. S., Jr, T. S., Balázsi, G., & Pál, C. (2017). Phenotypic heterogeneity promotes adaptive evolution. *PLOS Biology*, *15*(5), e2000644. https://doi.org/10.1371/journal.pbio.2000644

Butow, R. A., & Avadhani, N. G. (2004). Mitochondrial Signaling: The Retrograde Response. *Molecular Cell*, *14*(1), 1–15. https://doi.org/10.1016/S1097-2765(04)00179-0

Cabib, E., Sburlati, A., Bowers, B., & Silverman, S. J. (1989). Chitin synthase 1, an auxiliary enzyme for chitin synthesis in Saccharomyces cerevisiae. *The Journal of Cell Biology*, *108*(5), 1665–1672. https://doi.org/10.1083/jcb.108.5.1665

Cabib, E., Silverman, S. J., & Shaw, J. A. (1992). Chitinase and chitin synthase 1: Counterbalancing activities in cell separation of Saccharomyces cerevisiae. *Journal of General Microbiology*, *138*(1), 97–102. https://doi.org/10.1099/00221287-138-1-97

Carey, L. B., van Dijk, D., Sloot, P. M. A., Kaandorp, J. A., & Segal, E. (2013). Promoter sequence determines the relationship between expression level and noise. *PLoS Biology*, *11*(4), e1001528. https://doi.org/10.1371/journal.pbio.1001528

Chen, D.-D., Wang, Z.-B., Wang, L.-X., Zhao, P., Yun, C.-H., & Bai, L. (2023). Structure, catalysis, chitin transport, and selective inhibition of chitin synthase. *Nature Communications*, *14*(1), 4776. https://doi.org/10.1038/s41467-023-40479-4

Choi, J. K., & Kim, Y.-J. (2009). Intrinsic variability of gene expression encoded in nucleosome positioning sequences. *Nature Genetics*, *41*(4), 498–503. https://doi.org/10.1038/ng.319

Chuffart, F., Richard, M., Jost, D., Burny, C., Duplus-Bottin, H., Ohya, Y., & Yvert, G. (2016). Exploiting Single-Cell Quantitative Data to Map Genetic Variants Having Probabilistic Effects. *PLoS Genetics*, *12*(8), e1006213. https://doi.org/10.1371/journal.pgen.1006213

Chuffart, F., & Yvert, G. (2014). MyLabStocks: A web-application to manage molecular biology materials. *Yeast (Chichester, England)*, *31*(5), 179–184. https://doi.org/10.1002/yea.3008

Conlan, R. S., Gounalaki, N., Hatzis, P., & Tzamarias, D. (1999). The Tup1-Cyc8 protein complex can shift from a transcriptional co-repressor to a transcriptional co-activator. *The Journal of Biological Chemistry*, *274*(1), 205–210. https://doi.org/10.1074/jbc.274.1.205

Coomer, M. A., Ham, L., & Stumpf, M. P. H. (2022). Noise distorts the epigenetic landscape and shapes cell-fate decisions. *Cell Systems*, *13*(1), 83-102.e6. https://doi.org/10.1016/j.cels.2021.09.002

Deutschbauer, A. M., & Davis, R. W. (2005). Quantitative trait loci mapped to single-nucleotide resolution in yeast. *Nature Genetics*, *37*(12), Article 12. https://doi.org/10.1038/ng1674

Dhar, R., Missarova, A. M., Lehner, B., & Carey, L. B. (2019). Single cell functional genomics reveals the importance of mitochondria in cell-to-cell phenotypic variation. *eLife*, *8*, e38904. https://doi.org/10.7554/eLife.38904

Dimitrov, L. N., Brem, R. B., Kruglyak, L., & Gottschling, D. E. (2009). Polymorphisms in Multiple Genes Contribute to the Spontaneous Mitochondrial Genome Instability of Saccharomyces cerevisiae S288C Strains. *Genetics*, *183*(1), 365–383. https://doi.org/10.1534/genetics.109.104497

Duveau, F., Hodgins-Davis, A., Metzger, B. P., Yang, B., Tryban, S., Walker, E. A., Lybrook, T., & Wittkopp, P. J. (2018). Fitness effects of altering gene expression noise in Saccharomyces cerevisiae. *eLife*, *7*, e37272. https://doi.org/10.7554/eLife.37272

Duveau, F., Metzger, B. P. H., Gruber, J. D., Mack, K., Sood, N., Brooks, T. E., & Wittkopp, P. J. (2014). Mapping small effect mutations in Saccharomyces cerevisiae: Impacts of experimental design and mutational properties. *G3 (Bethesda, Md.)*, *4*(7), 1205–1216. https://doi.org/10.1534/g3.114.011783

Duveau, F., Vande Zande, P., Metzger, B. P., Diaz, C. J., Walker, E. A., Tryban, S., Siddiq, M. A., Yang, B., & Wittkopp, P. J. (2021). Mutational sources of trans-regulatory variation affecting gene expression in Saccharomyces cerevisiae. *eLife*, *10*, e67806. https://doi.org/10.7554/eLife.67806

Ehrenreich, I. M., Torabi, N., Jia, Y., Kent, J., Martis, S., Shapiro, J. A., Gresham, D., Caudy, A. A., & Kruglyak, L. (2010). Dissection of genetically complex traits with extremely large pools of yeast segregants. *Nature*, *464*(7291), 1039–1042. https://doi.org/10.1038/nature08923

Eldar, A., & Elowitz, M. B. (2010). Functional roles for noise in genetic circuits. *Nature*, *467*(7312), 167–173. https://doi.org/10.1038/nature09326

Elowitz, M. B., Levine, A. J., Siggia, E. D., & Swain, P. S. (2002). Stochastic gene expression in a single cell. *Science (New York, N.Y.)*, *297*(5584), 1183–1186. https://doi.org/10.1126/science.1070919

Fehrmann, S., Bottin-Duplus, H., Leonidou, A., Mollereau, E., Barthelaix, A., Wei, W., Steinmetz, L. M., & Yvert, G. (2013). Natural sequence variants of yeast environmental sensors confer cell-to-cell expression variability. *Molecular Systems Biology*, *9*(1). https://doi.org/10.1038/msb.2013.53

Fu, A. Q., & Pachter, L. (2016). Estimating intrinsic and extrinsic noise from single-cell gene expression measurements. *Statistical Applications in Genetics and Molecular Biology*, *15*(6), 447–471. https://doi.org/10.1515/sagmb-2016-0002

Gamba, P., Jonker, M. J., & Hamoen, L. W. (2015). A Novel Feedback Loop That Controls Bimodal Expression of Genetic Competence. *PLoS Genetics*, *11*(6), e1005047. https://doi.org/10.1371/journal.pgen.1005047

Gietz, R. D., & Schiestl, R. H. (2007). High-efficiency yeast transformation using the LiAc/SS carrier DNA/PEG method. *Nature Protocols*, *2*(1), Article 1. https://doi.org/10.1038/nprot.2007.13

Guantes, R., Rastrojo, A., Neves, R., Lima, A., Aguado, B., & Iborra, F. J. (2015). Global variability in gene expression and alternative splicing is modulated by mitochondrial content. *Genome Research*, *25*(5), 633–644. https://doi.org/10.1101/gr.178426.114

Hanekamp, T., & Thorsness, P. E. (1996). Inactivation of YME2/RNA12, which encodes an integral inner mitochondrial membrane protein, causes increased escape of DNA from mitochondria to the nucleus in Saccharomyces cerevisiae. *Molecular and Cellular Biology*, *16*(6), 2764–2771. https://doi.org/10.1128/MCB.16.6.2764

Harper, C. V., Finkenstädt, B., Woodcock, D. J., Friedrichsen, S., Semprini, S., Ashall, L., Spiller, D. G., Mullins, J. J., Rand, D. A., Davis, J. R. E., & White, M. R. H. (2011). Dynamic Analysis of Stochastic Transcription Cycles. *PLOS Biology*, *9*(4), e1000607. https://doi.org/10.1371/journal.pbio.1000607

Hill, M. S., Vande Zande, P., & Wittkopp, P. J. (2021). Molecular and evolutionary processes generating variation in gene expression. *Nature Reviews. Genetics*, *22*(4), 203–215. https://doi.org/10.1038/s41576-020-00304-w

Hornung, G., Bar-Ziv, R., Rosin, D., Tokuriki, N., Tawfik, D. S., Oren, M., & Barkai, N. (2012). Noise–mean relationship in mutated promoters. *Genome Research*, *22*(12), 2409. https://doi.org/10.1101/gr.139378.112

Huang, W., Carbone, M. A., Magwire, M. M., Peiffer, J. A., Lyman, R. F., Stone, E. A., Anholt, R. R. H., & Mackay, T. F. C. (2015). Genetic basis of transcriptome diversity in Drosophila melanogaster. *Proceedings of the National Academy of Sciences*, *112*(44), E6010–E6019. https://doi.org/10.1073/pnas.1519159112

Jazwinski, S. M., & Kriete, A. (2012). The Yeast Retrograde Response as a Model of Intracellular Signaling of Mitochondrial Dysfunction. *Frontiers in Physiology*, *3*. https://doi.org/10.3389/fphys.2012.00139

Jia, Y., Rothermel, B., Thornton, J., & Butow, R. A. (1997). A basic helix-loop-helix-leucine zipper transcription complex in yeast functions in a signaling pathway from mitochondria to the nucleus. *Molecular and Cellular Biology*, *17*(3), 1110–1117. https://doi.org/10.1128/MCB.17.3.1110

Johnston, I. G., Gaal, B., Neves, R. P. das, Enver, T., Iborra, F. J., & Jones, N. S. (2012). Mitochondrial Variability as a Source of Extrinsic Cellular Noise. *PLOS Computational Biology*, *8*(3), e1002416. https://doi.org/10.1371/journal.pcbi.1002416

Kapust, R. B., Tözsér, J., Fox, J. D., Anderson, D. E., Cherry, S., Copeland, T. D., & Waugh, D. S. (2001). Tobacco etch virus protease: Mechanism of autolysis and rational design of stable mutants with wild-type catalytic proficiency. *Protein Engineering*, *14*(12), 993–1000. https://doi.org/10.1093/protein/14.12.993

Keren, L., van Dijk, D., Weingarten-Gabbay, S., Davidi, D., Jona, G., Weinberger, A., Milo, R., & Segal, E. (2015). Noise in gene expression is coupled to growth rate. *Genome Research*, *25*(12), 1893–1902. https://doi.org/10.1101/gr.191635.115

Laughery, M. F., Hunter, T., Brown, A., Hoopes, J., Ostbye, T., Shumaker, T., & Wyrick, J. J. (2015). New Vectors for Simple and Streamlined CRISPR-Cas9 Genome Editing in Saccharomyces cerevisiae. *Yeast (Chichester, England)*, *32*(12), 711–720. https://doi.org/10.1002/yea.3098

Levy, S. F., Ziv, N., & Siegal, M. L. (2012). Bet hedging in yeast by heterogeneous, age-correlated expression of a stress protectant. *PLoS Biology*, *10*(5), e1001325. https://doi.org/10.1371/journal.pbio.1001325

Liao, X., & Butow, R. A. (1993). RTG1 and RTG2: Two yeast genes required for a novel path of communication from mitochondria to the nucleus. *Cell*, *72*(1), 61–71. https://doi.org/10.1016/0092-8674(93)90050-z

Liao, X. S., Small, W. C., Srere, P. A., & Butow, R. A. (1991). Intramitochondrial functions regulate nonmitochondrial citrate synthase (CIT2) expression in Saccharomyces cerevisiae. *Molecular and Cellular Biology*, *11*(1), 38–46. https://doi.org/10.1128/mcb.11.1.38-46.1991

Liu, J., Martin-Yken, H., Bigey, F., Dequin, S., François, J.-M., & Capp, J.-P. (2015). Natural yeast promoter variants reveal epistasis in the generation of transcriptional-mediated noise and its potential benefit in stressful conditions. *Genome Biology and Evolution*, *7*(4), 969–984. https://doi.org/10.1093/gbe/evv047

Liu, P., Song, R., Elison, G. L., Peng, W., & Acar, M. (2017). Noise reduction as an emergent property of single-cell aging. *Nature Communications*, *8*(1), 680. https://doi.org/10.1038/s41467-017-00752-9

Liu, Z., & Butow, R. A. (2006). Mitochondrial retrograde signaling. *Annual Review of Genetics*, *40*, 159–185. https://doi.org/10.1146/annurev.genet.40.110405.090613

Loell, K., Wu, Y., Staller, M. V., & Cohen, B. (2022). Activation domains can decouple the mean and noise of gene expression. *Cell Reports*, *40*(3), 111118. https://doi.org/10.1016/j.celrep.2022.111118

Lu, Y., Biancotto, A., Cheung, F., Remmers, E., Shah, N., McCoy, J. P., & Tsang, J. S. (2016). Systematic Analysis of Cell-to-Cell Expression Variation of T Lymphocytes in a Human Cohort Identifies Aging and Genetic Associations. *Immunity*, *45*(5), 1162–1175. https://doi.org/10.1016/j.immuni.2016.10.025

Magwene, P. M., Willis, J. H., & Kelly, J. K. (2011). The statistics of bulk segregant analysis using next generation sequencing. *PLoS Computational Biology*, *7*(11), e1002255. https://doi.org/10.1371/journal.pcbi.1002255

Martinez-Jimenez, C. P., Eling, N., Chen, H.-C., Vallejos, C. A., Kolodziejczyk, A. A., Connor, F., Stojic, L., Rayner, T. F., Stubbington, M. J. T., Teichmann, S. A., de la Roche, M., Marioni, J. C., & Odom, D. T. (2017). Aging increases cell-to-cell transcriptional variability upon immune stimulation. *Science (New York, N.Y.)*, *355*(6332), 1433–1436. https://doi.org/10.1126/science.aah4115

Metzger, B. P. H., Duveau, F., Yuan, D. C., Tryban, S., Yang, B., & Wittkopp, P. J. (2016). Contrasting Frequencies and Effects of cis- and trans-Regulatory Mutations Affecting Gene Expression. *Molecular Biology and Evolution*, *33*(5), 1131–1146. https://doi.org/10.1093/molbev/msw011

Metzger, B. P. H., Yuan, D. C., Gruber, J. D., Duveau, F., & Wittkopp, P. J. (2015). Selection on noise constrains variation in a eukaryotic promoter. *Nature*, *521*(7552), 344–347. https://doi.org/10.1038/nature14244

Mineta, K., Matsumoto, T., Osada, N., & Araki, H. (2015). Population genetics of non-genetic traits: Evolutionary roles of stochasticity in gene expression. *Gene*, *562*, 16–21.

Morgan, M. D., Patin, E., Jagla, B., Hasan, M., Quintana-Murci, L., & Marioni, J. C. (2020). Quantitative genetic analysis deciphers the impact of cis and trans regulation on cell-to-cell variability in protein expression levels. *PLoS Genetics*, *16*(3), e1008686. https://doi.org/10.1371/journal.pgen.1008686

Neves, R. P. das, Jones, N. S., Andreu, L., Gupta, R., Enver, T., & Iborra, F. J. (2010). Connecting Variability in Global Transcription Rate to Mitochondrial Variability. *PLOS Biology*, *8*(12), e1000560. https://doi.org/10.1371/journal.pbio.1000560

Newman, J. R. S., Ghaemmaghami, S., Ihmels, J., Breslow, D. K., Noble, M., DeRisi, J. L., & Weissman, J. S. (2006). Single-cell proteomic analysis of S. cerevisiae reveals the architecture of biological noise. *Nature*, *441*(7095), 840–846. https://doi.org/10.1038/nature04785

Ohnishi, Y., Huber, W., Tsumura, A., Kang, M., Xenopoulos, P., Kurimoto, K., Oleś, A. K., Araúzo-Bravo, M. J., Saitou, M., Hadjantonakis, A.-K., & Hiiragi, T. (2014). Cell-to-cell expression variability followed by signal reinforcement progressively segregates early mouse lineages. *Nature Cell Biology*, *16*(1), 27–37. https://doi.org/10.1038/ncb2881

Pal, S., & Dhar, R. (2024). Living in a noisy world—Origins of gene expression noise and its impact on cellular decision-making. *FEBS Letters*, *598*(14), 1673–1691. https://doi.org/10.1002/1873-3468.14898

Parab, L., Pal, S., & Dhar, R. (2022). Transcription factor binding process is the primary driver of noise in gene expression. *PLOS Genetics*, *18*(12), e1010535. https://doi.org/10.1371/journal.pgen.1010535

Park, S., Hanekamp, T., Thorsness, M. K., & Thorsness, P. E. (2006). Yme2p is a mediator of nucleoid structure and number in mitochondria of the yeast Saccharomyces cerevisiae. *Current Genetics*, *50*(3), 173–182. https://doi.org/10.1007/s00294-006-0087-9

Parks, T. D., Leuther, K. K., Howard, E. D., Johnston, S. A., & Dougherty, W. G. (1994). Release of proteins and peptides from fusion proteins using a recombinant plant virus proteinase. *Analytical Biochemistry*, *216*(2), 413–417. https://doi.org/10.1006/abio.1994.1060

Partow, S., Siewers, V., Bjørn, S., Nielsen, J., & Maury, J. (2010). Characterization of different promoters for designing a new expression vector in Saccharomyces cerevisiae. *Yeast (Chichester, England)*, *27*(11), 955–964. https://doi.org/10.1002/yea.1806

Pedraza, J. M., & Paulsson, J. (2008). Effects of molecular memory and bursting on fluctuations in gene expression. *Science (New York, N.Y.)*, *319*(5861), 339–343. https://doi.org/10.1126/science.1144331

Puzović, N., Madaan, T., & Dutheil, J. Y. (2023). Being noisy in a crowd: Differential selective pressure on gene expression noise in model gene regulatory networks. *PLoS Computational Biology*, *19*(4), e1010982. https://doi.org/10.1371/journal.pcbi.1010982

Quarton, T., Kang, T., Papakis, V., Nguyen, K., Nowak, C., Li, Y., & Bleris, L. (2020). Uncoupling gene expression noise along the central dogma using genome engineered human cell lines. *Nucleic Acids Research*, *48*(16), 9406–9413. https://doi.org/10.1093/nar/gkaa668

Raser, J. M., & O'Shea, E. K. (2004). Control of stochasticity in eukaryotic gene expression. *Science (New York, N.Y.)*, *304*(5678), 1811–1814. https://doi.org/10.1126/science.1098641

Raser, J. M., & O'Shea, E. K. (2005). Noise in Gene Expression: Origins, Consequences, and Control. *Science (New York, N.Y.)*, *309*(5743), 2010–2013. https://doi.org/10.1126/science.1105891

Richard, A., Boullu, L., Herbach, U., Bonnafoux, A., Morin, V., Vallin, E., Guillemin, A., Gao, N. P., Gunawan, R., Cosette, J., Arnaud, O., Kupiec, J.-J., Espinasse, T., Gonin-Giraud, S., & Gandrillon, O. (2016). Single-Cell-Based Analysis Highlights a Surge in Cell-to-Cell Molecular Variability Preceding Irreversible Commitment in a Differentiation Process. *PLOS Biology*, *14*(12), e1002585. https://doi.org/10.1371/journal.pbio.1002585

Richard, M., & Yvert, G. (2014). How does evolution tune biological noise? *Frontiers in Genetics*, *5*, 374. https://doi.org/10.3389/fgene.2014.00374

Rocabert, C., Beslon, G., Knibbe, C., & Bernard, S. (2020). Phenotypic noise and the cost of complexity. *Evolution*, *74*(10), 2221–2237. https://doi.org/10.1111/evo.14083

Sanchez, A., & Golding, I. (2013). Genetic determinants and cellular constraints in noisy gene expression. *Science (New York, N.Y.)*, *342*(6163), 1188–1193. https://doi.org/10.1126/science.1242975

Sarkar, A. K., Tung, P.-Y., Blischak, J. D., Burnett, J. E., Li, Y. I., Stephens, M., & Gilad, Y. (2019). Discovery and characterization of variance QTLs in human induced pluripotent stem cells. *PLOS Genetics*, *15*(4), e1008045. https://doi.org/10.1371/journal.pgen.1008045

Schmiedel, J. M., Carey, L. B., & Lehner, B. (2019). Empirical mean-noise fitness landscapes reveal the fitness impact of gene expression noise. *Nature Communications*, *10*(1), 3180. https://doi.org/10.1038/s41467-019-11116-w

Schmutzer, M., & Wagner, A. (2020). Gene expression noise can promote the fixation of beneficial mutations in fluctuating environments. *PLOS Computational Biology*, *16*(10), e1007727. https://doi.org/10.1371/journal.pcbi.1007727

Schor, I. E., Degner, J. F., Harnett, D., Cannavò, E., Casale, F. P., Shim, H., Garfield, D. A., Birney, E., Stephens, M., Stegle, O., & Furlong, E. E. M. (2017). Promoter shape varies across populations and affects promoter evolution and expression noise. *Nature Genetics*, *49*(4), 550–558. https://doi.org/10.1038/ng.3791

Shaffer, S. M., Dunagin, M. C., Torborg, S. R., Torre, E. A., Emert, B., Krepler, C., Beqiri, M., Sproesser, K., Brafford, P. A., Xiao, M., Eggan, E., Anastopoulos, I. N., Vargas-Garcia, C. A., Singh, A., Nathanson, K. L., Herlyn, M., & Raj, A. (2017). Rare cell variability and drug-induced reprogramming as a mode of cancer drug resistance. *Nature*, *546*(7658), 431–435. https://doi.org/10.1038/nature22794

Sharon, E., van Dijk, D., Kalma, Y., Keren, L., Manor, O., Yakhini, Z., & Segal, E. (2014). Probing the effect of promoters on noise in gene expression using thousands of designed sequences. *Genome Research*, *24*(10), 1698–1706. https://doi.org/10.1101/gr.168773.113

Sherman, M. S., Lorenz, K., Lanier, M. H., & Cohen, B. A. (2015). Cell-to-cell variability in the propensity to transcribe explains correlated fluctuations in gene expression. *Cell Systems*, *1*(5), 315–325. https://doi.org/10.1016/j.cels.2015.10.011

Siciliano, V., Garzilli, I., Fracassi, C., Criscuolo, S., Ventre, S., & di Bernardo, D. (2013). miRNAs confer phenotypic robustness to gene networks by suppressing biological noise. *Nature Communications*, *4*(1), 2364. https://doi.org/10.1038/ncomms3364

Snijder, B., Sacher, R., Rämö, P., Damm, E.-M., Liberali, P., & Pelkmans, L. (2009). Population context determines cell-to-cell variability in endocytosis and virus infection. *Nature*, *461*(7263), 520–523. https://doi.org/10.1038/nature08282

Stewart-Ornstein, J., Weissman, J. S., & El-Samad, H. (2012). Cellular Noise Regulons Underlie Fluctuations in Saccharomyces cerevisiae. *Molecular Cell*, *45*(4), 483–493. https://doi.org/10.1016/j.molcel.2011.11.035

Stuckey, S., Mukherjee, K., & Storici, F. (2011). In Vivo Site-Specific Mutagenesis and Gene Collage Using the Delitto Perfetto System in Yeast Saccharomyces cerevisiae. In H. Tsubouchi (Ed.), *DNA Recombination* (Vol. 745, pp. 173–191). Humana Press. https://doi.org/10.1007/978-1-61779-129-1_11

Sukys, A., & Grima, R. (2025). Cell-cycle dependence of bursty gene expression: Insights from fitting mechanistic models to single-cell RNA-seq data. *Nucleic Acids Research*, *53*(7), gkaf295. https://doi.org/10.1093/nar/gkaf295

Sun, M., & Zhang, J. (2020). Allele-specific single-cell RNA sequencing reveals different architectures of intrinsic and extrinsic gene expression noises. *Nucleic Acids Research*, *48*(2), 533–547. https://doi.org/10.1093/nar/gkz1134

Suter, D. M., Molina, N., Gatfield, D., Schneider, K., Schibler, U., & Naef, F. (2011). Mammalian genes are transcribed with widely different bursting kinetics. *Science (New York, N.Y.)*, *332*(6028), 472–474. https://doi.org/10.1126/science.1198817

Tan, R. Z., & van Oudenaarden, A. (2010). Transcript counting in single cells reveals dynamics of rDNA transcription. *Molecular Systems Biology*, *6*(1), 358. https://doi.org/10.1038/msb.2010.14

Taniguchi, Y., Choi, P. J., Li, G.-W., Chen, H., Babu, M., Hearn, J., Emili, A., & Xie, X. S. (2010). Quantifying E. coli proteome and transcriptome with single-molecule sensitivity in single cells. *Science (New York, N.Y.)*, *329*(5991), 533–538. https://doi.org/10.1126/science.1188308

Tirosh, I., & Barkai, N. (2008). Two strategies for gene regulation by promoter nucleosomes. *Genome Research*, *18*(7), 1084–1091. https://doi.org/10.1101/gr.076059.108

Trinh, D.-C., Martin, M., Bald, L., Maizel, A., Trehin, C., & Hamant, O. (2023). Increased gene expression variability hinders the formation of regional mechanical conflicts leading to reduced organ shape robustness. *Proceedings of the National Academy of Sciences of the United States of America*, *120*(30), e2302441120. https://doi.org/10.1073/pnas.2302441120

Triqueneaux, G., Burny, C., Symmons, O., Janczarski, S., Gruffat, H., & Yvert, G. (2020). Cell-to-cell expression dispersion of B-cell surface proteins is linked to genetic variants in humans. *Communications Biology*, *3*(1), 346. https://doi.org/10.1038/s42003-020-1075-1

Vande Zande, P., Hill, M. S., & Wittkopp, P. J. (2022). Pleiotropic effects of trans-regulatory mutations on fitness and gene expression. *Science*, *377*(6601), 105–109. https://doi.org/10.1126/science.abj7185

Verhagen, P. G. A., & Hansen, M. M. K. (2025). Exploring the Central Dogma Through the Lens of Gene Expression Noise. *Journal of Molecular Biology*, 169202. https://doi.org/10.1016/j.jmb.2025.169202

Vlková, M., & Silander, O. K. (2022). Gene regulation in Escherichia coli is commonly selected for both high plasticity and low noise. *Nature Ecology & Evolution*, *6*(8), 1165–1179. https://doi.org/10.1038/s41559-022-01783-2

Wang, Z., & Zhang, J. (2011). Impact of gene expression noise on organismal fitness and the efficacy of natural selection. *Proceedings of the National Academy of Sciences*, *108*(16), E67–E76.

https://doi.org/10.1073/pnas.1100059108

Wernet, M. F., Mazzoni, E. O., Çelik, A., Duncan, D. M., Duncan, I., & Desplan, C. (2006). Stochastic spineless expression creates the retinal mosaic for colour vision. *Nature*, *440*(7081), 174–180. https://doi.org/10.1038/nature04615

Wittkopp, P. J., Haerum, B. K., & Clark, A. G. (2004). Evolutionary changes in cis and trans gene regulation. *Nature*, *430*(6995), 85–88. https://doi.org/10.1038/nature02698

Wolf, L., Silander, O. K., & van Nimwegen, E. (2015). Expression noise facilitates the evolution of gene regulation. *eLife*, *4*, e05856. https://doi.org/10.7554/eLife.05856

Yang, S., Kim, S., Rim Lim, Y., Kim, C., An, H. J., Kim, J.-H., Sung, J., & Lee, N. K. (2014). Contribution of RNA polymerase concentration variation to protein expression noise. *Nature Communications*, *5*(1), 4761. https://doi.org/10.1038/ncomms5761

You, S.-T., Jhou, Y.-T., Kao, C.-F., & Leu, J.-Y. (2019). Experimental evolution reveals a general role for the methyltransferase Hmt1 in noise buffering. *PLoS Biology*, *17*(10), e3000433. https://doi.org/10.1371/journal.pbio.3000433

Yvert, G. (2014). 'Particle genetics': Treating every cell as unique. *Trends in Genetics: TIG*, *30*(2), 49–56. https://doi.org/10.1016/j.tig.2013.11.002

Zenklusen, D., Larson, D. R., & Singer, R. H. (2008). Single-RNA counting reveals alternative modes of gene expression in yeast. *Nature Structural & Molecular Biology*, *15*(12), 1263–1271. https://doi.org/10.1038/nsmb.1514

Zhang, Z., Qian, W., & Zhang, J. (2009). Positive selection for elevated gene expression noise in yeast. *Molecular Systems Biology*, *5*, 299. https://doi.org/10.1038/msb.2009.58

Zopf, C. J., Quinn, K., Zeidman, J., & Maheshri, N. (2013). Cell-Cycle Dependence of Transcription Dominates Noise in Gene Expression. *PLOS Computational Biology*, *9*(7), e1003161. https://doi.org/10.1371/journal.pcbi.1003161